Linear and Nonlinear Optical Effects in Sub-wavelength Structures

By
SAMIR KUMAR

PHYS11201204015

National Institute of Science Education and Research, Bhubaneswar

A thesis submitted to the

Board of Studies in Physical Sciences

In partial fulfillment of requirements

for the Degree of

DOCTOR OF PHILOSOPHY

of

HOMI BHABHA NATIONAL INSTITUTE

January, 2019

Homi Bhabha National Institute[1]

Recommendations of the Viva Voce Committee

As members of the Viva Voce Committee, we certify that we have read the dissertation prepared by Samir Kumar entitled "Linear and Nonlinear Optical Effects in Sub-wavelength Structures" and recommend that it may be accepted as fulfilling the thesis requirement for the award of Degree of Doctor of Philosophy.

Chairman – Prof. Bedangadas Mohanty   Date:

Guide / Convener – Dr. Ritwick Das   Date:

Co-guide -   Date:

External- Examiner – Prof. Achanta Venugopal   Date:

Member 1- Dr. Pratap Kumar Sahoo   Date:

Member 2- Dr. Kartikeswar Senapati   Date:

Member 3- Dr. Rajan Jha   Date:

Final approval and acceptance of this thesis is contingent upon the candidate's submission of the final copies of the thesis to HBNI.

I/We hereby certify that I/we have read this thesis prepared under my/our direction and recommend that it may be accepted as fulfilling the thesis requirement.

Date: 28/01/2019

Place: BHUBANESWAR

Dr Ritwick Das

---

[1] This page is to be included only for final submission after successful completion of viva voce.

ii

STATEMENT BY AUTHOR

This dissertation has been submitted in partial fulfillment of requirements for an advanced degree at Homi Bhabha National Institute (HBNI) and is deposited in the Library to be made available to borrowers under rules of the HBNI.

Brief quotations from this dissertation are allowable without special permission, provided that accurate acknowledgment of the source is made. Requests for permission for extended quotation from or reproduction of this manuscript in whole or in part may be granted by the Competent Authority of HBNI when in his or her judgment the proposed use of the material is in the interests of scholarship. In all other instances, however, permission must be obtained from the author.

Samir Kumar

Samir Kumar

DECLARATION

I, hereby declare that the investigation presented in the thesis has been carried out by me. The work is original and has not been submitted earlier as a whole or in part for a degree/diploma at this or any other Institution / University.

Samir Kumar

List of Publications arising from the thesis

Journal

1. "Refractive index sensing using a light trapping cavity: A theoretical study", S. Kumar and R. Das, *J. Appl. Phys*, **2018**, *123*, 233103.

2. "Coupling to Tamm-plasmon-polaritons: dependence on structural parameters", A. Kumari, S. Kumar, M.K. Shukla, G. Kumar, P.S. Maji, R. Vijaya, R. Das, *Journal of Physics D: Applied Physics*, **2018,** 51 (25), 255103.

3. "Self-referenced refractive index sensing with hybrid-Tamm-plasmon-polariton modes in sub-wavelength analyte layers", S. Kumar, M.K. Shukla, P.S. Maji, R. Das *Journal of Physics D: Applied Physics*, **2017**, 50 (37), 375106.

4. "On the tunability of quality-factor for optical Tamm plasmon modes", S. Kumar, R. Das, *Journal of Optics*, **2017**, 19 (9), 095001.

5. "Tamm-plasmon resonance based temperature sensor in a Ta_2O_5/SiO_2 based distributed Bragg reflector", S. Kumar, P.S. Maji, R. Das, *Sensors and Actuators A: Physical* , **2017**, 260, 10-15.

6. "Phase-dependent ultrafast third-order optical nonlinearities in metallophthalocyanine thin films", S. Kumar, K.V.A. Kumar, S.M. Dharmaprakash, R. Das, *J. Appl. Phys,* **2016**, 120 (12), 123104.

7. "Impact of $\alpha \rightarrow \beta$ transition in the ultrafast high-order nonlinear optical properties of metal-free phthalocyanine thin films", K.V.A. Kumar, S. Kumar, S.M. Dharmaprakash, R. Das, *J. Phys. Chem. C*, **2016,** 120 (12), 6733-6740.

8. "Defect-assisted saturable absorption characteristics in Mn-doped ZnO nano-rods", A. Singh, S. Kumar, R Das, P.K. Sahoo, *RSC Advances*, **2015,** (108), 88767-88772.

Conferences

1. "Refractive Index Sensing With 1D Photonic Crystal", S. Kumar and R. Das, *Frontiers in Optics/Laser Science,* **September 2017**.

2. "On the Coupling Efficiency of Tamm Plasmon Polaritons", S. Kumar, M. K. Shukla and R. Das, *Frontiers in Optics/Laser Science,* **September 2017.**

3. "Refractive Index Sensor Based On Hybrid-Tamm Plasmon-Polariton And Cavity Mode", S. Kumar, M. K. Shukla, P. S. Maji, R. Das, *CLEO-PR, OECC & PGC Singapore*, **August 2017**.

4. "Q-factor enhancement in Optical Tamm Plasmon Modes", S. Kumar and R. Das, *International Conference on Fiber Optics and Photonics*, IIT Kanpur, **Dec. 2016.**

5. "Ultrafast optical nonlinearities in 2, 9, 16, 23 -Tetra -tert - butyl - 29H, 31H - Phthalocyanine thin films", S. Kumar, K. V. Anil Kumar, S. M. Dharmaprakash, and R. Das, *Advanced Photonics Congress*, Vancouver Canada, **July 2016**.

6. "Femtosecond Nonlinear Optical Properties of as Grown and Annealed Phthalocyanine Thin Films", S. Kumar, R. Das, K.V. Anil Kumar and S.M. Dharmaprakash, *Workshop on Recent Advances in Photonics* (*WRAP),* IIsc. Bangalore*,* **Dec. 2015**.

7. "Single-pass, multi-watt second-harmonic generation in congruent and Stoichiometric $LiTaO_3$", M. K. Shukla, S. Kumar, and R. Das, *IEEE Photonics conference*, Reston, Virginia, USA, **Oct. 2015**.

8. "Tamm-plasmon states in the broadband dielectric-coated mirror", S. Kumar and R. Das, Proc. 99th Optical Society of America Annual Meeting: *Frontiers in Optics/Laser Science*, San Jose, USA, **Oct. 2015.**

9. "High-power frequency-doubled Yb-fiber lase", M. K. Shukla, S. Kumar, and R. Das, *International Conference on Fiber Optics and Photonics*, IIT Kharagpur, **Dec 2014.**

10. "High-power, single-frequency, single-pass second-harmonic generation by optimally focused Yb-fiber lase", M. K. Shukla, S. Kumar and R. Das, *Advanced Solid State Lasers (ASSL)*, Shanghai China, **Nov. 2014.**

Others

1. "A comparative study of optical nonlinearities of trans-A 2 B-corroles in solution and in aggregated state", A. Garai, S. Kumar, W. Sinha, C.S. Purohit, R. Das, S. Kar, *RSC Advances* , **2015**, 5 (36), 28643-28651.

2. "Single-pass, multi-watt second-harmonic-generation in congruent and stoichiometric $LiTaO_3$", M Shukla, S Kumar, R. Das, *Photonics Technology Letters*, **2015**, 27 (13), 1379 -1382.

3. "Single-pass, efficient type-I phase-matched frequency doubling of high-power ultrashort-pulse Yb-fiber laser using LiB3O5", M.K. Shukla, S. Kumar, R. Das, *Applied Physics B*, **2016**, 122 (5), 114.

Samir Kumar

Samir Kumar

To My Parents Ramashish Prasad Singh and Sulochna Devi,

 And My Brother Saurabh Kumar

Acknowledgments

First of all, I would like to express my deep-felt gratitude to my thesis supervisor Dr. Ritwick Das, for his support, guidance, care, and patience. What has been achieved is because of the never-ending encouragement and support that I have received from him. He showed great patience in guiding me, which has helped me in many ways, without which it would not have been possible to complete this thesis.

I am thankful to Dr. Pratap Kumar Sahoo, Dr. Kartikeswar Senapati, Dr. Rajan Jha (IIT Bhubaneswar) and the chairman of the doctoral committee Prof. Bedangadas Mohanty for agreeing to serve on my Ph. D. committee and for their feedback and support on how to improve my Ph. D. thesis. Prof. Bedangadas Mohanty valuable discussions and healthy criticism ensured success and clarity during the PhD. tenure. I would like to thank Prof. David Hagan of CREOL, University of Central Florida, for valuable discussions on nonlinear optics and Z-scan technique and accepting my invitation to visit and deliver a talk in NISER Bhubaneswar OSA Student Chapter. I thank Dr. Sachin Srivastava for valuable discussions on self reference refractive index sensor. Faculty member at School of Physical Sciences, NISER have been a source of many important insights, for this I thank them all. I thank all the staff and administrators of the NISER for the assistant, support and friendly nature.

I would like to thank Dr. Pratap Kumar Sahoo, Dr. S M Dharmaprakash and Dr. Sanjiv Kar for the collaboration from which my results on nonlinear optics resulted. Most of the results presented in Chapters 3 and 4 of this thesis is an outcome of

Samir Kumar

Samir Kumar

CONTENTS

SYNOPSIS

(Limited to 10 pages in double spacing)

Nonlinear optical (NLO) effects have been subject of extensive research ever since the first observation of NLO phenomena known as second harmonic generation (SHG) because of its broad range of applications [1]. Currently, there is a great deal of interest in NLO phenomena as it holds great promises for a broad range of applications in a variety of aspects of human life as well as in the areas of science and technology [2]. Some examples of the areas of human life are communication, medicine, and military [1,2]. Among those in the areas of science and technology are nonlinear microscopy, wavelength conversion, optical switching, photonic devices, quantum computing and material processing [1,2]. This growing interest in the field of NLO effects due to its different applications creates a need for new nonlinear optical materials suitable for the development of integrated optics. Therefore the realization of NLO applications is closely connected with the development of novel materials and nonlinear optics [3]. In general, a nonlinear response could occur in a material when the intensity of the light beam is large enough to overdrive the physical system [1]. This causes the resulting polarization to behave nonlinearly, leading to the occurrence of several interesting phenomena such as self-focusing and self-phase modulation [2]. The underlying processes resulting in such nonlinear phenomenon are intensity-dependent refractive index and attenuation [1,2]. The degree of nonlinear polarization primarily depends on the electric field strength and oscillator strength of constituent atoms and molecules which is expressed in terms of linear and nonlinear susceptibility.

This thesis work was motivated by the necessity to characterize and explore the nonlinear optical properties of novels materials to assess their capabilities towards

varied NLO applications. Also, the necessity to tailor and control the linear and nonlinear optical properties of novel materials for practical applications in numerous technologies has driven me to work on this project [1,2]. The work is divided into three parts, a theoretical background section, nonlinear optical properties of organic and inorganic semiconductors and the linear optical properties of metal-distributed Bragg reflector (M-DBR) structure. In the theory section, we describe the factors and mechanism affecting the NLO responses in the sample. This section also presents the different techniques utilized for the NLO characterization of the samples. The second part of the present research focuses on the investigation of NLO properties of organic and inorganic semiconductors as well as investigates the methods to control or tune their NLO properties. There are many approaches that can help us to modify the linear and NLO optical properties of materials [1-3]. Amongst the methods that I have studied is the impact of the structural configuration of the organic semiconductors i.e. Phthalocyanine thin films [4]. An important cause for NLO interest is that the Phthalocyanine can be synthesized and their optical properties can be modified through different metal substitution and peripheral substitution with ease [4]. Their properties are suited to many applications like optical limiting. An important property of Phthalocyanine is the presence of Q- band whose properties can be controlled by changing the phase of the Pc films. An alternate route that we have adopted for the purpose of controlling the optical properties is by means of doping the semiconductors and creating defects [5]. Doping in semiconductor thin films and nanorods is a popular way of controlling the linear and nonlinear optical properties of materials. It is important to mention here that doping leads to the development of new materials with enhanced NLO properties such as nonlinear absorption and nonlinear refraction [6]. We have also looked at the sub-wavelength structures with the perspective that can help us to enhance linear and nonlinear optical effects. The interaction of light with these sub-wavelength structures (such as metal-photonic

crystal structures) leads to the confinement of the electromagnetic field and hence significantly enhances the light-matter interactions and hence, linear and NLO effects [7,8].

For the study of nonlinear optical properties i.e. nonlinear refractive index and nonlinear absorption, we used the closed-aperture (CA) and open aperture (OA) Z-Scan technique [9]. The Z-scan technique is a simple, sensitive, uses single beam and highly effective method to measure the nonlinear refractive index and nonlinear absorption of a material. In the CA Z-scan technique, we measure the transmittance of the nonlinear medium through a finite aperture in the far-field as the sample is translated across the focus of the Gaussian beam. The phase extracted from the CA measurements is related to the nonlinear refraction of the sample. In the OA Z-scan technique, we measure the transmittance as a function of sample position as the sample is translated through the focus of the Gaussian beam [9].

In order to study the impact of phase change ($\alpha \rightarrow \beta$) of Tetra-tert-butyl-phthalocyanine (H_2Pc) on NLO properties; 2,9,16,23-Tetra-tert-butyl-29H,31H-Phthalocyanine powder was used for the preparation of Phthalocyanine thin films. We prepared H_2Pc thin-films at room temperature on an ultrasonically cleaned glass substrate at a base pressure of 10^{-5} Torr using thermal-evaporation-technique. The prepared thin-films exist in the α-phase form of H_2Pc (UTT) which was further annealed at 473 K for 90 minutes using a muffle furnace to obtain the corresponding thermally-stable β-phase i.e. ATT [10]. The structural modifications in H_2Pc films showed distinct signature in UV-visible absorption spectra, powder X-ray diffraction and Raman spectra which were employed for identifying the transformation from α-phase to β-phase. The NLO characteristics which include nonlinear refractive indices such as n_2 and n_4, as well as nonlinear absorption coefficient (β_{eff}), were measured by using a single beam Z-scan technique [11,12]. Using an ultrashort pulsed fiber-laser at 1064 nm central wavelength, we performed the OA and CA Z-scan experiment. In

OA experiment, we obtained a smaller value of β_{eff} in α-phase as compared to β-phase due to a smaller value of saturation intensity (I_s) which, in turn, is a consequence of ground state bleaching in the thermally unstable amorphous state of the molecule. The impact of $\chi^{(5)}$ nonlinearity in the CA Z-scan transmittance of α-phase was apparent from the dual peak-valley behavior and interestingly, the optical phase changes due to $\chi^{(3)}$ and $\chi^{(5)}$ nonlinearities bear opposite sign [11]. In addition, they alter their signs as the laser intensity increases. A dominant fifth-order NLO contribution in the PC films was mainly a consequence of inherently large $\chi^{(5)}$ as well as two-photon assisted nonlinear refraction as a result of excited state absorption (ESA). It is worthwhile to mention that α-polymorphs are comparatively less stable and more susceptible to distortion as a consequence of molecular architecture and molecular stacking arrangement on the substrate. Therefore, UTT films are expected to undergo the greater change in dipole moment as compared to ATT films when appropriate vibrational modes (with different scales of disorder) in the polymorph are excited by the external electric field. As a consequence, the structural orientation has a strong influence on the electrical as well as optical properties. The NLO study of metal-free Pc films revealed that the switching characteristics of n_2 and n_4 in α-polymorphs could be a promising candidate for devising controlled switches and gates in modern photonic integrated circuitry. On the other hand, H_2PC films existing in β-phase are better suited for optical limiting applications by virtue of their improved saturable absorption properties.

In another study, the impacts of phase transformations of metallophthalocyanine (MPc) thin films on their third-order nonlinear optical (NLO) properties were investigated. In order to do so, MPc thin films are prepared by thermally evaporating the commercially available Copper(II)2,9,16,23-Tetra-tert-butyl-29H,31H-phthalocyanine (CuPc) and Zinc(II) 2,9,16,23-Tetra-tert-butyl-29H,31H-

phthalocyanine (ZnPc) powder on glass substrate. Thermal annealing causes a phase transformation which has a distinct signature in powder X-ray diffraction and UV-Vis-NIR spectroscopy [10]. The NLO characteristics which include nonlinear refractive index n_2, as well as nonlinear absorption coefficient (β_{eff}), were measured using a single beam Z-scan technique [9]. The CA Z-scan reveal opposite sign of nonlinear refractive indices for CuPc and ZnPc thin films. It was also observed that the n_2 values are affected by the central metal atom and the phases of the MPc molecules. In the case of ZnPc thin films, the value of nonlinear refractive index varies marginally on phase transition. The case of CuPc is completely different. The as-prepared CuPc has the highest value of the nonlinear refractive index. The value of n_2 decreased from 9.6×10^{-15} m^2/W to 2.2×10^{-15} m^2/W on annealing the CuPc thin films at 473 K. An explanation of this observation for CuPc is strongly connected with the phase change [13]. The OA Z-scan investigation reveals that annealed CuPc phase exhibits strong NLA which is essentially a consequence of a singlet ESA assisted TPA. Due to strong NLA, CuPc films can be employed as optical limiters at 1064 nm. The as-prepared and annealed ZnPc thin films are found to exhibit optically induced transparency or saturable absorption behavior at 1064 nm. This difference in NLA for CuPc and ZnPc can be attributed to their different absorption mechanism and excited state dynamics.

In addition to the nonlinear optical properties of organic semiconductors, we have also studied the NLO properties of inorganic semiconductors Zinc Oxide (ZnO). The work is motivated by the necessity to control the interaction between light and matter. In order to do so, we doped Manganese (Mn) in ZnO sub-wavelength rods and investigated its nonlinear optical properties, namely two-photon absorption (TPA) and nonlinear refraction using single-beam Z−scan technique utilizing sub picoseconds 532 nm laser [9]. Mn-doped ZnO nanorods (NRs) were prepared by low-temperature

aqueous growth technique. The results showed that Mn-doping concentration primarily determines the interaction between light and Mn-doped ZnO nanorods. We observed that Mn-doping concentration primarily determines whether ZnO NRs would exhibit saturable absorption (SA) or two-photon-absorption (TPA) characteristics in the OA Z-scan experiment. At high Mn-doping concentrations, ZnO NRs exhibit strong SA behavior displaying an increase in transmittance which could be attributed to high occupation probability of defects states as well as saturation of linear absorption of sub-wavelength rod aggregates at high optical fluence. In addition to this, a residual absorption originated by the tail of the absorption edge or the product of the mid-gap states produced by the high doping concentration of the sample could be expected and deriving in a saturable absorption behavior [14]. In contrast to high Mn-doping concentration in ZnO NRs, we observed TPA feature in undoped and 0.5% Mn-doped ZnO NRs. The employability of such structures in the area of optical limiting and switching is essentially derived from the possibility to tune their nonlinear optical absorption which could be realized by appropriate Mn-doping in ZnO NR architecture. In CA Z-scan measurements, all the samples with varying concentration of Mn-doping exhibited self-defocusing effect with significantly higher n_2 values as compared to ZnO thin films. The significantly large third-order NLO behavior could be appreciated by observing the modifications in geometrical arrangement and band structure of ZnO NRs as a function of Mn-doping.

In the subsequent section of my thesis work, we have investigated the properties of Optical Tamm plasmon (OTP) resonances in metal-distributed Bragg reflector (M-DBR) geometry [15]. OTP resonances in M-DBR geometry can be put to many practical uses [8,16]. For example, excitation of OTP helps us to achieve light localization which in turn leads to an enhanced nonlinear response. Light localization also helps us to enhance the sensitivity of the optical sensors. OTP has also great

potential to be applied in the field of optical switches, OTP based laser, light trapping in a nano and microcavity and in enhancing the fluorescence [17]. To begin with, we present a comprehensive investigation of the impact of metal films on tuning the quality-factor (Q-factor) of OTP modes in M-DBR structure. The lifetime and the Q-factor of OTP in gold and silver deposited films on DBR mirror were determined from OTP resonance linewidth. The lifetime and the Q-factor of OTP modes are found to depend on DBR bilayers, metal film thickness as well as on different plasmon active metals. This is because of the fact that lifetime and Q-factor are dictated by the sharpness of the OTP resonance and sharpness of the resonance curve depends upon the imaginary part of the dielectric constant of the metal, number of DBR bilayers and metal thickness [16]. In general, Q-factor is a measure of the rate at which optical energy is dissipated from within the cavity (due to absorption, scattering, or mirror leakage) and hence, it signifies the strength of confinement of electromagnetic energy in a given volume. We observed that the linewidth of OTP modes turns smaller when the intrinsic reflectivity of the metal layer or the DBR geometry increases. The Q-factor of OTP modes in case Ag-DBR geometry was measured to be almost $\approx$ 1.65 times than that for Au-DBR geometry. We also observed that the average photon lifetime in OTP mode strongly depends on metal thickness as well as nature of plasmon-active metal for a different number of DBR bilayers. This investigation provides a plausible route to optimally choose the metal and DBR architecture so as to satisfy the requirement for a particular application.

 Another part of this work presents a comprehensive analysis for enhanced coupling of light to TPP mode based on the observations of reflectance minima in the reflectivity spectra [18]. The coupling efficiency of TPP modes is strongly influenced by the thickness of metal, choice of plasmon active metals as well as the number of bilayers [16]. In order to attain a condition of efficient coupling, the DBR structure

should undergo concomitant changes in the number of bilayers together with the metal thickness. Also, a shift in the resonance wavelength was achieved through varying DBR top layer thickness and varying the metal thickness. Our proposed design scheme resulted in controlling the reflectivity minima for TPP resonance based on requirements of applications. In a separate work, we have presented a plausible route to realize a refractive-index sensor using hybrid-modes in dual `Ag-DBR' geometry supporting hybrid-modes formed as a consequence of coupling between individual TPP modes at the metal-DBR interface [19]. Since the coupling between the TPP modes is carried out through the sub-wavelength sized analyte medium, the symmetric hybrid-mode undergoes appreciable change when analyte refractive index alters. This forms the basis of the refractive-index sensing mechanism. Our analysis shows that hybrid-mode sensor performance is comparable to that for interferometer based sensor as well as SPR sensors. The proposed scheme can be potentially applied to biochemical sensors with the integrated nanofluidic channel.

Another study is intended to propose a practically feasible refractive index sensor based on a cavity mode. The cavity mode based sensor is realized by a "metal-cavity-DBR" configuration in which the refractive index of the cavity varies. Consequently, there is a spectral shift of cavity resonance wavelength which forms the basis of refractive index sensing [20]. The sub-wavelength sized cavity substantially enhances the field concentration between metal and DBR due to excitation of cavity mode which results in high sensitivity and improved detection accuracy. Both the wavelength and angular spectral sensitivities of the biochemical sensors based on cavity mode reveal a strong dependence of sensitivity and linewidth on the angle of incidence and polarization of the light. The proposed scheme and associated design can be potentially applied to other desired wavelength as well by optimally designing the DBR structure. The significant advantages of the

presented sensor suggest the use of this sensor for biochemical applications and can be integrated to the nanofluidic channel. In another work, we also proposed and experimentally realized Tamm-plasmon-polariton (TPP) based temperature sensor [21]. The sensing architecture is comprised of thin silver (Ag) film on a broadband dielectric coated mirror. The OTP mode excitation is characterized by a sharp dip in reflectivity within the high reflectivity band of the dielectric mirror. It was observed that the TPP reflectivity dip reduces uniformly as a function of temperature without affecting the sharpness of the dip. Defining temperature sensitivity in terms of change in reflectivity from the composite structure, a sensitivity of 7.8 $\times 10^{-4}$ / ^{0}C was determined.

Bibliography

[1] R. W. Boyd. *Nonlinear Optics*. Academic Press, second edition, 2003.

[2] R. L. Sutherland. *Handbook of Nonlinear Optics*. Marcel Dekker, Inc.,1996.

[3] X. Liu, Q. Guo, and J. Qiu, "Emerging low-dimensional materials for nonlinear optics and ultrafast photonics," Adv. Mater. **29(14)**, 1605886 (2017).

[4] G. de la Torre, P. Vazquez, F. Agullo-Lopez, T. Torres, "Role of Structural Factors in the Nonlinear Optical Properties of Phthalocyanines and Related Compounds," Chem. Rev. **104**, 3723-3750 (2004).

[5] B. Anand, S. R.Krishnan, R. Podila, S S Sai, A. M Rao, R. Philip. "The role of defects in the nonlinear optical absorption behavior of carbon and ZnO nanostructures," Phys Chem Chem Phys **16(18)**, 8168-77 (2014).

[6] V. Krishnakumar, G. Shanmugam, R. Nagalakshmi, "Large third-order optical nonlinearity of Mg-doped PbS/PVA freestanding nanocomposite films," J Phys D **45**, 165102–165108 (2012).

[7] M. Soljacic and J. D. Joannopoulos, "Enhancement of nonlinear effects using photonic crystals," Nature Materials **3**, 211-219(2004).

[8] K. J. Lee, J. W. Wu, and K. Kim, "Enhanced nonlinear optical effects due to the excitation of optical Tamm plasmon polaritons in one-dimensional photonic crystal structures," Opt. Express **21**, 28817–28823 (2013).

[9] M. Sheik-Bahae, A. A. Said, T.-H. Wei, D. J. Hagan, and E. W. Van Stryland, " Sensitive measurement of optical nonlinearities using a single beam," IEEE Journal of Quantum Electronics **26(4)**, 760-769(1990).

[10] S. Yim, S. Heutz, T. S. Jones, "Model for the $\alpha \rightarrow \beta 1$ Phase Transition in Phthalocyanine Thin Films," J. Appl. Phys **91**, 3632-3626 (2002).

[11] B. Gu, J. Chen, Y. Fan, J. Ding, H. T. Wang, "Theory of Gaussian Beam Z scan With Simultaneous Third- and Fifth-Order Nonlinear Refraction Based on a Gaussian Decomposition Method," J. Opt. Soc. Am. B **22**, 2651-2659(2005).

[12] H. Zhang, S. Lu, J. Zheng, J. Du, S. Wen, D. Tang, K. Loh, "Molybdenum Disulfide (MoS_2) as a Broadband Saturable Absorber for Ultra-Fast Photonics," Opt. Express **22**, 7249-7260 (2014).

[13] A. Zawadzka, P. Plociennik, J. Strzelecki, M. Pranaitis, S. D. Seignon and B. Sahraoui, "Structural and nonlinear optical properties of as-grown and annealed metallophthalocyanine thin films," Thin Solid Films **545**, 429-437 (2013).

[14] C. Torres-Torres, B. A. Can-Uc, R. Rangel-Rojo, L. Castañeda, R. Torres- Martínez, C. I. García-Gil, and A. V. Khomenko, "Optical Kerr phase shift in a nanostructured nickel-doped zinc oxide thin solid film," Opt. Express **21(18)**, 21357-64 (2013).

[15] M. Kaliteevski, I. Iorsh, S. Brand, R. A. Abram, J. M. Chamberlain, A.V. Kavokin and I. A. Shelykh, "Tamm plasmon-polaritons: Possible electromagnetic states at the interface of a metal and a dielectric Bragg mirror," Phys. Rev. B **76**, 165415(2007).

[16] C.Y. Chang, Y. H. Chen, Y. L. Tsai, H. C. Kuo, K. P. Chen, "Tunability and Optimization of Coupling Efficiency in Tamm Plasmon Modes," IEEE J. Sel. Top. Quantum Electron **21**, 460020 (2015).

[17] S. Kumar and R. Das, "On the tunability of quality-factor for optical Tamm plasmon modes," J. Opt. **19**, 095001 (2017).

[18] B. Auguie, A. Bruchhausen, and A. Fainstein, "Critical coupling to Tamm plasmons," J. Opt. 17, 035003(2015).

[19] Y. Fang, L Yang, K. Wa, and Z. Na, "Tunable coupled states of a pair of Tamm plasmon polaritons and a microcavity mode," J. Opt **15**, 125703(2013).

[20] M. Shaban, A. M. Ahmed, E. Abdel-Rahman and H. Handy, "Tunability and sensing properties of the plasmonic/1D photonic crystal," Sci. Rep. 7 41983(2017).

[21] L. J. Davis, M. Deutsch, "Surface plasmon-based thermo-optic and temperature sensor for microfluidic thermometry," Rev. Sci. Instrum. **81**, 114905(2010).

Publications in Refereed Journal:

 a. Published

  1. Antara Garai, **Samir Kumar**, Woormileela Sinha, Chandra Shekhar Purohit, Ritwick Das, Sanjib Kar, "A comparative study of optical nonlinearities of trans-A 2 B-corroles in solution and in aggregated state," *RSC Advances*, **5**, 28643-28651 (2015).

2. [#]Avanendra Singh, [#]**Samir Kumar**, Ritwick Das, Pratap K Sahoo, "Defect-assisted saturable absorption characteristics in Mn-doped ZnO nano-rods," *RSC Advances*, **5**, 88767-88772 (2015).

3. Mukesh Kumar Shukla, **Samir Kumar** and R. Das "Single-Pass Multi-Watt Second-Harmonic-Generation in Congruent and Stoichiometric LiTaO3," *IEEE Photon. Technol. Lett.*, **27**, 1379 –1382 (2015).

4. [#]KV Anil Kumar, [#]**Samir Kumar**, SM Dharmaprakash, Ritwick Das, "Impact of $\alpha \rightarrow \beta$ Transition in the Ultrafast High-Order Nonlinear Optical Properties of Metal-Free Phthalocyanine Thin Films," *J. Phys. Chem. C* **120**, 6733–6740 (2016).

5. **Samir Kumar**, K V Anil Kumar, S. M. Dharmaprakash, Ritwick Das, Phase-dependent ultrafast third-order optical nonlinearities in metallophthalocyanine thin films," *J. Appl. Phys.* **120**, 123104 (2016).

6. Mukesh Kumar Shukla, **Samir Kumar**, Ritwick Das, "Single-pass, efficient type-I phase matched frequency doubling of high-power ultrashort-pulse Yb-fiber laser using LiB_3O_5," *Appl. Phys. B* 122 (2016).

7. **Samir Kumar**, Partha Sona Maji, Ritwick Das, "Tamm-plasmon resonance based temperature sensor in a Ta_2O_5/SiO_2 based distributed Bragg reflector," *Sensors and Actuators A* **260**, 10-15(2017).

8. **Samir Kumar** and Ritwick Das, "On the tunability of quality-factor for optical Tamm plasmon modes," J. Opt, **19** 095001 (2017).

9. **Samir Kumar**, Mukesh Kumar Shukla, Partha Sona Maji, Ritwick Das, " Self-referenced refractive index sensing with hybrid-Tamm-plasmon-

polariton modes in sub-wavelength analyte layers," J. Phys. D: Appl. Phys. **50**,(2017).

 # Equal Contributions

b. **To be Communicated:**

1. **S. Kumar** *et al.* "Optimization of structural parameters for efficient coupling of light to OTP Modes," (Manuscript Under preparation).

2. **S. Kumar** *et al.* "Refractive Index Sensing Characteristics of Tamm-Plasmon-Polaritons with Light Trapping Cavity," (manuscript under preparation).

Other Publications:

Conference/Symposium

1 M. K. Shukla, **S. Kumar** and R. Das "High-power, single-frequency, single-pass second-harmonic generation by optimally focused Yb-fiber laser" *Advanced Solid State Lasers (ASSL),* Shanghai China, 2014.

2 M. K. Shukla, **S. Kumar,** and R. Das "High-power frequency-doubled Yb-fiber laser" Conference Papers, *Photonics,* S5A , Page S5A.29, 2014.

3 **S. Kumar** and R. Das "Tamm-plasmon states in the broadband dielectric-coated mirror" Proc. 99th Optical Society of America Annual Meeting: *Frontiers in Optics/Laser Science*, San Jose, USA, Oct.2015.

4 M. K. Shukla, **S. Kumar**, and R. Das, "Single-pass, multi-watt second-harmonic generation in congruent and Stoichiometric $LiTaO_3$" *IEEE Photonics conference*, Reston, Virginia, USA, Oct.2015.

5 **S. Kumar**, R. Das, K.V. Anil Kumar and S.M. Dharmaprakash "Femtosecond Nonlinear Optical Properties of as Grown and Annealed

Phthalocyanine Thin Films" *Workshop on Recent Advances in Photonics (WRAP),* IIsc. Bangalore, Dec. 2015.

6 **S. Kumar**, K. V. Anil Kumar, S. M. Dharmaprakash, and Ritwick Das "Ultrafast optical nonlinearities in 2, 9, 16, 23 -Tetra -tert - butyl - 29H, 31H - Phthalocyanine thin films" *Advanced Photonics Congress*, Vancouver Canada, July 2016.

7 **S. Kumar** and R. Das, "Q-factor enhancement in Optical Tamm Plasmon Modes" *International Conference on Fiber Optics and Photonics*, IIT Kanpur, Dec. 2016

8 **S Kumar**, Mukesh Kumar Shukla, Partha Sona Maji, Ritwick Das, "Refractive Index Sensor Based On Hybrid-Tamm Plasmon-Polariton And Cavity Mode, *CLEO-PR, OECC & PGC* Singapore 2017.

9 **S Kumar**, M K Shukla and R Das, "On the Coupling Efficiency of Tamm Plasmon Polaritons" *Frontiers in Optics/Laser Science 2017*

10 **S Kumar** and R Das "Refractive Index Sensing With 1D Photonic Crystal," *Frontiers in Optics/Laser Science 2017*

LIST OF FIGURES

ZnO rods with 532 nm wavelength and 0.7 ns pulses.

LIST OF TABLES

LIST OF ABBREVIATIONS

NLO	Nonlinear Optical
SHG	Second Harmonic Generation
M-DBR	Metal-Distributed Bragg Reflectors
Pc	Phthalocyanine
MPc	Metalophthalocyanine
CA	Closed-aperture
OA	Open Aperture
UTT/α-phase	As Prepared phthalocyanine film
ATT/β-phase	Annealed phthalocyanine film
H_2Pc	Metal-free Phthalocyanine
CuPc	Copper(II)2,9,16,23-Tetra-tert-butyl-29H,31H-phthalocyanine
ZnPc	Zinc(II) 2,9,16,23-Tetra-tert-butyl-29H,31H-phthalocyanine
n_2	Third- Order Nonlinear Refractive Index
n_4	Fifth-Order Nonlinear Refractive Index
β_{eff}	Effective Two Photon Absorption
TPA	Two Photon Absorption
MPA	Multi Photon Absorption
NLA	Nonlinear Absorption
NLR	Nonlinear Refraction

ESA	Excited State Absorption
THG	Third Harmonic Generation
SNR	Signal to Noise Ratio
SFG	Sum Frequency Generation
DFG	Difference Frequency Generation
FOM	Figure of Merit
FWM	Four Wave Mixing
DFWM	Degenerate Four Wave Mixing
Fs	Femtosecond
Ns	Nanosecond
CW	Continuous Wave
ZnO	Zinc Oxide
Mn	Manganese
NRs	Nanorods
SA	Saturable Absorption
RSA	Reverse Saturable Absorption
OTP	Optical Tamm Plasmon
TPPs	Tamm Plasmon Polaritons
DBR	Distributed Bragg Reflector
Q-factor	Quality Factor
$\chi^{(1)}$	First - Order Susceptibilty
$\chi^{(3)}$	Third-Order Susceptibilty
$\chi^{(5)}$	Fifth -Order Susceptibilty

NLT	Nonlinear Transmission
I_s	Saturation Intensity
I_0	Peak Intensity
L_{eff}	Effectice Sample Thickness
α_0	Linear Absorption
Z_0	Rayleigh Length
w_0	Beam waist
NT	Normalized Transmission
T_p	Peak
T_v	Valley
NIR	Near Infrared
VB	Valence Band
CB	Conduction Band
E_g	Band gap or Energy gap
FWHM	Full Width Half Maxima
TIR	Total Internal Reflection
SPPs	Surface Plasmon Polaritons
d_m	Metal Thickness
d_a/ d_c	Analyte or Cavity Thickness
N	Number of DBR Bilayers
R_{min}	Reflectivity Minima
WLS	White Light Source
λ_{tp}	Tamm Resonance Wavelength

τ_{tp}	Cavity Lifetime
TE and TM	Transverse Electric and Transverse Magnetic
RIS	Refractive Index Sensing
Ta_2O_5	Tantalum Pentoxide
SiO_2	Silicon Oxide
S_n	Sensitivity
RIU	Refractive Index Unit
AOI	Angle of Incidence
n_a	Analyte Refractive Index
TMM	Transfer Matrix Method
DA	Detection Accuracy
ΔR_{min}	Variation in Reflectivity Minima
dn/dT	Thermo-Optic Coefficient

Chapter 1
Introduction

1.1 Motivation

The nonlinear optical response of a medium to an intense laser beam could result in polarization at frequencies not present in the incident radiation [1]. If the light beam is intense enough, different nonlinear optical (NLO) effects like Sum Frequency Generation (SFG), Difference Frequency generation (DFG), Intensity-dependent refractive index (nonlinear refraction), nonlinear absorption (NLA) could come into effect [1,2]. Such NLO effects have a broad range of applications in different areas of science and technology which touch human life in a variety of ways e.g. through communication, medicine and military [3-5]. In science and technology, nonlinear optics play an indispensable role in the areas of nonlinear microscopy, frequency conversion, optical switching & limiting, photonic devices, quantum computing and material processing and many more [2-6]. However, the lack of suitable photonic materials offering requisite functionality is often the chief limitation in efficiently catering to the aforementioned applications. Therefore, strong emphasis is being laid in the research for exploring novel materials in nonlinear optics in order to expand the scope of these applications and refine those which are already in the matured stage. In this direction, material technology and nonlinear optics are working hand-in-hand for the realization of efficient and reliable NLO devices. Amongst the materials that are being investigated for the NLO applications are polymers, semiconductors and plasmonic materials [7-12].

The motivation behind the present thesis work is essentially aimed at exploring a variety of artificially prepared materials which exhibit interesting NLO characteristics.

The explored materials constituents are expected to significantly contribute towards developing more efficient systems for the optoelectronic industry as well as delving deeper into basic science [2]. Through the investigations, we aim to gain a fair bit of physical insight of underlying mechanisms which are playing a vital role and subsequently, design recipes for controlling the linear as well as NLO properties of novel materials for a broad range of applications. The present thesis work will be primarily focusing on two aspects. The first part will be primarily focusing on various $\chi^{(3)}$ based NLO interactions such as nonlinear refraction (NLR) and nonlinear absorption (NLA). In the remaining part of the thesis, I will present examples of light-matter interaction in the periodically stratified medium through our investigations of optical surface modes [2,13-15].

1.2 Aim and Objectives

The primary objective of the present Ph.D. thesis is to study the NLO properties of organic and inorganic semiconductors as well as investigate the methods to control their NLO characteristics. There are many approaches that can help us to modify the linear and NLO optical properties of materials [7,15, 16-22]. Amongst the methods which I have focussed on the impact of the structural configuration of the organic semiconductors i.e. Phthalocyanine thin films [7]. The research in Phthalocyanine thin films is not limited to the field of organic chemistry. It is a crucial material under investigation in the semiconductor industry as well. Phthalocyanine films could be synthesized through well-established routes and their optical properties can be modified through different metallic substitutions and peripheral substitutions which could be realized with ease [23-26]. Their properties are suited to many applications including optical-switching and optical limiting [22, 26, 27]. An important property of

Phthalocyanine is the presence of Q-band in the visible region which could be optimally tailor altering the morphological phase of the Pc films [23,24,28].

Another technique that we have deployed for controlling as well as manipulating the nonlinear optical characteristics is through doping of semiconducting sub-wavelength materials and creating defects [29]. Doping in semiconductor thin films and nanorods (sub-wavelength rods) has been a popular route for controlling the linear and NLO properties of materials over the last few years [30-33]. For example, in case of optical limiting, doping leads to the development of new functionalities without affecting the primary application and at times, enhances the listing efficiency [29, 34].

Our prime motivation has been to focus on the periodic sub-wavelength semiconducting as well as insulating geometries with a perspective of understanding the light-matter interaction mechanisms which are responsible for enhancing the linear and NLO effects [15-17]. The thesis explores the consequences of the interaction of light with periodic subwavelength architectures (such as Metallo-dielectric photonic crystals) which results in the electromagnetic field localization and hence, significantly enhances the light-matter interaction [16, 35]. This, at times, has a direct and decisive role to play in enhancing the NLO effects [15,35].

1.3 Thesis Outline

My thesis work is divided into 6 chapters. In chapter 2, I introduce the theoretical principles and the derivation of the expression for various NLO concepts like NLR and NLA that form the basis of my research [2,36]. This is followed by a detailed description of the origin of NLO response in different novel optical materials [1]. A comprehensive description of the nonlinear measurement Z-scan technique follows this [36-38].

In chapter 3, the Z-scan results obtained from investigations on organic semiconductor is presented [29,36]. Here, Z-scan measurements on metal-doped Phthalocyanine (Pc) thin films and metal-free Phthalocyanine thin films are discussed in detail [39.40]. To be precise, this chapter deals with characterization and optimization of nonlinear optical coefficients in different phases of Phthalocyanine thin films. The impact of morphological and structural phase-change on high-order NLO properties in different phases of phthalocyanine (metal and metal-free) thin films are studied using the Z-scan method [36]. Furthermore, the CA Z-scan results revealed a strong fifth-order nonlinear refraction in as-prepared (α-phase) metal-free Pc thin-films. The intensity dependent fifth-order NLR is investigated and discriminated by the third-order NLO refractive-index. In subsequent sections of this chapter, I investigated the impact of the metal atom in the Pc ring and their effects on nonlinear properties [40]. This study revealed that the linear, as well as nonlinear characteristics of Phthalocyanines, depend on their phases due to the difference in their intramolecular arrangement. The ultrashort fiber laser based Z-scan experiment facilitated the study of both the saturable absorption (SA) and Excited-state-absorption (ESA) in Pc thin films.

Chapter 4 presents the results that I have obtained from the investigations on inorganic semiconducting sub-wavelength structures [29]. Here, the Z-scan measurements performed on Mn-doped ZnO nanorods is presented. To begin with, a discussion about the NLO properties of the bulk ZnO is presented. Thereafter, the NLR and NLA coefficients for different concentrations of Mn-doped ZnO rods which are determined from the Z-scan measurements have been presented. The results reveal that the increase in Mn-doping concentrations leads to SA phenomena in ZnO nanorods. This observation is explained by the concept of elongated lifetimes of the defect states.

As an important aspect of present thesis, the associated research has investigated the characteristics and utility of Optical Tamm plasmons (OTP) which are optical surface states existing at an interface between an optically periodic and continuous media [38]. In chapter 5, I present the investigations on ascertaining basic features of OTP [41]. To begin with, the fundamental aspects of light propagation in composite dielectric and metallic geometries are presented. Using the theoretical model, the excitation mechanism is explored and the dependence of propagation features on Metallo-dielectric configuration is presented. Finally, the ideas have been deployed to ascertain the possibility of devising an OTP based temperature and refractive-index sensor [42-43].

Finally, chapter 6 summarizes the results described in previous chapters and conclusions. Furthermore, this chapter briefly suggests the possible future.

Bibliography

[1] R. W. Boyd. *Nonlinear Optics*. Academic Press, second edition, 2003.

[2] D. N. Christodoulides, I. C. Khoo, G. J. Salamo, G. I. Stegeman, and E. W. Van Stryland, Nonlinear refraction and absorption: mechanisms and magnitudes, Adv. Opt. Photon. **2(1)**, 60–200 (2010).

[3] R. L. Sutherland. *Handbook of Nonlinear Optics*. Marcel Dekker, Inc., 1996.

[4] B. R. Masters. *Handbook of Biomedical Nonlinear Optical Microscopy*. Oxford University Press.

[5] J. A. Miragliotta. Analytical and device-related applications of nonlinear optics. *Johns Hopkins APL Technical Digest* **16(4),** 348-357 (1995).

[6] J. E. Midwinter, editor. *Photonics in Switching*. Quantum Electronics -Principles and Applications. Academic Press, 1993.

[7] G. de la Torre, P. Vazquez, F. Agullo-Lopez, T. Torres, Role of Structural Factors in the Nonlinear Optical Properties of Phthalocyanines and Related Compounds, Chem. Rev. 104, 3723-3750 (2004).

[8] H. S. Nalwa, S. Miyata, Nonlinear Optics of Organic Molecules and Polymers; CRC Press: New York, 1997.

[9] Y. Wang, N. Herron, W. Mahler, and A. Suna, Linear- and nonlinear-optical properties of semiconductor clusters, J. Opt. Soc. Am. B **6**, 808-813 (1989)

[10] C. Klingshirn, Non-linear optical properties of semiconductors, Semicond. Sci. Technol. 5, 457(1990).

[11] I. De Leon, Z. Shi, A. C. Liapis, and R. W. Boyd, Measurement of the complex nonlinear optical response of a surface plasmon-polariton, Opt. Lett. **39**, 2274-2277 (2014).

[12] R. W. Boyd, Z. Shi, and I. De Leon, The third-order nonlinear optical susceptibility of gold, Opt. Commun. **326**, 74–79 (2014).

[13] R. S. Bennink, Y.-K. Yoon, and R. W. Boyd. Accessing the optical nonlinearity of metals with metal-dielectric photonic bandgap structures, Optics Letters **24 (20),** 1416-1418, (1999).

[14] G. J. Lee, Y. P. Lee, S. G. Jung, C. K. Hwangbo, S. Kim, and K. Park, Linear and nonlinear optical properties of one-dimensional photonic crystals containing ZnO defects, J. Appl. Phys. **102**, 073528 (2007).

[15] N. N. Lepeshkin, A. Schweinsberg, G. Piredda, R. S. Bennink, and R. W. Boyd, Enhanced nonlinear optical response of one- dimensional metal-dielectric photonic crystals, Physical Review Letters **93(12),**123092(2004).

[16] M. Soljacic and J. D. Joannopoulos, Enhancement of nonlinear effects using

photonic crystals, *Nature Materials* **3**, 2 11-219 (2004).

[17] R. S. Bennink, Y.-K. Yoon, and R. W. Boyd. Accessing the optical nonlinearity of metals with metal-dielectric photonic bandgap structures, Optics Letters **24(20),** 1416-1418, (1999).

[18] G. L. Fischer, R. W. Boyd, R. J. Gehr, S. A. Jenekhe, J. A. Osaheni, J. E. Sipe, and L. A.Weller-Brophy, the Enhanced nonlinear optical response of composite materials, Phys. Rev. Lett. **74**, 1871-1874(1995).

[19] J. Butet, T. V. Raziman, K-Y Yang, G. D. Bernasconi, and Olivier J. F. Martin, Controlling the nonlinear optical properties of plasmonic nanoparticles with the phase of their linear response, Opt. Express **24**, 17138-17148 (2016)

[20] J. A. Reyes-Esqueda *et al.,* Anisotropic linear and nonlinear optical properties from anisotropy-controlled metallic nanocomposites, Opt. Express **17**, 12849-12868 (2009)

[21] D. Compton, L. Cornish and E. van der Lingen, The third order nonlinear optical properties of gold nanoparticles in glasses: I Gold Bull. **36**, 10–6(2003).

[22] S. M. O'Flaherty, S. V. Hold, M. J. Cook, T. Torres, Y. Chen, M. Hanack, W. J. Blau, Molecular Engineering of Peripherally and Axially Modified Phthalocyanines for Optical Limiting and Nonlinear Optics, Adv. Mater. **15**, 19-32 (2003).

[23] S. Heutz, S.M. Bayliss, R. L. Middleton, T. S. Jones, Polymorphism in Phthalocyanine Thin Films: Mechanism of the α→ β Transition, J. Phys. Chem. B **104**, 7124-7129 (2000).

[24] S. Yim, S. Heutz, T. S. Jones, Model for the α→ β1 Phase Transition in Phthalocyanine Thin Films, J. Appl. Phys. **91**, 3632-3636 (2002).

[25] B. Derkowska, M. Wojdyła, R. Czaplicki, W. Bała, B. Sahraoui, Influence of the central metal atom on the nonlinear optical properties of MPcs solutions and thin films, Optics Communications **274**, 206-212 (2007)

[26]   Y. Chen, M. Hanack, Y. Araki,   and O. Ito, Axially   modified   gallium phthalocyanines and naphthalocyanines for optical limiting Chem. Soc. Rev. **34(6)**, 517–529 (2005).

[27] M. Hanack, D. Dini, M. Barthei, S. Vagin, S. Conjugated Macrocycles as Active Materials in Nonlinear Optical Processes: Optical Limiting Effect with Phthalocyanines and Related Compounds, Chem. Rec. **2**, 129-148 (2002).

[28] A. Zawadzka, P. Plociennik, I. Czarnecka, J. Strzelecki, and Z. Lukasiak, The effects of annealing process influence on optical properties and the molecular orientation of selected organ metallic compounds thin films, Opt. Mater. **34**, 1686-1691 (2012).

[29] A. Singh, S. Kumar, R. Das, and P. K. Sahoo, Defect-assisted saturable absorption characteristics in Mn-doped ZnO nano-rods, RSC Adv. **5**, 88767 (2015).

[30] C. Torres-Torres, B. A. Can-Uc, R. Rangel-Rojo, L. Castañeda, R. Torres-Martínez, C. I. García-Gil, and A. V. Khomenko, Optical Kerr phase shift in a nanostructured nickel-doped zinc oxide thin solid film, Opt. Express **21**, 21357-21364 (2013).

[31] Kenji Imakita, Masahiko Ito, Minoru Fujii, and Shinji Hayashi, Nonlinear optical properties of Phosphorous-doped Si nanocrystals embedded in phosphosilicate glass thin films, Opt. Express **17**, 7368-7376 (2009).

[32] Y. Q. Li, C. C. Sung, R. Inguva, and C. M. Bowden, Nonlinear-optical properties of semiconductor composite materials, J. Opt. Soc. Am. B **6**, 814-817 (1989).

[33] G. Banfi, V. Degiorgio, and D. Ricard, Nonlinear optical properties of semiconductor nanocrystals, Adv. Phys. **47**, 447 (1998).

[34] P. Roussignol, D. M. Rioard, and C. Flytzanis, Nonlinear optical properties of commercial semiconductor-doped glasses, Appl. Phys. A 44, 285 (1987).

[35] Kwang Jin Lee, J. W. Wu, and Kihong Kim Enhanced nonlinear optical effects due to the excitation of optical Tamm plasmon polaritons in one-dimensional photonic crystal structures, Opt. Express **21**, 28817-28823 (2013).

[36] M. Sheik-Bahae, A. A. Said, T. H. Vei, D. J. Hagan, and E. W. Van Stryland, Sensitive measurement of optical nonlinearities using a single beam, IEEE J. Quantum Electron. **26**, 760–769 (1990).

[37] M. Sheik-Bahae and M. P. Hasselbeck, Third-order optical nonlinearities, in OSA Handbook of Optics, (McGraw-Hill2001), Vol. IV, Chap. 17.

[38] Y.V.G.S. Murti and C. Vijayan, Essentials of Nonlinear Optics, John Wiley, 2014. [39] K. V. Anil Kumar, S. Kumar, S. M. Dharmaprakash, and R. Das, Impact of $\alpha \rightarrow \beta$ Transition in the Ultrafast High-Order Nonlinear Optical Properties of Metal-Free Phthalocyanine Thin Films, J. Phys. Chem. C **120**, 6733−6740 (2016).

[40] S. Kumar, K. V. Anil Kumar, S. M. Dharmaprakash, and R. Das, Phase-dependent ultrafast third-order optical nonlinearities in metallophthalocyanine thin films, J. Appl. Phys. **120**, 123104 (2016).

[41] S. Kumar, R. Das, On the tunability of quality-factor for optical Tamm plasmon modes, Journal of Optics **19** (9), 095001(2017).

[42] S. Kumar, PS Maji, R. Das, Tamm-plasmon resonance based temperature sensor in a Ta2O5/SiO2 based distributed Bragg reflector, Sensors and Actuators A: Physical **260**, 10-15 (2017).

[43] S. Kumar, M. K. Shukla, P. S. Maji, R Das, Self-referenced refractive index sensing with hybrid-Tamm-plasmon-polariton modes in sub-wavelength analyte layers, Journal of Physics D: Applied Physics **50** (37), 375106(2017).

Chapter 2
Third Order Optical Nonlinearities: Mechanisms and Measurement Method

In this chapter, I present an overview of nonlinear optics (NLO), underlying mechanisms as well as the experimental techniques which have been rigorously deployed in the present thesis work. The first section of this chapter gives a brief introduction to the concept of NLO that results in the nonlinear optical phenomena like NLR and the concept of NLA. The second section of this chapter discussed the mechanisms or the origin of third-order susceptibility. In the third section, I present the detail description of the Z-scan experimental technique used to study the third-order susceptibility i.e. $\chi^{(3)}$. This is followed by features as well as factors contributing to the error in the measurement of NLR and NLA response.

2.1 Nonlinear Optics

Study of laser light-matter interaction changes the optical properties of a medium [1]. When any real physical system is overdriven, then it gives rise to change in its optical response which is expressed as nonlinear dependence polarisability on the electric field of an electromagnetic wave [2]. At low input power in an optical system, the optical response changes linearly with the electric field (E). However, at high input intensity, light-matter interaction leads to a rapid change optical response from any material [2]. A few mW of moderately focused laser light is intense enough to cause this change of the material optical properties. This change in the material properties gives rise to nonlinear optical-effects like self-focusing, NLA, harmonic generation and solitons etc [1]. In presence of laser light, this change in material optical properties is expressed through the polarization (P) of the optical medium [2].

Therefore, the polarization **P** of the material system does not vary linearly with the electric field (**E)** and contains contributions from higher power **E** as described by the Taylor series [1].

$$P=(\varepsilon_0\chi^{(1)}E+\varepsilon_0\chi^{(2)}E^2+\varepsilon_0\chi^{(3)}E^3+...) \qquad 2.1$$

where ε_0 is the permittivity of free space, $\chi^{(1)}$ is the first-order susceptibility and $\chi^{(2)}, \chi^{(3)}$ are the second and third-order susceptibility. $\chi^{(1)}$ describes the regime of linear optics. The real part of $\chi^{(1)}$ is associated with the linear refractive index (n_0) whereas imaginary part of $\chi^{(1)}$ is related to linear absorption (α_0) [1,2]. Second order susceptibility $\chi^{(2)}$ give rise to phenomena like second-harmonic generation (SHG), difference frequency generation (DFG) and optical parametric processes [1]. Third-order susceptibility i.e. $\chi^{(3)}$ cover a large area of NLO and is responsible for many phenomena like the intensity-dependent refractive index, NLA, four-wave mixing, third harmonic generation etc [1]. In this work, we are basically interested in phenomena giving rise to nonlinear refraction (NLR) and NLA. It is important to mention here that the Taylor series expression for the NLO properties expressed by the equation (2.1) is assumed to converge quickly under the perturbative approach [3]. Also as the equation assumes the response is instantaneous, therefore the equation (2.1) is true and valid under the conditions of bound-electronic nonlinearity [1,3]. This is mainly because of the fact that, the NLO response is fast under bound-electronic nonlinearity condition. Since the magnitude of linear susceptibility $\chi^{(1)}$ is very large as compared to the $\chi^{(2)}$ and $\chi^{(3)}$ susceptibility, therefore their response can be observed only at high input intensity or at long laser-matter interaction length [1].

2.1.1 Third-order Nonlinear Properties

Third-order nonlinear optical properties stem from the third term ($\chi^{(3)}E^3$) of the

equation 2.1. This term implies that the frequency mixing by the interaction of three fields leads to the generation of fourth field [2]. Therefore $\chi^{(3)}$ is a 4 photon process. In this section, nonlinear optical properties like intensity-dependent refractive index and NLA associated with $\chi^{(3)}$ are analyzed and discussed. $\chi^{(3)}$ is complex in nature and is the tensor of rank 4. The real and imaginary parts of $\chi^{(3)}$ are associated with NLR and NLA.

2.1.2 Nonlinear Refractive Index

Generally, the nonlinear refractive index is referred to the spatial variation in refractive index of material due to the presence of intense laser field [1,2]. This change in refractive index is caused by several mechanisms. Out of these mechanisms, one is optical Kerr effect [1,4]. Optical Kerr effect is related to the electronic contribution to the nonlinear refractive index change i.e. third term contribution of equation (2.1). In particular

$$P^{NL}(\omega) = 3\varepsilon_0 \chi^{(3)} \left|E_0\right|^2 E(\omega) \qquad 2.2$$

For a monochromatic field of the form

$$E(t) = E_0\, e^{-i\omega t} + c.c. \qquad 2.3$$

Therefore, the total polarization of the optical medium at frequency ω can be written as

$$P^{tot}(\omega) = \varepsilon_0 \left(\chi^{(1)} + 3\chi^{(3)} \left|E_0\right|^2 \right) E(\omega) \qquad 2.4$$

$$P^{tot}(\omega) = \varepsilon_0 \chi_{eff} E(\omega) \qquad 2.5$$

where χ_{eff} is the effective susceptibility and is described by the expression

$$\chi_{eff} = \chi^{(1)} + 3\chi^{(3)} \left|E_0\right|^2 \qquad 2.6$$

As the linear refractive index (n_0) is associated with the $\chi^{(1)}$, therefore the concept of effective susceptibility leads to the idea of effective refractive index described by the following equation[1].

$$n^2 = 1 + \chi_{eff} \qquad \qquad 2.7$$

$$\chi_{eff} = \chi^{(1)} + 3\chi^{(3)} |E_0|^2 \qquad \qquad 2.8$$

Equation (2.8) shows that refractive index is irradiance dependent.

$$n = n_0 \sqrt{1 + \frac{3}{n_0^2} \chi^{(3)} |E_0|^2} \qquad \qquad 2.9$$

As $\dfrac{\chi^3 E_0^2}{n_0^2} < 1$ therefore the equation (2.9) can be expressed as

$$n = n_0 \left(1 + \frac{3\chi^3 E_0^2}{2n_0^2} \right) \qquad \qquad 2.10$$

$$n \approx n_0 + \frac{3\chi^3 E_0^2}{2n_0} \qquad \qquad 2.11$$

Now the intensity in terms of the electric field is expressed by the relation

$$I = 2\varepsilon_0 c n_0 |E_0|^2 \qquad \qquad 2.12$$

Therefore equation 2.11 can be written as

$$n = n_0 + n_2 I \qquad \qquad 2.13$$

where $n_2 = \dfrac{3\chi^3}{4n_0^2 c\varepsilon_0}$ and is called the nonlinear refractive index. In general equation

2.13 can be rewritten as

$$n = n_0 + n_2 I + n_4 I^2 \qquad \qquad 2.14$$

where n_2 and n_4 are the contributions from the real part of $\chi^{(3)}$ and $\chi^{(5)}$ respectively. Equation 2.14 shows that refractive index of a medium is irradiance dependent. This

14

change in refractive index leads to few effects such as self-defocusing, self-focusing, four-wave mixing, self-phase modulation, photorefractivity, phase conjugation, spatial solitons, optical bistability, nonlinear waveguides, and interfaces etc. [1,5-7].

2.1.3 Nonlinear Absorption (NLA)

Unlike linear absorption process where a material system absorbs a photon and is excited to a higher energy state, NLA involves simultaneous absorption of two or more photons and excitations to a higher energy state [1]. Therefore we can say that NLA is an absorption phenomenon that can occur in the presence of strong electromagnetic fields. It is an intensity dependent phenomenon and is expected to be maximum when the sample is at the focal point of a laser beam. NLA is associated with the imaginary part of $\chi^{(3)}$. The phenomenon of NLA requires an energy resonance and is observable only at high intensity. NLA is associated with the change in the amplitude of pump beam on propagation through a medium with a non-zero value of imaginary part of $\chi^{(3)}$ [2]. In order to determine NLA coefficients, the total power of a focused laser beam transmitted by the sample is measured by a photodetector. The phenomena of NLA could occur due to a variety of processes like multiphoton absorption (MPA), reverse Saturable absorption (RSA) and SA. The aforementioned NLA mechanism processes also depend on laser wavelength, laser pulse duration, and the pump intensities. It is important to note that the magnitude of the imaginary part of $\chi^{(3)}$ for a material determines the actual value of intensity necessary for NLA to be observed. In other words, the probability that an optical system will show NLA when a light of given wavelength is launched on it depends on the intrinsic properties of materials [8]. The process of simultaneous absorption of two photons for excitation from the ground state to excited state is referred to as two-photon absorption (TPA) as

shown in Fig 2.1. Fig 2.1 illustrates the phenomena of one photon absorption (1PA) as well as TPA. For example, if E_1 *and* E_2 are the two photon energies, then for TPA process to occur $E_1 + E_2$ must be greater than the difference in energy between the ground and excited state. In other words, $E_1 + E_2$ must be in resonance with one of the electronic states of the system. As a result of TPA, there is a decrease in the pump intensity and system is pumped t to the excited state (state "e" in Fig 2.1) from the ground state (state "g" as shown in Fig. 2.1). TPA was first theoretically described by Maria Goppert-Mayer in 1931 and in 1961 Kaiser and Garrett observed it experimentally [1, 8,11, 12]. However, when more than two-photon is absorbed to make a transition from ground to the excited state, the process is referred to as multi-photon absorption (MPA) [10].
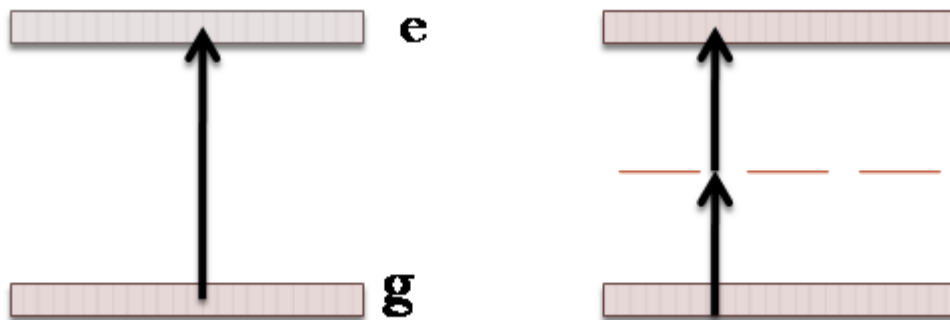
Fig 2.1 Schematic diagram showing one photon absorption and TPA. "g" is the ground state and "e" is the excited state.

With the advances in science and technology, a number of experimental techniques have been developed to study the NLA spectra of the optical system as well as to determine TPA or MPA absorption cross-section. The methods are classified into two categories:

1. **Direct Methods**

2. **Indirect Methods**

In the direct methods, optical power loss in the pump beam is measured. Therefore, in the direct method, the change in intensity of the pump beam is measured which is an extension of linear absorption measurement method. Nonlinear transmission (NLT) and Z-scan technique are the examples of direct measurements of NLA methods. In NLT method, the sample is placed in the path of a focussed Gaussian laser beam and laser power is measured before and after the sample by varying the input power. In the Z-scan method, the transmittance is measured by moving the sample along the direction of the laser beam. The Z-scan method is used for the NLO study in this thesis work and will be discussed in detail in the later part of this chapter. In indirect methods, the effects of TPA or MPA like TPA induced fluorescence, phosphorescence is monitored. Also, effects like temperature change in the materials due to NLA are monitored. Due to the simplicity and the fact that it can be applied to all kinds of materials like solid and liquid, direct method is mainly utilized for NLA coefficients measurements.

It is worthwhile to note that the nonlinear optical phenomenon has important implications in the field of spectroscopy.

- ❖ TPA and MPA have been deployed as a nonlinear spectroscopic technique for probing molecular properties like two or three photon resonance higher active excited state which are not accessible due to selection rules [1]

- ❖ TPA microscopy has also been utilized to remove the background in the imaging process in the highly scattering medium [1].

- ❖ Two-photon fluorescence imaging [8]

- ❖ Laser-induced breakdown spectroscopy (LIBS).

- ❖ 3D microfabrication [8]

❖ Optical limiting [1,8]

❖ Optical data storage [8,9]

❖ For a permanent change of materials via MPA or multiphoton ionization [9].

However, NLA phenomena like TPA and MPA also leads to losses in an optical system and hence, this limits the uses and effects of devices based on the NLO.

2.2 Physical Mechanisms behind Nonlinear Refractive Index

There are number of physical processes which are responsible for the change in refractive index at high intensity. We describe some of the important mechanism in this section briefly. It is important to mention here that not all the mechanisms are present in all the materials exhibiting optical nonlinearity. Most of the mechanisms depend on the type of materials probed [4]. Here, we discuss the physics of these mechanisms and provide the typical values of refractive index and response time [1, 4,15]. The different physical processes that contribute to third-order nonlinear susceptibility are

- Electronic Polarization

- Molecular Orientation

- Photorefractive Effects

- Electrostriction

- Thermal Nonlinearities

Electronic Polarization

It is a well-known fact that when we apply an electric field to an atom or molecules, it distorts the electron cloud of the atoms or molecules. The distortion of the electron

cloud produces a net dipole moment which is linearly proportional to the applied field. However, with laser light, the net dipole moment has a significant contribution from the higher-order electric field. Although its magnitude is small it turns prominent at higher values. In case of electronic polarization, the change in refractive index is local and the response is very fast $\approx 10^{-15}$ s [1]. The response is appreciably fast due to the involvement of virtual transitions. As electron distortion is easy in large size macromolecules essentially due to the wide distribution of electrons and decrease in binding energy, we expect large nonlinear contributions from macromolecules.

Molecular Orientation

This mechanism is responsible for large variation in the nonlinear refractive index in anisotropic molecules. Linear molecules of liquids and liquid crystals mainly exhibit molecular orientation that contributes to n_2. This contribution is due to the tendency of a molecule to reorient itself along the polarization axis of the applied field. Therefore, the orientation of molecules in presence of strong field leads to an induced dipole. Hence, the molecule experiences a torque caused by the electric field and induced dipole interaction. Due to this torque experienced by the molecules, it tries to reorient itself parallel to the field [1,4]. The net effect is the change in polarizability which manifests in intensity dependent refractive index. Response time for refractive index change due to molecular orientation is $\approx 10^{-12}$ s [1].

Photorefractive Effects

This effect is due to absorption in the maedium [1]. The absorption leads to the redistribution of electrons and holes. Due to the spatial variation of laser light and distribution of electrons and holes, the observed change in the refractive index is local. This nonlocality in index change is the cause for a number of effects like two-beam

coupling and beam fanning [4]. The contribution of photorefractive effects to the changes in refractive index is appreciably large and they play a dominant role in case of semiconductors. Also, it is important to mention that the contribution of photorefractive effects is intensity independent.

Electrostriction

Electrostriction is the property of a dielectric in which an application of an external electric field in the dielectric tends to deform or change its shape [1,15]. However, on changing the direction of the electric field, it does not change or reverse the deformation. The deformation in such dielectric materials is due to the internal forces produced by the non-uniform electric field. The value of nonlinear refractive index change due to electrostriction is $\approx 10^{-14} \, cm^2/W$ and response time is $10^{-9} \, s$ [1,4].

Thermal Nonlinearities

Thermal contribution to nonlinear refractive index comes from the absorption. Absorption leads to local heating and hence, there is a temperature gradient which in turns changes the density of a medium. This change in local density modifies the refractive index which could be attributed to thermal effects. It has been observed that the refractive index (n) monotonically decreases for fluids as a function of temperature. However, for solid samples, change in refractive index could exhibit an increasing or decreasing trend with the increasing temperature. The response time for thermal contribution is $\approx 10^{-3} \, s$ [1]. Therefore, thermal contribution leads to strong nonlinear response [4].

2.3 Nonlinear Measurement: Z-Scan Method

There are quite a few numbers of experimental methods for nonlinear optical characterization of the materials. Some of the experimental technique includes four-

wave mixing (FWM), time-resolved pump-probe technique, interferometric technique, Z-scan technique, beam-deflection [3,6,16-18]. The advantage of one over other depends on the mechanism of the nonlinearity as well as the physical quantity that we are aiming to determine. For example, with four-wave mixing (FWM) technique, we characterize the different components of $\chi^{(3)}$ a tensor. However, this method cannot be employed for determining the sign of $\chi^{(3)}$ [6]. Additionally, in FWM method, both NLR and NLA contribute to the mixing process and consequently, the contributions to real and imaginary components of $\chi^{(3)}$ cannot be determined simultaneously. On the other hand, the interferometric method assists in circumventing this issue [6]. However, the implementation of the interferometric technique is a bit complex as it requires precise beam alignment and stable environment. A very simple and sensitive method for investigating the third-order nonlinearities is Z-scan [18,19]. There are various forms of Z-scan methods like transmission Z-scan, reflection Z-scan,
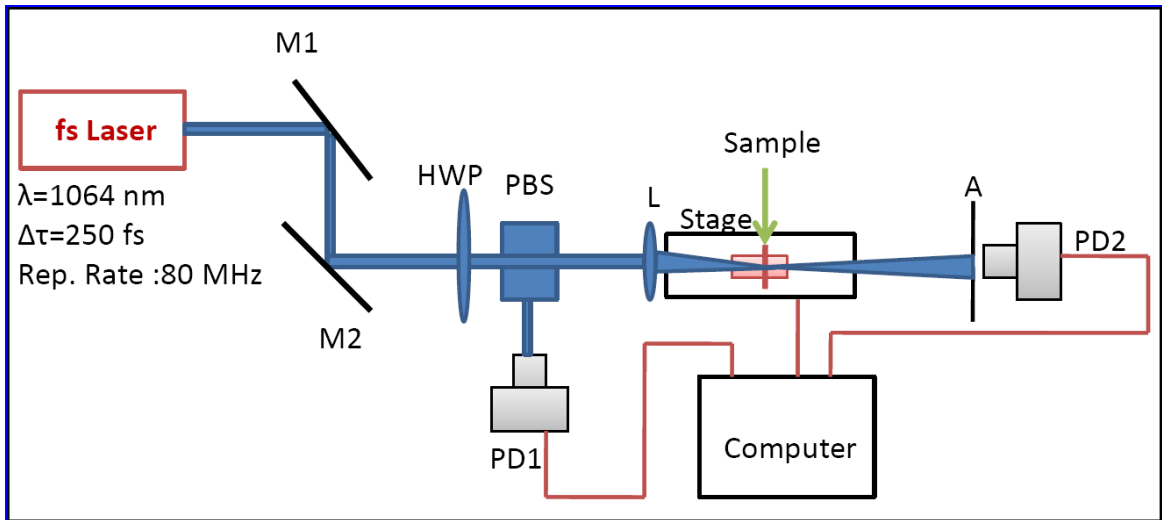
Fig 2.2 Z-scan method schematic. HWP: Half-wave plate, PBS: Polarizing beam-splitter, Stage: Translation stage (10 cm travel), A: Aperture; M1, M2: Mirror, PD1, and PD2: Large Area Detector, L: Lens (f =100 mm).

Eclipsing Z-scan, time-resolved Z-scan [19-23]. Here we give a comprehensive description of the transmission Z-scan method used to determine the optical nonlinearity of organic semiconductors in this work. Using this technique, real and imaginary contributions to $\chi^{(3)}$ could be ascertained [18]. Additionally, NLR and NLA sign could be determined with the conventional Z-scan method. In the present thesis, the Z-scan method is employed for studying the NLO properties in Mn-doped ZnO nanorods, phthalocyanine, and metal phthalocyanine thin films. A schematic of the transmission Z scan is illustrated in Fig 2.2.

There are basically two forms of Z-scan.

1. **Closed-aperture (CA)**

2. **Open Aperture (OA)**

In the CA Z-scan method, transmittance through an aperture (as shown in Fig.2.2) is monitored at a far distance as the sample is translated across the focal plane. In OA method, we remove the aperture and measure the transmission of the sample as it is translated with respect to the focus. In OA measurements, it is to be ensured that the optical detector sensitive area is significantly large so as to capture the total energy or power transmitted through the sample. Therefore, in the OA Z-scan transmission method, only nonlinear absorption (NLA) is expected to cause variation in transmission as the sample is translated. When the sample is far from focus, the irradiance is low and therefore, no nonlinear effects are present. This leads to constant transmission. When sample approaches the focal point, the intensity increases due to small spot size, thus it will induce nonlinear optical effects and hence, a change in transmission.

2.3.1 Closed-aperture Z-scan Method

The CA Z-scan method is illustrated in Fig. 2.3. As observed from Fig.2.3, the transmittance of the sample at the far field is monitored through an aperture. An aperture in front of the photodetector is placed so that only a fraction of light passes through it and enters the
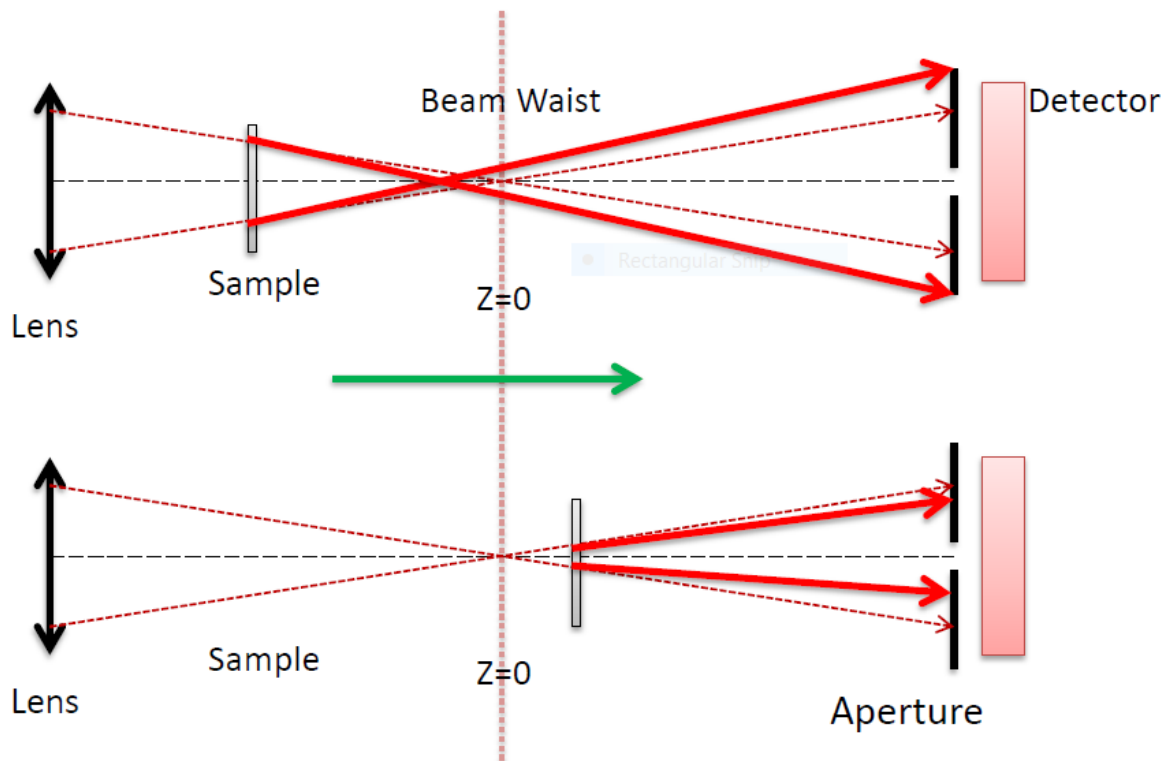
Fig 2.3 CA Z-scan Schematic

photodetector. By far field, we mean that the distance of the aperture from the focal plane is very large as compared to the Rayleigh length [24]. Fig 2.4 shows the schematic of a CA Z-scan signal for the positive and negative n_2 values. When a sample has a positive nonlinear refractive index, it will cause self-focusing effect called optical Kerr effect. When the sample is near the focal plane, the self-focusing phenomena cause the laser light to focus before the actual focal point and hence, it tends to diverge more near the detector plane. Due to this divergence and presence of an aperture, there is a decrease in the detector power and hence creating a "valley".

When the sample is moved to the post-focal point, the beam collimated due to self-focusing. Collimation of beams in front of the aperture causes more light to enter the detector and therefore, we observe a "peak". Again as the sample reaches far-field, the irradiance decreases and hence, no NLO effects are observed. So, a sample with positive n_2 will yield a "valley" followed by a "peak" as the sample is translated through the focus of the beam. Similarly, a sample with negative n_2 exhibits a peak in the pre-focal point and a
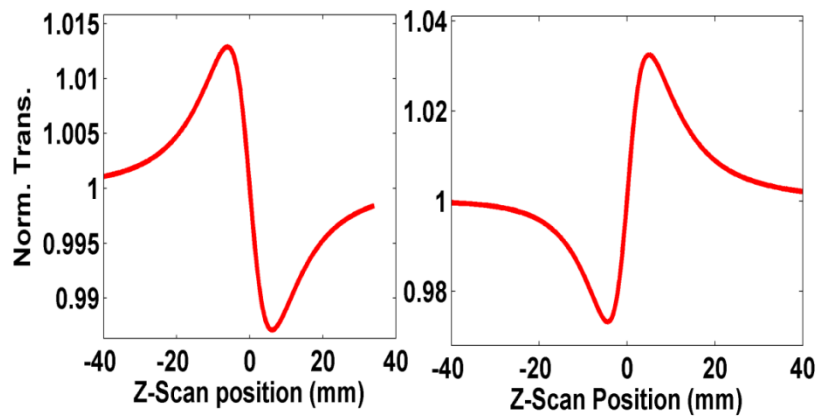
Fig 2.4 Closed-aperture Characteristic curve for positive and negative nonlinear refractive index

valley in the post-focal plane. The CA Z-scan gives us the phase change from which we can determine the nonlinear refractive index.

The valley-peak or peak-valley signature is symmetric with respect to the focal plane in absence of NLA. However, if there is NLA in the samples, then the CA Z-scan transmittance curves are asymmetric about the focus. In case phase shift due to NLA is large, then also CA Z-scan transmittance curves become asymmetric about the focus. Depending upon the NLA mechanism, the peak or the valley would be enhanced and suppressed. SA tends to enhance the peak and suppress the valley. However, TPA and MPA enhance the valley and suppress the peak. In order to

remove the contribution of NLA to NLR, the CA and OA data are taken simultaneously using a 50:50 beam splitter and the CA Z- transmission data are divided by the OA Z scan transmission data. This result in a typical CA Z-scan curve, similar to that would be observed in absence of NLA.

For a small phase change in a nonlinear medium, ($|\Delta\varphi|<<1$), as well as samples having TPA, the simple theoretical equation can be used to obtain the NLR coefficients.

$$T(z, s \approx 0) = 1 - \frac{4\Delta\Phi_0 x}{(x^2+9)(x^2+1)} - \frac{2(x^2+3)\Delta\Psi_0}{(x^2+1)(x^2+9)} \qquad 2.16$$

where $x = z/z_0$, $\Phi_0 = kn_2 I_0 L_{eff}$ is the phase change due to nonlinear refraction and $\Delta\psi_0 = \beta I_0 L_{eff}/2$ [25].

With higher order contributions from φ_0 and ψ_0, the expression for CA becomes

$$T(x, s \approx 0) = 1 + \frac{1}{\sqrt{2}} \frac{4x\Delta\Phi_0 - (x^2+3)q_0}{(x^2+1)(x^2+9)} + \frac{4\Phi_0^2(3x^2-5) + q_0^2(x^4+17x^2+40) - 8\Phi_0 q_0 x(x^2+9)}{(x^2+1)^2(x^2+9)(x^2+25)} 2.17$$

In presence of higher order ($\chi^{(3)}$, $\chi^{(5)}$) contributions to the change in refractive index, the experimental data is fitted using the relation

$$T(z, \varphi_{01}, \varphi_{02}) = 1 + \frac{4x\varphi_{01}}{(x^2+1)(x^2+9)} + \frac{8x\varphi_{02}}{(x^2+1)^2(x^2+25)} \qquad 2.18$$

Here $x = z/z_0$, $\varphi_{01} = kn_2 I_0 L_{eff1}$, $\varphi_{02} = kn_4 I_0 L_{eff2}$ are the phase changes due to $\chi^{(3)}$ and $\chi^{(5)}$, $L_{eff1} = (1-\exp(-\alpha_0 L))/\alpha_0$ and $L_{eff2} = (1 - \exp(-2\alpha_0 L))/2\alpha_0$ is the effective sample length [26].

2.3.2 Open-Aperture Z-scan Method

The OA Z-scan method is illustrated in Fig 2.5. The Fig. 2.5, represent the effect of a sample with negative nonlinear absorption. The dashed lines represent the propagation

of a focused laser beam in the absence of a sample and the solid red lines represent the propagation of the focused laser beam in presence of sample with negative nonlinear absorption. The power transmitted through the sample decreases or increases depending upon whether the sample exhibit two-photon absorption on saturable absorption.

As the name suggests aperture is removed and all the transmitted power is captured in a far field detector as the sample is translated. Unlike CA which is sensitive to both NLA and NLR, OA is sensitive to only NLA and hence contribute to the variation in transmission.
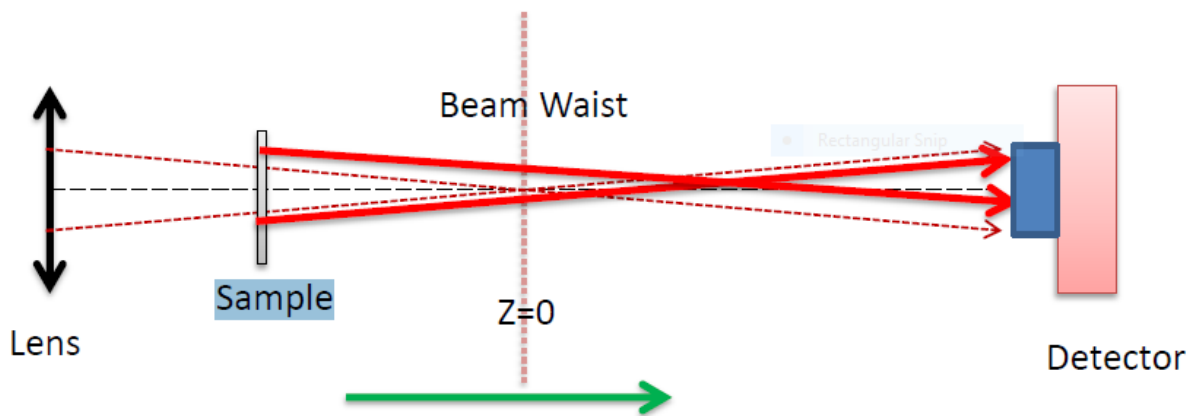
Fig. 2.5 A schematic representation of OA Z-scan method

A few representative examples of OA Z-scan curves are shown in Fig. 2.6. As irradiance is high at the focal plane, therefore, NLA will be large at the focus. Consequently, a dip in the OA transmission is observed at the focus when the sample is translated. If the mechanism responsible for NLA is SA instead of MPA, then a peak will be created symmetrically around the focus. The OA signal is fitted using the relation given by
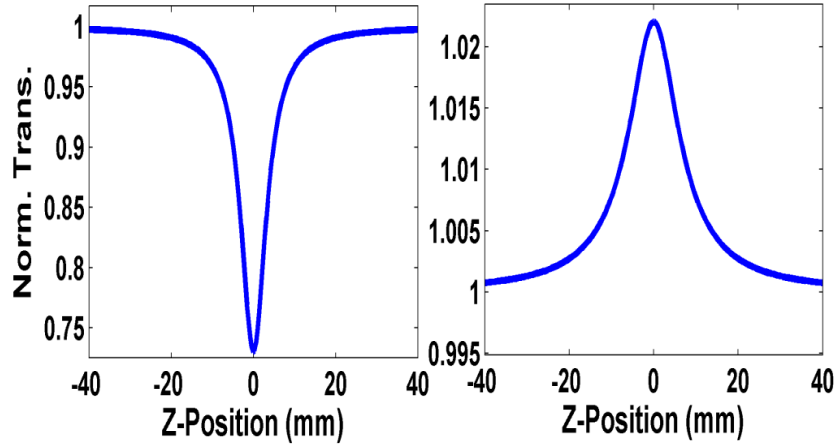
Fig 2.6 Schematic of OA Z-scan signal

Sheik-Bahae *et. al.*

$$T(z, S=1) = 1 - \frac{\beta_{eff} I_0 L_{eff}}{2^{3/2}(1+x^2)}$$

2.19

β_{eff} is the effective nonlinear absorption coefficient, I_0 is intensity at the focal plane, L_{eff} is the effective length of the sample thickness [18]. If there is the contribution of SA as well as MPA in the samples, then the Z–scan transmittance is fitted using the following relation for determining the NLA coefficients.

$$T(z) = \left[1 - \frac{\alpha_0 L I_s}{I_s + I_0/(1+x^2)} - \frac{\beta_{eff} I_0 L}{1+x^2} \right] / \left(1 - \alpha_0 L\right)$$

2.20

I_s is the saturation intensity [27].

2.3.3 Factors Contributing to Experimental Errors

In order to use the above-mentioned theoretical equations to fit the Z-scan transmittance, we have to measure a number of parameters accurately. Accurate measurements of parameters such as laser pulse-width, beam waist, aperture

27

transmission, linear absorption coefficients of the sample, sample thickness, pulse energy, wavelength of the laser and uncertainties in the spatial and temporal variation of the beam are essential for accurately determining the nonlinear coefficients [28]. If not accurately measured, the above-mentioned parameters give rise to the experimental errors which need to be accounted for.

2.3.4 Merits and demerits of Z-scan Method

Following are the merits of the Z-scan method

1. Simple, sensitive and single-beam method.

2. NLA and NLR magnitude, as well as their sign, can be determined.

3. The beam alignment is fairly straightforward, unlike interferometric technique.

4. Higher contribution to NLR and NLA can also be determined.

Demerits of Z-scan Method

1. It cannot differentiate between different mechanisms which are responsible for a nonlinear optical response.

2. Response time cannot be determined by transmission Z scan method. However two-color Z-scan and times resolved Z-scan allows separation of nonlinearities having a different response time.

3. It requires a very good quality Gaussian laser beam emitting in TEM_{00} mode.

4. Accurate determination of a wide variety of parameters for ascertaining n_2.

5. Solid samples must have a good optical surface for reducing unwanted scattering and maximizing transmission.

6. Background subtraction: In order to remove the effect of sample inhomogeneities and substrate effects on nonlinear measurements, it is

important to perform two Z-scans, one at high and another at very low irradiance level. The Z-scan data at low irradiance is then subtracted from the Z-scan data at high irradiance. Following two conditions must be mate for effective background subtraction. First the sample positions to be reproducible and secondly the z-scan data must be normalized before subtraction.

2.4 Summary

In this chapter, I have presented the basic features associated with nonlinear optics, its origin and the experimental technique (Z-scan) which is employed for investigating the nonlinear optical properties. The different physical process causing the change in nonlinear optical properties is discussed briefly. The mathematical expressions for evaluating the intensity-dependent refractive index are derived. A detailed description of the Z-scan is also presented in this chapter. The analytical expressions which have been used for determining NLR and NLA coefficients are stated and discussed briefly. Finally, the chapter concludes with a discussion on the advantages and disadvantages of the Z-scan technique.

Bibliography

[1] R. W. Boyd, Nonlinear Optics, 2nd ed. (Academic Press, Boston, 2003).

[2] M. Sheik-Bahae and E. W. Van Stryland, optical nonlinearities in the transparency region of bulk semiconductors, in Nonlinear Optics in Semiconductors I, E. Garmire and A. Kost, Eds., Semiconductors and Semimetals, vol. 58 (Academic, Boston, 1999).

[3] M. Sheik-Bahae and M. P. Hasselbeck, "Third-order optical nonlinearities," in OSA Handbook of Optics, (McGraw-Hill2001), Vol. IV, Chap. 17.

[4] D. N. Christodoulides, I. C. Khoo, G. J. Salamo, G. I. Stegeman, and E. W. Van Stryland, Nonlinear refraction and absorption: mechanisms and magnitudes, Adv. Opt. Photon. **2(1)**, 60-200 (2010).

[5] R. Boyd, S. Lukishova, Y. R. Shen, and A. Campillo, Self-focusing: Past and Present (Springer, Berlin, 2009), p. 157.

[6] R. L. Sutherland, *Handbook of Nonlinear Optics* (Marcel Dekker, New York, 1996)

[7] T. Schneider, Self- and Cross-Phase Modulation. In: Nonlinear Optics in Telecommunications. Advanced Texts in Physics. Springer, Berlin, Heidelberg (2004).

[8] M. Rumi and J. W. Perry, Two-photon absorption: an overview of measurements and principles, Adv. Opt. Photon. **2**, 451-518 (2010).

[9] E. Garmire, Nonlinear optics in daily life, Opt. Express **21**, 30532-30544 (2013).

[10] G. S. He, L.-S. Tan, Q. Zheng, and P. N. Prasad, Multiphoton absorbing materials: molecular designs, characterizations, and applications, Chemical Review **108**,1245-1330(2008).

[11] G. Mayer and M. Uber, *Elementarakte Mit Zwei Quantensprüngen,* Ann. Phys. **401**, 273-294 (1931).

[12] W. Kaiser, and C.G.B. Garrett, Two-Photon Excitation in CaF2: Eu2+, Phys. Rev. Lett. **7**(6), 229-231(1961).

[13] Y-P Chan, J-H Lin, C-C Hsu, and W-F Hsieh, Near-resonant high order nonlinear absorption of ZnO thin films, Opt. Express **16**, 19900-19908 (2008).

[14] R. A. Ganeev, Nonlinear refraction and nonlinear absorption of various media, J. Opt. Pure Appl. Opt. **7**, 717 (2005).

[15] Y.V.G.S. Murti and C. Vijayan, Essentials of Nonlinear Optics, John Wiley, 2014.

[16] W. B. Jackson, N. M. Amer, A. C. Boccara, and D. Fournier, Photothermal deflection spectroscopy, and detection, Appl. Opt. **20**, 1333-1344 (1981)

[17] A. C. Boccara, D. Fournier, Warren Jackson, and Nabil M. Amer, Sensitive photothermal deflection technique for measuring absorption in optically thin media, Opt. Lett. **5**, 377-379 (1980).

[18] M. Sheik-Bahae, A. A. Said, T.-H. Wei, D. J. Hagan and E. W. Van Stryland, Sensitive measurement of optical nonlinearities using a single beam, IEEE J. Quantum Electron. **26**, 760–769 (1990).

[19] M. Sheik-Bahae, A. A. Said, and E. W. Van Stryland, High-sensitivity, single-beam n_2 measurements, Opt. Lett. **14**, 955-957 (1989)

[20] J. Wang, M. Sheik-Bahae, A. A. Said, D. J. Hagan, and E. W. Van Stryland, Time-resolved Z-scan measurements of optical nonlinearities, J. Opt. Soc. Am. B **11**, 1009-1017 (1994)

[21] T. Xia, D. J. Hagan, M. Sheik-Bahae, and E. W. Van Stryland, Eclipsing Z-scan measurement of $\lambda/10^4$ wave-front distortion, Opt. Lett. **19**, 317-319 (1994).

[22] D. V. Petrov, A. S. L. Gomes, and Cid B. de Araujo, Reflection *Z*-scan technique for measurements of optical properties of surfaces, Appl. Phys. Lett. **65**, 1067 (1994).

[23] M. Martinelli, S. Bian, J. R. Leite, and R. J. Horowicz, Sensitivity-enhanced reflection Z-scan by oblique incidence of a polarized beam, Appl. Phys. Lett. **72**, 1427 (1998).

[24] L. C. Andrews, R. L. Phillips, Laser Beam Propagation through Random Media (SPIE Press, Bellingham, Washington, 1998).

[25] R. A. Ganeev, M. Suzuki, M. Baba, M. Ichihara, and H. Kuroda, Low- and high-order nonlinear optical properties of Au, Pt, Pd, and Ru nanoparticles, J. Appl. Phys. **103**, 063102 (2008).

[26] B.Gu, J. Chen, Y. Fan, J. Ding, H. T. Wang, Theory of Gaussian Beam Z-scan With Simultaneous Third- and Fifth-Order Nonlinear Refraction Based on a Gaussian Decomposition Method, J. Opt. Soc. Am. B **22**, 2651-2659 (2005).

[27] H. Zhang, S. B. Lu, J. Zheng, J. Du, S. C. Wen, D. Y. Tang, and K. P. Loh, Molybdenum Disulfide (MoS_2) as a Broadband Saturable Absorber for Ultra-Fast Photonics, Opt. Express **22**, 7249-7260 (2014).

[28] G. Piredda. Materials for Nonlinear Optics: Semicontinuous Gold Films and Fast Saturable Absorbers Ph.D. thesis, University of Rochester, Rochester, New York.

Chapter 3
Nonlinear Optical Properties of Organic Semiconductors

In this chapter, we present the impact of morphological phase transformation in organic semiconductors (metal-free phthalocyanine and Metal phthalocyanines) thin films on their nonlinear optical (NLO) characteristics. The NLO characterization has been carried out by a Z-scan method using a 1064 nm femtosecond pulse laser. The chapter is organized as follows: A brief description of physical properties of Phthalocyanine (Pc) is discussed in section 3.1 which dictates the motivation for this work. This is followed by the description of the Pc samples in section 3.2. The experimental technique employed to determine the NLO properties is described in section 3.3. In section 3.4 and 3.5, we present the NLO characterization of the thermally prepared metal-free phthalocyanine (Pc) and Metalophthalocyanine (MPc) thin films on glass substrate. The NLO characteristics are depicted by saturable absorption (I_s), the effective two-photon absorption coefficient (β_{eff}) and nonlinear refractive indices. The NLO properties are determined at an operating wavelength of 1064 nm where the optical transmission is $\geq 90\%$. Our study shows a large value for fifth-order nonlinearity in as prepared metal-free Pc films as compared to annealed and stable phases. These Pc films also show phase-dependent nonlinear absorption (NLA). The variations in the NLO characteristics in different phases of Pc and MPc are discussed in terms of their structural arrangements.

3.1 Introduction

Over the past few decades, NLO properties of organic semiconductors have been investigated for a wide range of applications like electronic, optoelectronic and

photonics. This is due to their large NLO properties [1, 2]. Over the past two decades, NLO properties of various conjugated polymers, molecular solids, organic and organo-metallic composites and compounds have been the subject of experimental investigations [3,4]. In this regard, phthalocyanine (Pc), Metalophthalocyanine and related compounds hold a considerable promise for the development of many nonlinear optical devices because of their large third-order nonlinearity, fast response time, unique electronic absorption characteristics, high thermal stability and environmental stability [5]. The strong and large NLO response originates from the highly delocalized aromatic 18 π-electron system of Phthalocyanines [5]. They are highly stable and have been extensively investigated as being among the most promising NLO materials due to their architectural flexibility. Axial and peripheral substitutions in Pc and MPc impact its linear and NLO properties [6]. Also, 70 different elements can be inserted into the Pc ring cavity [6,7]. Such modifications give rise to different phthalocyanine analogs and favorably affect their linear as well as NLO properties.

Another useful feature of these macro compounds is their ability to exist in different morphological phases. As demonstrated by Heutz *et al.* Pc predominantly exists in different phases [8]. Mainly they are found in amorphous, α, β and γ phases [7-9]. The structural configurations or the morphological phases of thin-films essentially depend on techniques employed to prepare them, substrate, temperature, and annealing [8,9]. Based on the above-mentioned conditions, investigations of NLO properties in organic thin films have its own importance in varying and controlling its NLO properties. In this regard, T. Ning *et al.* have demonstrated that CaCu3Ti4O12 thin films on different substrates exhibit different NLO response [10]. In another study,

H.M. Zeyada *et al*. have shown that pristine and annealed variant of the α-PbO$_2$ thin film has different values of NLO constants [11]. In theoretical investigations carried out by R. Kishi *et al,* it has been said that from the perspective of NLO applications organic semiconductors in thin films is of prime importance [12]. Investigation of femtosecond laser irradiation carried out by Rafique *et al*. shows that structural changes in thin films strongly influence its NLA properties [13]. Also, there are various studies that show a change in MPC structural, linear and NLO properties due to variation in phase, and metal atom [14-22]. However, the impact of metal atom and phase change on NLO properties in Pc and Metalophthalocyanine (MPc) thin films by the Z-scan technique is yet to be carried out. Alkyl phthalocyanine in solutions shows large NLA with nanosecond pulse laser [18]. Another study reveals that Pc films exhibit strong NLO properties with picoseconds laser pulse [23]. C. Nitschke *et al*. have demonstrated the effect of quantum confinement in Zinc Phthalocyanine (ZnPc) nanoparticles [17]. Anil Kumar *et. al.* investigations reveal strong wavelength-dependent NLO properties in Copper and Zinc Phthalocyanine [24, 25]. Mathews *et. al.* investigated the optical limiting characteristics of Pc in solutions and thin film. The study was aimed at understanding the impact of the continuous-wave laser on NLO properties and to determine the influence of thermal effects [26]. A couple of studies demonstrate the dependence of the NLO properties in Pc films on their phases. Phase dependence results from the variation in dipole moment of the structure [27,28]. Nalwa *et al.* studies of NLO properties in TiOPc reveal that $\chi^{(3)}$ for the as-prepared film was 5-times larger as compared to annealed or stable phase [29]. Another researcher demonstrated that thermal phase change increases the $\chi^{(3)}$ by a factor of 2-5 times in VOPc (Vanadium oxide Pc) and TiOPc films [30]. The NLO investigations in

organic semiconductors show that $\chi^{(3)}$ value depends on a number of factors like the temperature, metal atom present in the ring and metal size [27]. A few studies also show the influence of heating. The heating changes the phase by virtue of structural alteration and hence change the optical properties [29, 30].

It is important to mention that as prepared and stable annealed Pc films mainly exist in α-phase and β-phase. α-phase and β-phase have herringbone structure and are different from each other by the angle between the molecular plane and the stacking axis [8,9]. As reported previously, the phase change is done by heating the sample during or after the sample preparation [8,9]. The as-prepared Pc films at room temperature results in the formation of the α-phase whereas annealing during or after the Pc films results in β-phase [9]. The structural variation of the different Pc films affects its physical-chemical, electronic and optical properties.

The primary objectives for the present study on NLO properties in these molecules are two folds (a) understanding the impact of central metal atom on NLO properties and (ii) how the structural alteration or the phase change causes variations in intermolecular interactions which tend to alter the NLO behavior. Therefore, we expect that due to variation in intermolecular interactions, the present study on optical nonlinearity of thin films in different phases and the different central metal atom has practical significance in optimizing the NLO properties.

3.2 Description of the Phthalocyanines Samples

In the present study, we have investigated three different kinds of samples prepared by thermal evaporation technique having different molecular arrangements. All the three samples have been prepared by Dr. S. M. Dharmaprakash and K. V. Anil Kumar at

Mangalore University. In order to prepare the Pc films, we used commercially available Tetra-tert-butyl-phthalocyanine, Copper (II) 2,9,16,23-Tetra-tert-butyl-29H,31H-phthalocyanine (CuPc) and Zinc(II) 2,9,16,23-Tetra-tert-butyl-29H,31H-phthalocyanine (ZnPC) powder. By thermal evaporation technique, Pc films of 200 nm thickness were prepared on the glass substrate. As mentioned previously, the as-prepared Pc films exist in α-phase. On annealing, the as-prepared Pc films at a temperature of 473 K for 90 minutes results in stable β-phase.

First, the influence of phase change (α→ β) on NLO properties in metal-free Pc thin films has been studied. Secondly, we investigate the impact of phase-change as well as the influence of central metal atom in CuPc and ZnPc thin films. As mentioned previously, Pc films mainly exist in α-phase and β-phase [8,9]. A schematic of α- and β- phases of MPc are illustrated in Fig 3.1. It is clear from the Fig that the molecular arrangements of β-phase are such that it has the minimum energy for intermolecular interactions. CuPc exists in a planar molecular structure having D_{4h} symmetry and ZnPc exists in a non-planar structure with C_{4v} symmetry.
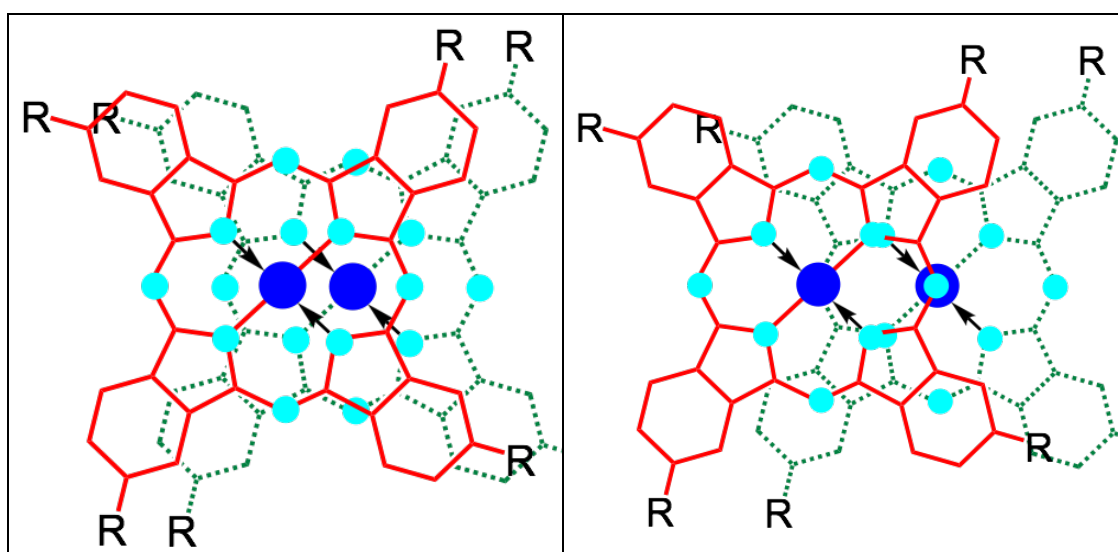
Fig. 3.1 α and β-phases schematics for Metalophthalocyanine.

This difference in molecular structure causes changes in the intermolecular interactions and therefore, both phases are expected to vary in NLO response [31]. Also, R. F. Theisen *et al.* investigations reveal that ZnPc has D_{4h} symmetry and a C_{4v} symmetry in the ground and excited-state respectively [32].

3.3 Experimental Section: Z-Scan Method

In order to investigate the NLO characteristics in different phases of Pc and MPc thin films, the Z-scan method was employed [33]. The Z-scan method is a simple, sensitive single beam and highly effective method to measure the NLR and NLA of a material. Closed-aperture (CA) and open aperture (OA) are two types of transmission Z-scan. In CA Z-scan method, the transmittance of the nonlinear medium through an aperture is measured as the sample is translated across the focus of a Gaussian beam. The phase extracted from the CA measurements is related to the nonlinear refraction of the sample which is also discussed previously in chapter 2. In the OA Z-scan technique, we measure the transmittance through the sample as it is translated through the focus of the Gaussian beam [34]. In OA measurements, it is to be ensured that the optical detector sensitive area is significantly large so as to capture the total energy or power contained in the beam. Therefore, in the OA Z-scan transmission measurements, only nonlinear absorption (NLA) is expected to cause variation in transmission as the sample is translated. Our Z-scan method utilizes a high power laser. The ultrafast high power fiber laser utilizes efficient pulse compression to deliver a linearly polarized pulse of ≈ 250 fs and at a repetition rate of 80 MHz [35]. The central wavelength of the laser is 1064 nm and delivers average power >5.0 W. We varied the intensity of the transmitted linearly polarized light on the sample, using a half wave plate (HWP)

and a polarizing beam-splitter (PBS). The laser light was focused to a spot size of 37±3 μm using a combination of concave (f = −50 mm) and a convex lens (f = +100 mm). The diffraction length (z_0) of the beam is then calculated to be 4 mm. Phthalocyanines samples were moved from z = −40 mm to z = +40 mm (total scanning length = 80 mm) using a motorized control translation unit. In order to remove the contribution of thermal effects on NLO properties, we performed the Z scan at 664 kHz repetition rate using a custom-made chopper wheel 35].

3.4 Nonlinear Optical Properties of Phthalocyanine Thin Films

3.4.1 Nonlinear Refraction

Under sufficiently intense illuminations, an optical system exhibits a nonlinear phase shift due to nonlinear refraction [36,37]. The concept of the intensity-dependent refractive index has already been discussed in chapter 2 and the measurements for estimating nonlinear refractive index coefficients, n_2, n_4 will be discussed here. In addition to this, the experimental results on the impact of positive or negative nonlinear phase shift in a Z-scan experiment will also be discussed.

Interestingly, Phthalocyanines exhibit significantly large phase shifts owing to nonlinear refraction which is essentially a consequence of large nonlinear refractive index [5,37]. The vast majority of the Z-scan measurements have been focused on investigating various kinds of phthalocyanine and the influence of central metal on the nonlinear refractive index values [5]. Various nonlinear measurements revealed that the nonlinear refraction of phthalocyanine is in the orders of ~10^{-16} - 10^{-11} cm^{2}W^{-1} [38].

Furthermore, NLO properties using degenerate four-wave mixing (DFWM) method in Metalophthalocyanine thin films and solutions have been reported [39]. DFWM allows the determination of an appropriate component of third order susceptibility tensor for Metalophthalocyanine thin films $\chi^{(3)} \approx 10^{-18} - 10^{-20}$ m^2/V^2 [39]. In addition, higher-order contributions turn significant at high irradiance or as the irradiance is increased above a certain threshold which is apart from the contribution from third-order susceptibility ($\chi^{(3)}$) [35].

It is important to mention that the nonlinear refraction of Pc films are proposed to be dependent on phases [29]. However, comprehensive measurements using Z-scan method were carried out to confirm the role of phases on nonlinear refractive index previously. The work performed in the present thesis work unambiguously verified the dependence of nonlinear refractive indices on Pc films phases [35, 38].

It has been found that the nonlinear refractive indices in Pc films are phase as well as irradiance dependent [35]. Furthermore, due to the large contribution of $\chi^{(5)}$ in as-prepared Pc film, we observed dual "peak-valley" in the transmission CA Z-scan method[35].

3.4.2 Closed-Aperture Z-scan Method

In order to study the NLR behavior of metal-free Pc films, we have performed the CA Z-scan using ultrashort fiber laser described in section 3.3 which exhibits excellent pulse-to-pulse stability and high average power [33, 34,35]. Nonlinear refractive properties of as-prepared, as well as annealed metal-free Pc, were investigated with intensity varying between 1.5×10^9 W/cm^2 to 5×10^9 W/cm^2. Fig 3.2(a) and (b) shows the experimentally measured (dotted values) CA Z-scan for as prepared and annealed

Pc films. As evident, the CA Z-scan data for the annealed film (Fig 3.2(b)) exhibits pre-focal minima and post-focal maxima. A pre-focal minimum followed by a post-focal maximum is an indication of positive n_2. However, the experimental data for CA Z-scan of the as-prepared film (Fig 3.2(a)) is complex as compared to the stable annealed film. The normalized transmittance shows two signatures for n_2 values. As observed CA Z-scan behavior of the as-prepared film displays a signature of negative n_2 values near ± 10 mm and positive values near close to the focus.
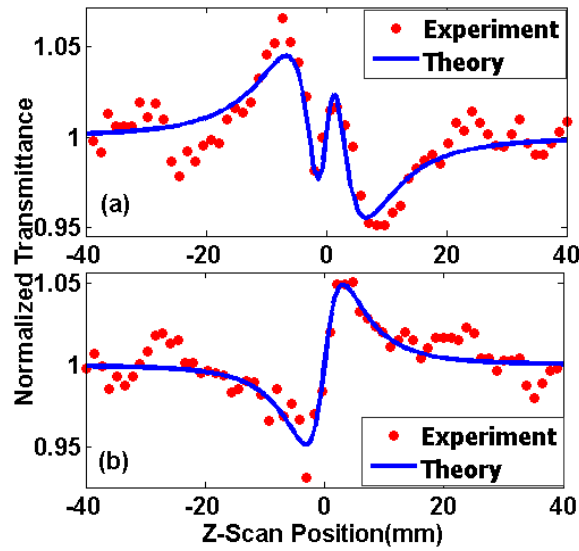
Fig 3.2 CA Z-scan experimental data (dots) of (a) As-prepared and (b) Annealed Pc film. Solid blue lines are the theoretical fitting with $\chi^{(3)}$ and $\chi^{(5)}$ contributions.

The theoretical fitting in Fig. 3.2 is carried out using equation 3.1 presented in the later part of this section. The transmittance behavior observed in this case has not been observed before for metal-free Pc films and due to the competition between $\chi^{(3)}$ and $\chi^{(5)}$ contributions [40]. Therefore, it becomes important to study the irradiance dependence of NLO properties for understanding the mechanism of such behavior. Therefore we performed the CA Z-scan measurements for both the phases of Pc films at different pulse fluence which are illustrated in Fig 3.3 (a-h). As can be seen from Fig 3.3(a-d)

the experimental data are quite complicated. From Fig 3.3(a-d), it is apparent that the difference between the peak (T_p) and valley (T_v) of the normalized transmittance (T_p-T_v) decreases with the increase in laser fluence around ±10 mm. However, the difference between the peak (T_p) and valley (T_v) of the normalized transmittance (T_p-T_v) (close to the focus) increases with the increase in laser intensity. To interpret such an unconventional CA Z- measurements, we take a note of the work carried out by B. Gu *et al.* [40]. Based on his theoretical observations, the authors conclude that a meager contribution of real part of $\chi^{(5)}$ would show the conventional "peak-valley" or "valley-peak" shape in the CA measurement.
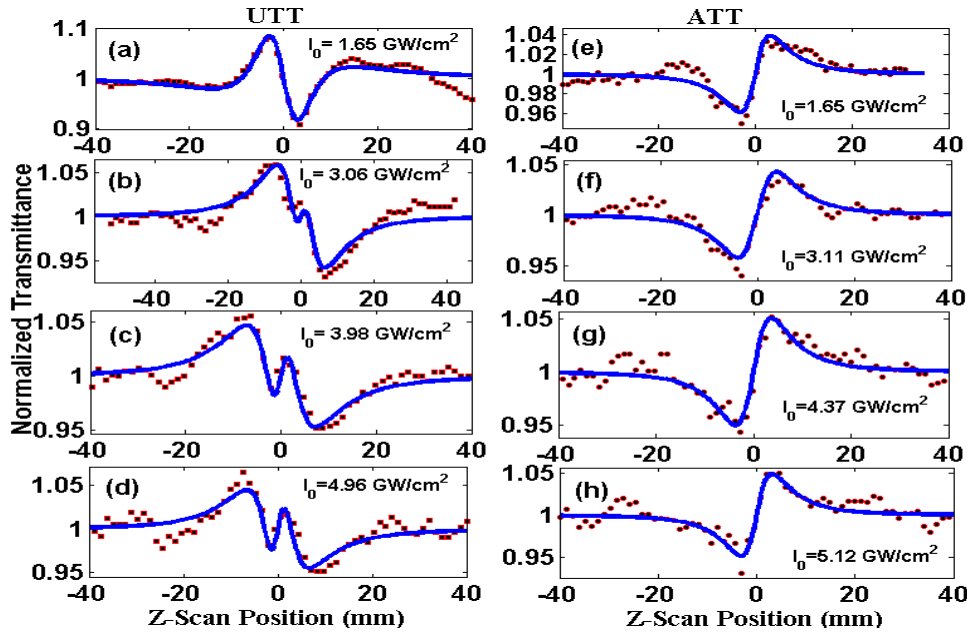
Fig 3.3 CA Z-scan experimental data (dots) for as prepared (a-d) and annealed PC films (e-h). Solid blue lines are the theoretical fitting with $\chi^{(3)}$ and $\chi^{(5)}$ contributions (Eqn. 3.1).

However, a large contribution of real part of $\chi^{(5)}$ results in dual "peak-valley" or "valley-peak" signature in the CA Z-scan measurements [35,40]. Such an observation could be appreciated from the fact that the contribution of $\chi^{(3)}$ NLO response is being

effectively compensated by $\chi^{(5)}$ NLO response having an opposite sign. In other words, the difference between $(T_p - T_v)$ of the CA measurements due to $-n_2$ decreases at the cost of an enhancement in the difference between $(T_p - T_v)$ close to the focus which sets in as a consequence of positive n_4. However, no such complicated behavior was noticed or detected in the case of annealed Pc film (Fig 3.3 (e-h)).

In order to measure n_2 and n_4 contributions, we performed the theoretical fitting to the experimentally measured CA Z-scan data using the equation (2.18) [40].

The values of the intensity-dependent nonlinear refractive indices obtained from the fit at different intensity are presented in table 3.1. As can be seen, metal-free Pc films exhibit significant third-order intensity-dependent nonlinear refraction of the order $\approx$ 10^{-14} m^2 W^{-1}. We can also observe from table-3.1 that the n_2 and n_4 values due to $\chi^{(3)}$ and $\chi^{(5)}$ contributions exhibits opposite signs for both the phases of Pc film. However, the competition between n_2 and n_4 is not observed in the CA measurements of annealed Pc film. This is due to the fact that the magnitude of n_4 for the stable annealed film is approximately two orders of magnitude lesser as compared to unstable as prepared Pc film. However, the n_2 values of both the phases are commensurate. As observed in table 3.1, n_2 and n_4 reverse their signs at higher intensities for as prepared Pc films. However, n_2 and n_4 values decrease with the increase in laser fluence for annealed Pc films. Although both the phases of Pc films exhibit a slight structural difference, its influence on NLO response is momentous which reveal markedly different phase variation [35]. It is important to mention here that the experiments have

Table 3.1 NLO coefficients for As-repared and Annealed Pc films calculated using Eq. (3.1).

	As-prepared			Annealed	
I_0 (GW/cm^2)	$n_2 \times 10^{-14}$ (m^2/W)	$n_4 \times 10^{-28}$ (m^4/W^2)	I_0 (GW/cm^2)	$n_2 \times 10^{-14}$ (m^2/W)	$n_4 \times 10^{-28}$ (m^4/W^2)
1.65	2.30±0.32	-(49±6.8)	1.65	0.98±0.14	-
3.1	-(1.66±0.23)	8.8±1.2	3.1	0.8±0.11	-(1.90.26)
4	-(1.15±0.16)	5.5±0.76	4.37	0.61±0.08	-(0.74±0.11)
5	-(0.93±0.13)	3.8±0.53	5.12	0.4±0.06	-(0.02±0.002)

performed with a femtosecond (fs) laser operating at 664 kHz. So, the main cause of the observed NLO response is electronic. Also, the equation 3.1 that includes phase change due to only electronic contribution gives a good fit to the measured CA Z-scan data. In order to understand the mechanisms and a possible explanation for such an observation, we note that as-prepared Pc films are comparatively less durable and more prone to distortion due to its molecular stricture [41]. Hence, as-prepared Pc films are expected to go through a larger change in the net dipole moment with respect to the annealed Pc [42]. This indicates that the molecule structural arrangement has a strong impact on its physical, electronic and optical properties. As mentioned previously, different phases have a different angle between the molecule plane and stacking axis; therefore the molecular arrangement could result in varied NLO response [6]. Also as explained in chapter 2, there is various physics process that contributes to n_2 values 27]. As observed in our case, similar switching of n_2 values have been reported previously in nanoparticles and nanostructures [43-45].

It is important to mention here that there are a number of physical process other than electronic contribution to $\chi^{(5)}$ NLR. Here, as observed in as prepared Pc thin films, the contribution as a result of ($\chi^{(5)}$) NLO response is noticeable from the experiments and

therefore, appropriate theoretical models are required for providing the justifications. The origin of fifth-order NLO term n_4 has been mainly associated with three physical processes [46]. The most fundamental being the electronic contribution at high intensity. Secondly, such an unconventional curve may be as a result of cascading of the third-order nonlinearities that result into a nonlinear response that appears like an equivalent $\chi^{(5)}$ nonlinearity [47]. Third, physical process that contributes to $\chi^{(5)}$ include phenomena like free-carrier and excited-state nonlinearities, etc [48]. Therefore, $\chi^{(5)}$ contribution to n_4 can be presented as a sum of these terms [49].

$$n_4 = n^{inhent} + n^{cascading} + n^{equivalent} \tag{3.1}$$

For example, negative values for n_4 may be due to TPA generated free carriers. The cascading of $\chi^{(3)}$-$\chi^{(3)}$ interaction takes place in the nanosecond (ns) time-scales, and therefore $n^{cascading}$ contribution to n_2 is also negligible. This is due to the fact that Z scan was performed with 250 fs laser (ii) n_4 decreases with the increase in laser intensities [46,47]. As will be observed in the subsequent section of OA Z-scan measurements, both variants of films exhibit TPA. This results in negative NLR behavior due to excited-states of the system, which could be seen in table 3.1. Therefore, the observed n_4 is associated to the TPA-supported generation of excited states, and meager universal $\chi^{(5)}$ contribution to NLR [50,51].

3.4.3 Nonlinear Absorption

Nonlinear absorption is an absorption phenomenon that can occur in the presence of strong electromagnetic fields, as discussed earlier in chapter 2 [33,34]. It is an intensity dependent phenomenon and is expected to be maximum when the sample is at the focal point of a laser beam. The concept of the nonlinear absorption coefficient

has already been discussed in chapter 2 and also the expression for estimating

nonlinear absorption coefficients (β) has been derived [37]. In order to determine β,

the total power of a focused laser beam transmitted by the sample is measured by a

photodetector. The phenomena of NLA could occur due to a variety of processes like

MPA, RSA, and SA as explained in chapter 2 [34].

3.4.4 Open Aperture Z-scan Measurements

In order to investigate the nonlinear absorption characteristics in metal-free Pc thin

films samples, I have used the OA Z-scan method [33]. In the OA Z-scan technique,

we measure the total power of the laser beam transmitted through the sample by a

photodetector and plotted against the sample position. A typical plot of the sample

transmittance exhibits a dip or a peak in the proximity of focal point. The occurrence

of a dip or a peak is dictated by the sign of nonlinear absorption coefficient β_{eff}. OA Z-

scan profile shows an increase in transmission at the focus due to SA i.e negative β

and decrease in transmission due to TPA, MPA for positive β_{eff}. The OA Z-scan data

for both the phases of Pc films are shown in Fig 3.4 (a) and (b) respectively. The OA

Z-scan measurements are characterized by a decrease in transmission at the focus (z =

0) which is mainly due to RSA [41]. We have performed the theoretical fitting (green

lines in Fig 3.4(a-b)) of the OA Z-scan experimental data (dots) using the relation

2.20[52]. β_{eff} and I_s were estimated to be $(2.60\pm0.360)\times10^{-9}$ m/W and 10×10^9 W/cm^2

respectively at $I_0 = 2.3 \times10^{10}$ W/cm^2 for as-prepared Pc film. However, β_{eff} and I_s were

found to be $(12.0\pm1.66)\times10^{-9}$ m/W and 20×10^9 W/cm^2 for the annealed film at

$I_0=3.3\times10^9$ W/cm^2. RSA behavior in OA is due to the combined effect of TPA and

singlet-ESA [6,22]. A minimal increase in β_{eff} for annealed Pc film is a result of

enhancement in absorption probability of the higher energy state. This enhancement is
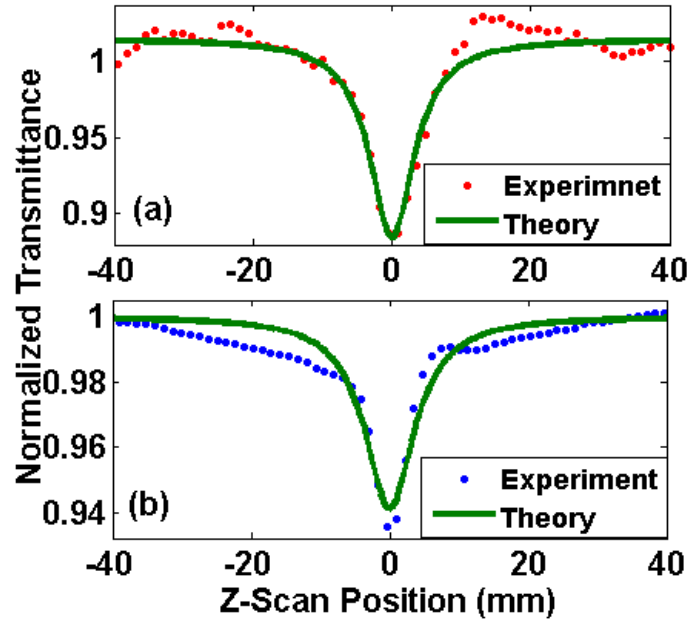
Fig 3.4. Measured transmittance trace for OA Z-scan experiment (dots) for (a) As prepared and (b) Annealed Pc films. Green lines are the theoretical fitting to the OA experimental data.

because of partial improvement in crystallinity of the annealed film [53].

3.4.5 Metal- Free Pc Thin Films: Figure of Merit

Finding materials for all-optical switching and nonlinear absorbers has been one of most active fields of research in the last couple of decades. However, it is important to mention that despite the substantial attention given to the investigations of third-order NLO properties, there are a few practical materials for realizing nonlinear refraction-based devices. At the same time, the number of optical systems considered for nonlinear absorption is considerably large [54,55]. From an application aspect, the utility of organic species for uses in photonics, nanophotonics, and biophotonics is evaluated in terms of materials Figure of merit (FOM) [55,35]. The two important FOM forms are defined as, FOM_1 (W) = $n_2 I_0 / \alpha_0 \lambda$ and FOM_2 (T^{-1}) = $n_2 / \beta_{eff} \lambda$ where

symbols have their usual meaning. FOM_1 is the result of dominant single-photon absorption and is required for all-optical switching devices whereas FOM_2 results from a dominant two-photon absorption which has wide applicability in optical-limiting processes. In contrast to FOM_1, FOM_2 has no dependence on light intensity as both β and n_2 are associated with the square of light intensity [55]. This figure of merit should be maximized such that W, as well as T^{-1} values, are greater than unity [54]. Therefore, an organic semiconductor with a greater FOM_1 value could be utilized for all-optical switching and other with a larger value of FOM_2 could be employed in sensor protection.

To determine the influence of phase changes in Pc films on the FOM factors, we note the NLO parameters for the as-prepared and annealed H_2Pc films. Based on our NLO measurements, we calculated the values of FOM and found, FOM_1 = 7.6 and 4.2 for as-prepared and annealed Pc films respectively whereas FOM_2 = 3.4 and 0.31 for as-prepared and annealed Pc films respectively. From the values of FOM_2, it is worth noting that as-prepared Pc films are good for all-optical switching in the NIR region with respect to annealed films. However, annealed H_2Pc films have higher values of NLA and consequently, they could be employed for optical devices protection based on optical limiting phenomena at 1064 nm wavelength.

3.5 NLO Properties of Metalophthalocyanine Thin Films

NLR due to bound electrons, also known as optical Kerr effect, is one of the important optical nonlinearities in the infrared region, resulting in nonlinear refractive index change Δn [36]. This change in the refractive index is proportional to the intensity with nonlinear coefficient n_2. Because phthalocyanine and Metalophthalocyanine

possess large $\chi^{(3)}$ NLO response with fast response time due to the highly delocalized aromatic 18 π-electron system, its NLO properties have been employed for optical limiting and pulse shaping, imaging and sensing, optical switching [56,57]

As mentioned in the previous section substrate type and heating influences the structural configurations of organic thin films. Therefore, investigations of NLO properties in low dimensional systems has its own significance in understanding the origin of the NLO mechanism and getting useful FOM [10-13,5 5]. Their phase dependent study is essential for maximizing FOM, with values greater than unity needed for the nonlinear applications process to be feasible at all [54,55].

We used to a Z-scan method to study the impact of phases and central metal atom NLO properties in Metalophthalocyanine thin films. A detail description of the experimental set up is given in section 3.3.

3.5.1. Closed-Aperture Z-scan Measurements

For determining the NLR coefficients of Metalophthalocyanine thin films, CA Z-scan experiment is performed [33]. The CA Z-scan transmittance for 30 nm thick MPc thin films with 1064 nm wavelength laser are presented in Fig. 3.5 (a-d). The CA Z-scan measurements on CuPc films as shown in Figs. 3.5(a-b) is characterized by "peak-valley" shape from which we conclude that it possesses negative n_2. However the CA Z-scan experiments for ZnPc (Fig. 3.5(c-d)), exhibits "valley-peak" signature positive values of n_2. We can notice in Fig.3.5 (a-d) that all the four samples exhibit a clear dependence of nonlinear refractive index on the phases of thin-films and the central metal of Pc. We expect that this dependence stems from optical Kerr effect in MPc films rather than a thermal manifestation [36]. Our conjecture seems reasonable because the measurements using < 250 femtoseconds (fs) laser
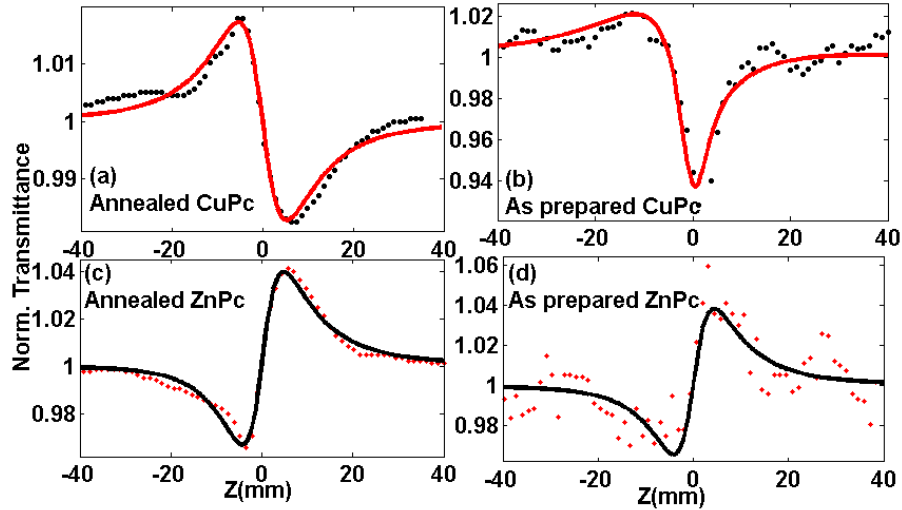
Fig. 3.5 CA Z-scan experimental data metal-phthalocyanine

beam pulses at 664 kHz repetition rate, the Z-scan measurements exhibit good correspondence to the theoretical models considering an only electronic contribution. The CA experimental Z-scan data was fitted using the CA expression (2.16 and 2.17)[58,59]. The CA fitted curves are shown in Fig. 3.5(a-d). The solid lines in Fig. 3.5 (a-d) represent the theoretical fits. Eq. (3.4) was used to fit the experimental data for CuPc films (Fig. 5(b)). Due to the fact that the glass substrate has very small or negligible nonlinear optical response, the strong NLO signals observed here result from MPc thin films. For comparison, we have summarized the nonlinear refractive index values from our findings as well as from previously reported one for MPc in table 3.2. It is clear that the sign and magnitude of n_2 for CuPc and ZnPc matches well with the already reported values [27]. Our finding also reveals that the phase shift due to nonlinear refraction (and hence, n_2) are influenced by the metal atom as well as the MPc phase. As observed in ZnPc thin films, n_2 values vary hardly at all for both the phases and matches well with the work of A. Zawadzka *et al.* [27].

Table 3.2. Summary of intensity dependent refractive index n_2 values

Sample	Laser Parameters	Techniques	n_2 (cm^2 W^{-1})	References
Alkyl Pc Nanoparticles	800 nm,100fs	Z-scan	-9.10×10^{-16}	10
Zinc Pc	800 nm,100fs 532nm, 6nm	Z-scan	1.14×10^{-15} 8.6×10^{-12}	12
CuPc Thin films	800,140 fs	Z-scan	7.00×10^{-09}	14
ZnPc Thin Films	800 nm, 100fs	Z-scan	-7.00×10^{-11}	27
Phenoxy Pc in DMF	800nm, 100fs	Z-scan	8.40×10^{-18}	60
CuPc in DMSO	532 nm,11ns	Z-scan	2.50×10^{-10}	61
CuPc Thin Films	750 nm, 150 fs	Z-scan	-1.10×10^{-10}	62
CuPc As prepared CuPc Annealed	1064 nm, 250 fs	Z-scan	-9.6×10^{-11} -2.2×10^{-11}	Thesis work
ZnPc As prepared ZnPc Annealed	1064 nm, 250 fs	Z-scan	3.65×10^{-11} 2.98×10^{-11}	Thesis work

The NLR properties of CuPc are different as compared to ZnPc. As evident from table 3.2, the as-prepared CuPc has the maximum value of the n_2. n_2 values reduce to 2.2×10^{-15} m^2/W from 9.6×10^{-15} m^2/W on phase change from as prepared to annealed one. The mechanism responsible for such an observation is strongly related to its phase change [27,31]. As reported in the literature, the position and size of the metal atom can greatly change the NLO behavior [3,5]. CuPc possesses flat structures as Cu

maintains a position inside the Pc ring's plane. Also, the lowest energy molecular orbitals of CuPc and ZnPc are different, which may result in varied electronic contribution. In the case of CuPc samples, the 3d orbitals are half occupied and are positioned in the gap between the Pc HOMO and LUMO. Therefore, the unfilled d-valence orbital can split into various levels due to the interaction between the d-electrons and π-conjugated electrons of Pc ring [27, 31]. This lowers the transition energy in low–lying d-orbital ligand or d-d transition. As reported previously, the existence of excited states with low transition energy will enhance the nonlinear optical susceptibilities of the material. The unfilled d-orbital of Cu atoms will couple with the conjugated electrons of phthalocyanine ring leading to the extension of the

conjugated systems. Consequently, the reason behind such large nonlinear response in case of CuPc is the large conjugated electron system [27]. To fully understand the variation in nonlinear refraction properties of MPc thin films, an explanation can be given on the basis of OA Z-scan measurements. In the case of CuPc, the effective two-photon absorption (Fig. 3.6(a-b)) possibly leads to negative nonlinearity and therefore, self-defocusing effect (Fig.3.6 (a-b)). For the ZnPc thin films, SA behavior is prominent which leads to focusing effect [44]. Our Z-scan results have shown that n_2 and β_{eff} values are different for as-prepared and annealed polymorphs. While the magnitude of n_2 decreases on annealing, the effective nonlinear absorption coefficient β follows an opposite trend. This peculiar behavior of n_2 is in accordance with that observed in metal phthalocyanine thin films by A. Zawadzka *et al.* [27].

3.5.2 Open Aperture (OA) Z-scan Measurements

NLA coefficients of MPc thin films have been determined using the OA Z-scan method [33]. All the Z-scan measurements described in this section were performed using a 250 fs laser at 1064 nm with pulse repetition rate 664 kHz [35]. The details of the experimental set up are given in section 3.3. The typical OA Z-scan profiles of the CuPc and ZnPc thin films measured at 2.5 GW/cm^2 to 5.0 GW/cm^2 intensity which is shown in Figs.3.6 (a-d) respectively. The OA Z scan data exhibits a dip (Fig3.6 (a-b)) or peak (Fig.3.6(c-d)) at the focus (z = 0) which is a consequence of NLA mechanism i.e. RSA or SA respectively. As observed from Fig.3,5 when the sample is at a far distance from the focus we observe normalized OA transmittance to be constant due
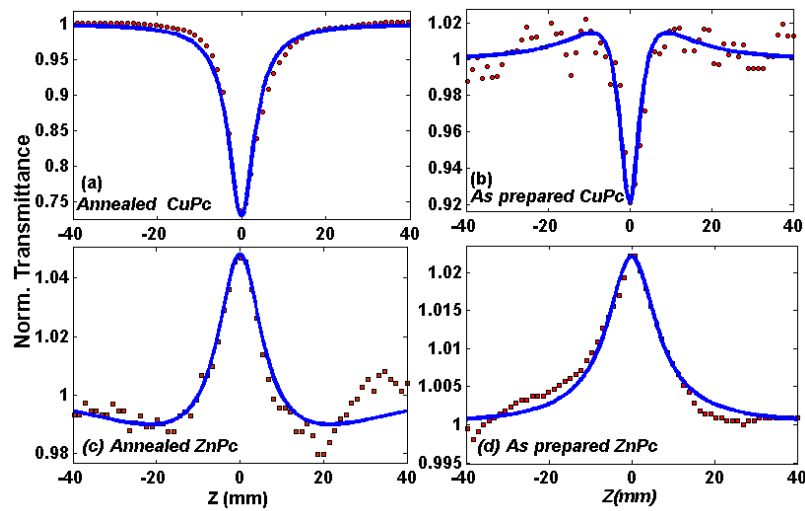
Fig 3.6 Open aperture Z- scan traces for metal-phthalocyanine

to negligible NLA. As the sample approaches the focal plane of the focused beam, the OA transmission decrease which is a clear indication of RSA (see Fig. 3.5(a)). However, in case of annealed ZnPc thin films (Fig. 3.6(b)), the OA Z-scan measurement shows a small but apparent increase around ±10 mm of the focal plane which is, a signature of SA characteristics. However, RSA mechanism is strong very close to the focal plane (highest intensity regime) and therefore, a dip or a minimum is

observed in the OA measurements. Therefore, the minima in OA Z-scan measurement at the focal plane in α-phase and β-phase of CuPc reveal that RSA is the mechanism for the observed NLA. This because the excited-state lifetimes for higher excited states in organic semiconductors responsible for RSA, typically vary from sub-picosecond to a few femtosecond [63]. Therefore, the decrease in OA transmission (near focus) is attributed to RSA as we employed an fs laser for the measurements. Basically, ESA is caused by MPA which results in RSA features in OA Z-scan in phthalocyanine [6,64]. Z-scan measurements for ZnPc thin films exhibit a peak in the transmission which is in contrast to the previous report in 0.5 mM solutions of ZnPc in DMF [22]. This difference in observation could be due to the different absorption mechanism in ZnPc thin films as compared to that for ZnPc in solutions. To determine the NLA coefficients, theoretical fitting of the normalized OA experimental data was done using the relation (2.10) [52]. Using Eq. (2.10), the OA Z-scan experimental measurement was fitted which is shown in Fig. 3.6 (a-d). The effective NLA coefficients β_{eff} and I_s were obtained to be (48.2±6.74) $\times 10^{-9}$ m W^{-1} and 6×10^{13} W m^{-2} respectively at a laser intensity of 2.86×10^{13} W m^{-2} for annealed CuPc thin film. On the other hand, β_{eff} and I_s were found to be (12.8±1.77)$\times10^{-9}$ m W^{-1} and 4.5×10^{13} W m^{-2} for as prepared CuPc at a laser intensity of 4.5×10^{13} W m^{-2}. SA characteristics of ZnPc results in β_{eff} and I_s to be $-(3.52\pm0.5)\times10^{-9}$ m W^{-1} and 5.6×10^{13} W m^{-2} respectively at a laser intensity of 5.2×10^{13} W m^{-2} for amorphous or as-prepared ZnPc thin films. While β_{eff} and I_s were found to be $-(3.8\pm0.54)\times10^{-9}$ m W^{-1} and 3×10^{13} W m^{-2} for annealed ZnPc respectively at a laser intensity of 3.8×10^{13} W m^{-2}. The OA Z-scan results show that effective nonlinear absorption coefficients β_{eff} increases for β-phase which may be due to efficient absorption of the excited state due to the

improved crystalline nature or crystallite size of the β- polymorphic forms or annealed film. The difference in OA transmission obtained for CuPc and ZnPc presented in Fig 3.6 (a-d) could be qualitatively explained as follows. CuPc has a long-lived lifetime (15 ns) from the S_1 states whereas ZnPc has a short-lived lifetime (9 ps). The long-lived lifetime results enhanced NLA observed in CuPc thin films [21,63].

In order to understand the usefulness of Pc films for integrated circuits, I have tabulated the NLO properties of TPA polymers and SiN in the table 3.2. The nonlinear refractive index value for polymers varies from $10^{-12}\,cm^2/W$ to $10^{-15}\,cm^2/W$. However the nonlinear refractive index values for SiN varies from $10^{-8}\,cm^2/W$ to $10^{-15}\,cm^2/W$ depending upon the Si concentration. As observed from our study the Phthalocyanines NLR values are of the same order as that of polymers. However the NLA values of SiN thin films is of the order of $10^{-5}\,cm/W$ and that of polymers is $10^{-9}\,cm/W$. Therefore our study reveals that the NLA and NLR values for polymers and phthalocyanine are of the same order of magnitude and hence Pc films can be utilized in place of commercial TPA polymers.

Table 3.3. Third order nonlinear optical properties of polymers and SiN

Sample	Laser Parameters	n_2 (cm^2/W)	β_{eff} (cm/W)	References
Silicon-rich nitride	1100-1500 nm 100 fs	$(1.5-4) \times 10^{-8}$	$(0.5-1) \times 10^{-5}$	65
SiN	1548 nm and 1558 nm	2.4×10^{-15}		66
SiN waveguide	1550 nm	6.94×10^{-15}		67
SiN waveguide	1550 nm	1.4×10^{-14}		68
SiN waveguide	1550 nm	9×10^{-15}		69
Polysterene	630 nm	2.4×10^{-15}		37
PPV	800 nm	$(1-10) \times 10^{-12}$	80×10^{-9}	37
2,5-Dimethxy p-PPV	800 nm	4×10^{-12}	$(25-80) \times 10^{-9}$	37
DBSA-PANI	1050	1.7×10^{-12}	42×10^{-9}	37
Polydiacetylene 4BCMU	1310	5×10^{-14}	0.25×10^{-9}	37
DANS	1060	8×10^{-14}		55
DAN2	1064	2×10^{-13}		55

3.5.3. Metal phthalocyanine Thin Films: Materials Figure of Merit

Based on the results NLR and NLA, it would be informative to compare FOMs (defined in section 3.4.5) for MPc thin-films. The linear properties, NLO properties, and FOM are summarised in Table 3.4. A recap of the section 3.4.5 reveals that an organic compound having a larger value of 'W' is useful for all-optical switching applications whereas the one having a larger value of 'T' would have more employability in optical limiting applications. Knowledge of FOM 'T' values is important in order to assess the strength of W with respect to NLA process [55]. Ideally, depending on the application, 'W' has a threshold value for a material to be of

any practical application. Also, T < 1 would not adversely affect the nonlinear absorption [65]. For example, a nonlinear Fabry-Perot resonator must have W>0.27,

Table 3.4. Summary of the linear and NLO characteristics

Sample	n_0	α_0 (10^6 m^{-1})	$n_2 \times 10^{-15}$ (m^2/W)	$\beta_{eff} \times 10^{-9}$ (m/W)	FOM (W)	FOM (T)
As prepared CuPc Film	2.3	1.32	-(9.64±1.45)	(12.7±1.77)	0.2724	0.028
Annealed CuPc Film	2.1	1.04	-(2.2±0.33)	(48.2±6.7)	0.0730	0.4662
As prepared ZnPc Film	2.45	1.5	(3.65±0.55)	-(3.52±0.5)	0.1189	0.0206
Annealed ZnPc Film	2.33	1.34	(2.98±0.45)	-(3.84±0.54)	0.1066	0.0274

whereas a half-beat length nonlinear directional coupler need W>1 [70]. In the present case, W > 0.27 always for as-prepared CuPc while T<1 for all the metal phthalocyanine thin films. Also as evident from table 3.4, the as-prepared MPc films possess larger values of W and smaller values of T in comparison to annealed one. Based on this, we could assert that the NLO devices using as-prepared MPc thin films are expected to deliver improved performance with respect to the annealed films for an operating wavelength of 1064 nm.

3.6 Summary

In this chapter, I have presented the impact of morphological phase change on NLO characteristics in metal-free and metal phthalocyanine thin films. The motivation behind this study is to explicitly show that the NLO properties of Pc depend on its phase due to the difference in intermolecular interactions. This is because the

molecular arrangements in MPc are very sensitive to thermal annealing. Therefore, the investigations on optical nonlinearity in thin-films with different phases have practical significance towards the optimizing the nonlinear Figure of merit. In the present study, we distinctly show the role of morphological phases in Tetra-tert-butyl-phthalocyanine (H_2Pc) thin films and the impact of the central metal and phases on NLO characteristics in Copper(II)2,9,16,23-Tetra-tert-butyl-29H,31H-phthalocyanine (CuPc) and Zinc(II) 2,9,16,23-Tetra-tert-butyl-29H,31H-phthalocyanine (ZnPC) thin films. The relevant NLO coefficients related to SA, TPA, and NLR were investigated and the associated coefficients were determined at an operating wavelength of 1064 nm wavelength using an ultrashort pulse laser. Our results reveal that as-prepared metal-free Pc and MPc exhibits large NLR and comparatively smaller NLA whereas the annealed variant has greater NLA. This suggests that morphological phase-dependent NLO study is important in optimizing the FOM. To the best of our knowledge, we report the first observation of fifth-order NLO response in as-prepared (α-phase) of metal-free Pc thin-film which was depicted in an unusual peak-valley feature in Z-scan transmittance. In order to improve the device functionality, the Figure of merit (FOM1 and FOM2) are estimated for metal-free Pc thin-films as well as Metalophthalocyanine thin-films. The FOMs suggest their suitability for devising solid-state based devices like all-optical switching based on either optical limiting or nonlinear refractive index and modern- monolithically-integrated photonic integrated circuitry.

Bibliography

[1] S. R. Forrest, Chem. Rev. **97**, 1793-1896 (1997)

[2] F. Kajzar, J. D. Swalan, *Organic thin films for wave guiding nonlinear optics*, 3 (Gordon and Breach Publishers 1996).

[3] P. N. Prasad, and D. J. Williams, *Introduction to Nonlinear Optical Effects in Molecules & Polymers*, Wiley, New York, 1990.

[4] H. Imahori, T. Umeyama; S. Ito, Large π-Aromatic Molecules as Potential Sensitizers for Highly Efficient Dye-Sensitized Solar Cells, Acc. Chem. Res. **42**, 1809-1818 (2009).

[5] S. M. O'Flaherty, S. V. Hold, M. J. Cook, T. Torres, Y. Chen, M. Hanack, W. J. Blau, Molecular Engineering of Peripherally and Axially Modified Phthalocyanines for Optical Limiting and Nonlinear Optics, Adv. Mater. **15,** 19-32 (2003).

[6] G. de la Torre, P. Vazquez, F. Agullo-Lopez, T. Torres, Role of Structural Factors in the Nonlinear Optical Properties of Phthalocyanines and Related Compounds, Chem. Rev. **104**, 3723-3750 (2004).

[7] M. A. Shaibat, L. B. Casabianca, D. Y. Siberio-Perez, A. J. Matzger, and Y. Ishii, Distinguishing polymorphs of the semiconducting pigment copper phthalocyanine by solid-state NMR and Raman spectroscopy, J. Phys. Chem. B, **114**, 4400-4406 (2010).

[8] S. Heutz, S.M. Bayliss, R. L. Middleton, T. S. Jones, Polymorphism in Phthalocyanine Thin Films: Mechanism of the $\alpha \rightarrow \beta$ Transition, J. Phys. Chem. B **104**, 7124-7129 (2000).

[9] S. Yim, S. Heutz, T. S. Jones, Model for the $\alpha \rightarrow \beta1$ Phase Transition in Phthalocyanine Thin Films, J. Appl. Phys. **91**, 3632-3636 (2002).

[10] T. Ning and Y. Zhou, J. Appl. Phys. **118**, 233103 (2015).

[11] H. M. Zeyada and M.M. Makhlouf, Effect of structure on nonlinear optical properties in $CaCu_3Ti_4O_{12}$ films, Opt. Mater. **54**, 181-189 (2016).

[12] R. Kishi, S. Ochi, S. Izumi, A. Makino, T. Nagami, J. Fujiyoshi, N. Matsushita, M. Saito, and M. Nakano, Third-Order Nonlinear Optical Properties of One-Dimensional Quinoidal Oligothiophene Derivatives Involving Phenoxyl Groups, Chem. Eur. J. **22**, 1493–1500 (2016).

[13] M. S. Rafique, S. Bashir, and A. Ajami, Nonlinear absorption properties correlated with the surface and structural changes of ultrashort pulse laser irradiated CR-39, Appl. Phys. A. **100**, 1183-1189 (2010).

[14] S. V. Rao, N. Venkatram, L. Giribabu, and D. N. Rao, Ultrafast nonlinear optical properties of alkyl-phthalocyanine nanoparticles investigated using Z-scan technique, J. Appl. Phys. **105**, 053109 (2009).

[15] Y. Zhou, T. Taima, T. Miyadera, T. Yamanari, and Y. Yoshida, Structural modifications of zinc phthalocyanine thin films for organic photovoltaic applications, J. Appl. Phys. **111**, 103117 (2012).

[16] R.S.S. Kumar, S. V Rao, L. Giribabu, and D. N Rao, Femtosecond and Nanosecond Nonlinear Optical Properties of Alkyl Phthalocyanines Studied Using Z-scan Technique, Chem. Phys. Lett. **447**, 274-278 (2007).

[17] C. Nitschke, S M O Flaherty, M. Kroll, J. J. Doyle, and W. J. Blau, Optical properties of zinc phthalocyanine nanoparticle dispersions, Chem. Phys. Lett. **283**, 555-560 (2004).

[18] M. Hanack, D. Dini, M. Barthei, S. Vagin, S. Conjugated Macrocycles as Active Materials in Nonlinear Optical Processes: Optical Limiting Effect with Phthalocyanines and Related Compounds, Chem. Rec. **2**, 129-148 (2002).

[19] B. Derkowska, M. Wojdyla, R. Czaplicki, W. Bała, B. Sahraoui, Influence of the Central Metal Atom on the Nonlinear Optical Properties of MPcs Solutions and Thin Films, Opt. Commun. **274,** 206-212 (2007).

[20] M. A. Diaz Garcia, Nonlinear Optical Properties of Phthalocyanines and Related Compounds, J. Porphyrins Phthalocyanines **13**, 652-667 (2009).

[21] A. Santhi, V. V. Namboodiri, P. Radhakrishnan, V. P. N. Nampoori, Spectral Dependence of Third-Order Nonlinear Optical Susceptibility of Zinc Phthalocyanine, J. Appl. Phys. **100**, 053109 (2006).

[22] A. Gadalla, O. Cregut, M. Gallart, B. Honerlage, J.-B. Beaufrand, M. Bowen, S. Boukari, E. Beaurepaire, P. Gilliot, Ultrafast Optical Dynamics of Metal-Free and Cobalt Phthalocyanine Thin Films, J. Phys. Chem. C **114**, 4086–4092 (2010).

[23] S. V. Rao, P. T. Anusha, T. S. Prashant, D. Swain, S. P. Tewari, Ultrafast Nonlinear Optical and Optical Limiting Properties of Phthalocyanine Thin Films Studied Using Z-Scan, Mater. Sci. Appl. **2**, 299-306 (2011).

[24] K. V. Anil Kumar, S. V. Rao, S. Hamas, and S. M. Dharmaprakash Wavelength dependent nonlinear optical switching in electron beam irradiated CuTTBPc thin film, RSC Adv **6,** 22083-22089 (2016).

[25] K.V. Anil Kumar, S. Raghavendra, S. V. Rao, S. Hamad, and S.M. Dharmaprakash, Optik **126**, 5918-5922 (2015).

[26] S. J. Mathews, S. C. Kumar, L. Giribabu, S. V. Rao, Nonlinear Optical and Optical Limiting Properties of Phthalocyanines in Solution and Thin Films of PMMA at 633 nm Studied Using a CW Laser, Mater. Lett. **61***,* 4426–4431 (2007).

[27] A. Zawadzka, P. Plociennik, J. Strzelecki, S. Dabos-Seignon, B. Sahraoui, Structural and Nonlinear Optical Properties of As-Grown and Annealed Metallophthalocyanine Thin Films, Thin Solid Films **545**, 429-437 (2013).

[28] M. Hosoda, T. Wada, A. Yamda, A. F. Garito, H. Sasabe, Phases and Third-Order Nonlinearities in Tetravalent Metallophthalocyanine Thin Films, Jpn. J. Appl. Phys. **30**, L1486- L1488 (1991).

[29] H. S. Nalwa, T. Saito, A. Kakuta, and T. Iwayanagi, Third-order nonlinear optical properties of polymorphs of oxotitanium phthalocyanine, J. Phys. Chem. **97**, 10515-10517 (1993).

[30] M. Hosoda, T. Wada, A. Yamada, A. F. Garito, and H. Sasabe, Phases and Third-Order Optical Nonlinearities in Tetravalent Metallophthalocyanine Thin Films**,** Jpn. J. Appl. Phys. **30**, L1486-L1488(1991).

[31] A. Zawadzka, P. Plociennik, I. Czarnecka, J. Strzelecki, and Z. Lukasiak, The effects of annealing process influence on optical properties and the molecular orientation of selected organ metallic compounds thin films, Opt. Mater. **34**, 1686-1691 (2012).

[32] F. Theisen, L. Huang, T. Fleetham, J. B. Adams, and J. Li, Ground and excited states of zinc phthalocyanine, zinc tetrabenzoporphyrin, and azaporphyrin analogs using DFT and TDDFT with Franck-Condon analysis**,** J. Chem. Phys. **142**, 094310 (2015).

[33] M. Sheik-Bahae, A. A. Said, T. H. Wei, D. J. Hagan, E. W. Van Stryland, Sensitive Measurement of Optical Nonlinearities Using a Single Beam, IEEE J. Quantum Electron. **26,** 760-769 (1990)

[34] G. Piredda. Materials for Nonlinear Optics: Semicontinuous Gold Films and Fast Saturable Absorbers Ph.D. thesis, University of Rochester, Rochester, New York 2008

[35] K. V. Anil Kumar, S. Kumar, S. M. Dharmaprakash, and R. Das, Impact of α→ β Transition in the Ultrafast High-Order Nonlinear Optical Properties of Metal-Free Phthalocyanine Thin Films, J. Phys. Chem. C **120**, 6733−6740 (2016).

[36] R. W. Boyd. *Nonlinear Optics*. Academic Press, second edition, 2003.

[37] D. N. Christodoulides, I. C. Khoo, G. J. Salamo, G. I. Stegeman, and E. W. Van Stryland, Nonlinear refraction and absorption: mechanisms and magnitudes, Adv. Opt. Photon. 2(1), 60–200 (2010).

[38] S. Kumar, K. V. Anil Kumar, S. M. Dharmaprakash, and R. Das, Phase-dependent ultrafast third-order optical nonlinearities in metallophthalocyanine thin films, J. Appl. Phys. **120**, 123104 (2016)

[39] B. Derkowska, M. Wojdyła, R. Czaplicki, W. Bała, B. Sahraoui, Influence of the central metal atom on the nonlinear optical properties of MPcs solutions and thin films, Optics Communications **274**, 206-212 (2007)

[40] B. Gu, J. Chen, Y. Fan, J. Ding, H. T. Wang, Theory of Gaussian Beam Z-scan With Simultaneous Third- and Fifth-Order Nonlinear Refraction Based on a Gaussian Decomposition Method, J. Opt. Soc. Am. B **22**, 2651-2659 (2005).

[41] J. V. Moloney In *Nonlinear Optical Materials,* IMA Volumes in Mathematics and Its Applications, M.I Stockman, L. N. Pandey, T. F. George, Enhanced Nonlinear-Optical Responses of Disordered Clusters and Composites, in Nonlinear Optical Materials, Springer-Verlag, New York, 225(1998).

[42] I. Gobernado-Mitre, R. Aroca, J. A. DeSaja, Vibrational Spectra and Molecular Organization in Thin Solid Films of 2, 3-Naphthalocyanines, Chem. Mater. **7**,118-122 (1995).

[43] R. A. Ganeev, A. I. Ryasnyansky, A. L. Stepanov, T. Usmanov, Saturated Absorption and Nonlinear Refraction of Silicate Glasses Doped with Silver Nanoparticles at 532 nm, Opt. Quantum Electron. **36**, 949-960 (2004).

[44] G. Fan, S. Qu, Q. Wang, C. Zhao, L. Zhang, Z. Li, Pd Nanoparticles Formation by Femtosecond Laser Irradiation and the Nonlinear Optical Properties at 532 nm Using Nanosecond Laser Pulses, J. Appl. Phys. **109**, 023102 (2011).

[45] V. Sreeramulu, K. K. Haldar, A. Patra D. N. Rao, Nonlinear Optical Switching and Enhanced Nonlinear Optical Response of Au−CdSe heterostructures, J. Phys. Chem. C **118**, 30333-30341(2014).

[46] A. I. Ryasnyansky, R. A. Ganeev, V. I. Redkorechev, T. Usmanov, G. Priebe, Fostiropoulos, K. Competition of Third and Fifth-Order Nonlinear Optical Processes in C_{60} Thin Film, Nanotubes, Carbon Nanostruct. **13**, 131-1409 (2005).

[47] S. Saltiel, S. Tanev, A. D. Boardman, High-Order Nonlinear Phase Shift Caused by Cascaded Third-Order Processes, Opt. Lett. **22**, 148-150 (1997).

[48]B. Gu, Y. Sun, W. Ji, Two-Photon-Induced Excited-State Nonlinearities, Opt. Express **16**, 17745-17751 (2008).

[49] R. A. Ganeev, M. Baba, M. Morita, A. I. Ryasnyansky, M. Suzuki, M. Turu, and H. Kuroda, Fifth-order optical nonlinearity of pseudoisocyanine solution at 529 nm, J. Opt. A: Pure Appl. Opt**. 6**, 282–287 (2004).

[50] A. A. Said, M. Sheik-Bahae, D. J. Hagan, T. H. Wei, J. Wang, J. Young, E.W. Van Stryland, Determination of Bound-Electronic and Free-Carrier Nonlinearities in ZnSe, GaAs, CdTe, and ZnTe, J. Opt. Soc. Am. B **9**, 405-414 (1992).

[51] C. Zhan, D. Zhang, D. Zhu, D. Wang, Y. Li, D. Li, Z. Lu, L. Zhao, Y. Nie, Third- and Fifth-Order Optical Nonlinearities in a New Stilbazolium Derivative, J. Opt. Soc. Am. B **19**, 369-375 (2002).

[52] H. Zhang, S. B. Lu, J. Zheng, J. Du, S. C. Wen, D. Y. Tang, and K. P. Loh, Molybdenum Disulfide (MoS_2) as a Broadband Saturable Absorber for Ultra-Fast Photonics, Opt. Express **22**, 7249-7260 (2014).

[53] H. J. Kim, H. S. Shim, J. W. Kim, H. H. Lee, J. J. Kim, CuI Interlayers in Lead Phthalocyanine Thin Films Enhance Near-Infrared Light Absorption, Appl. Phys. Lett. **100**, 263303 (2012).

[54] M. Samoc *et al*. Nonlinear absorption and nonlinear refraction: maximizing the merit factors, Proc. of SPIE **8258**, Organic Photonic Materials and Devices XIV (2012).

[55] J. L. Bredas, C. Adant, P. Tackx, and A. Persoons, Third-Order Nonlinear Optical Response in Organic Materials: Theoretical and Experimental Aspects, Chem. Rev. **94**, 243-278 (1994).

[56] B. Gu, C. Zhao, A. Baev, K. T. Yong, S. Wen, and P. N. Prasad, Molecular nonlinear optics: recent advances and applications, Adv. Opt. Photon. **8**, 328–369 (2016)

[57] G. de la Torre, C. G. Claessens, and T. Torres, Phthalocyanines: old dyes, new materials. Putting color in nanotechnology, Chem. Commun. **20**, 2000-2015 (2007).

[58] R. A. Ganeev, M. Suzuki, M. Baba, M. Ichihara, and H. Kuroda, Low- and high-order nonlinear optical properties of Au, Pt, Pd, and Ru nanoparticles, J. Appl. Phys. **103**, 063102 (2008).

[59] B. Gu, W. Ji, and X. Q. Huang, the Analytical expression for femtosecond-pulsed z scans on instantaneous nonlinearity, Appl. Opt. **47(9)**, 1187-1192 (2008).

[60] L. Ma, Y. Zhang, and P. Yuan, Nonlinear optical properties of phenoxy-phthalocyanines at 800nm with femtosecond pulse excitation, Opt. Express **18(17),** 17666–17671 (2010).

[61] J. Yang, C. He, Y. Song, and J. Gu, Concentration-dependent nonlinear refraction in tetrasulfonated copper phthalocyanine solution, J. Opt. A: Pure Appl. Opt. **11,** 065203 (2009).

[62] H. J. Chang, M.J. Shin, and J. W. Wu, Femtosecond Z-scan Measurement of the Third Order Nonlinear Optical Coefficient of CuPc Thin Film, Mol. Cryst. Liq. Cryst. **370**, 127 (2001).

[63] F. Li, P. Lu, H. Long, G. Yang, Y. Li, and Q. Zheng, Nonlinear absorption in CuPc-doped PMMA thin film in the femtosecond regime: Experimental and theoretical studies**,** Opt. Express **16(19),** 14571-14581 (2008).

[64]Y. Chen, M. Hanack, Y. Araki,and O. Ito, Axially modified gallium phthalocyanines and naphthalocyanines for optical limiting, Chem. Soc. Rev. **34(6),** 517–529 (2005).

[65] S. Minissale, S. Yerci, and L. Dal Negro, Nonlinear optical properties of low temperature annealed silicon-rich oxide and silicon rich nitride materials for silicon photonics, Appl. Phys. Lett. 100, 021109 (2012).

[66] K. Ikeda, Robert E. Saperstein, N. Alic, and Y. Fainman, Thermal and Kerr nonlinear properties of plasma-deposited silicon nitride/silicon dioxide waveguides, Opt. Express 16, 12987-12994 (2008).

[67] L. Wang, W. Xie, D. Van Thourhout, Y. Zhang, H. Yu, and S. Wang, Nonlinear silicon nitride waveguides based on a PECVD deposition platform, Opt. Express 26, 9645-9654 (2018).

[68] C. J. Krückel, A. Fulop, T. Klintberg, J. Bengtsson, P. A. Andrekson, and V. Torres-Company, Linear and nonlinear characterization of low-stress high-confinement silicon-rich nitride waveguides, Opt. Express 23(20), 25827–25837 (2015).

[69] M.-C. Tien, J. F. Bauters, M. J. R. Heck, D. J. Blumenthal, and J. E. Bowers, Ultra-low loss Si3N4 waveguides with low nonlinearity and high power handling capability, Opt. Express 18(23), 23562–23568 (2010).

[70] E. L. Falcao-Filho, C. A. C. Bosco, G. S. Maciel, L. H. Acioli, C. B. de Araujo, A. A. Lipovskii, and D. K. Tagantsev, Third-order optical nonlinearity of a transparent glass ceramic containing sodium niobate nanocrystals, Phys. Rev. B **69**, 134204 (2004)

Chapter 4
Nonlinear Optical Properties of Inorganic Semiconductors

Nonlinear optical (NLO) characteristics exhibited by inorganic semiconductors (Manganese (Mn)-doped ZnO) nanorods were investigated with nanosecond pulses utilizing the single beam Z-scan method. The samples were prepared by hydrothermal method. We observed opposite signs of nonlinear absorption (NLA) which primarily depends on Mn-doping concentration in ZnO nanorods. ZnO samples where Mn-doping concentrations are high showed saturable absorption (SA) behavior which could be attributed to change in band gap resonance as well as the creation of defects states. In contrary, we observed two-photon absorption (TPA) features in pure and 0.5% Mn-doped ZnO rods. Nonlinear refraction measurements through closed-aperture (CA) Z-scan technique exhibit negative values of intensity dependent refractive index (n_2) with reasonably high values of the for all the samples. Enhanced NLO response of defect induced by Mn-doping in ZnO nanorods and its stability offer the possibility of applications of those highly stable nanostructures in the area of nonlinear optical devices like optical limiting, saturable absorber, and optical switching.

4.1 Motivation

Various nonlinear optical (NLO) properties in solids have been extensively investigated in large bandgap semiconductor as well as narrow bandgap semiconductors [1,2]. It has been found out that band gap of semiconductors is an important parameter that affects the optical properties [1]. This is because of the fact that optical transitions that lead to the origin of third-order nonlinear properties are directly linked to the eigenstates of an unperturbed optical system [1,3]. These

68

energy eigenstates can be related to the motion of electrons, molecular rotation or molecular vibrations of the optical system [1,2]. It is important to note that the rotational transitions involve the smallest energy separation while the electronic transitions are associated with largest energy separation. In a given optical system, one or more of these transitions may contribute to the NLO response [1].

An important characteristic of semiconductor material is that their allowed eigenstates form broad bands (valence band, conduction band) which are separated by forbidden energy [2]. Valence bands (VB) are the energy bands are called completely filled or nearly filled whereas conduction band (CB) is the highest occupied band and are empty or nearly empty [2]. The energy difference between the highest occupied VB and the lowest occupied CB is known as the bandgap of the semiconductor. The band gap energy is denoted by E_g.
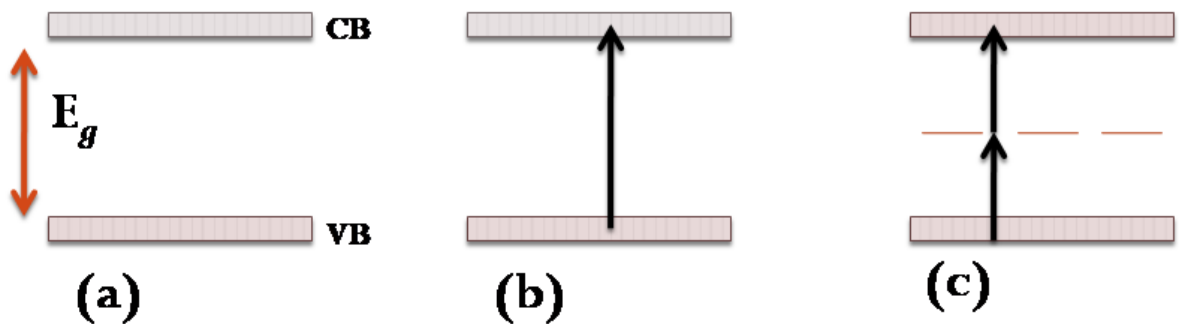
Fig.4.1 (a) Schematic of the band diagram of semiconductors. (b) For photon energy greater than bandgap, the NLO behavior is due to transfer of an electron to the conduction band (c) For photon energy less than bandgap, the NLO behavior involves virtual transitions.

The concepts of VB and CB are illustrated in Fig.4.1. The NLO response in

semiconductors is dictated by the fact that whether photon energy is greater or smaller than the forbidden band gap (E_g) [1,2]. When the energy of the photon (Fig 4.1(b)) is greater than the E_g, the NLO response is due to transfer of valence electrons to the CB. This transfer of electrons to the CB results in higher-order polarizabilities which are the origin of NLO properties of the semiconductor. For the case Fig4.1(c), NLO characteristics are essentially instantaneous and involve a transition between virtual levels [2].

However, in recent years, one of the important aims that the scientific community aspires the possibility to transfer large information, at a fast rate with appreciable accuracy using integrated optical devices [4,5]. In reference to the above-mentioned applications in the field of optoelectronics and photonics e.g. all-optical switching, optical limiting, and saturable absorbers, nanostructured semiconductor materials have been investigated extensively [4-7]. All-optical switching can potentially free us from our dependence on electronic signal processing [4,5]. Therefore, the first motivation behind efficient extraction of nonlinear optical response from semiconductor materials is that they possess very large and easily accessible optical nonlinearities [1,2,7-11]. This is primarily due to strong oscillator strength of semiconductor materials which leads to large NLO response [10,11]. Importantly, the possibility of dispersion engineering of semiconducting species facilitates strong electromagnetic field localization which results in substantial enhancement of the NLO responses [10,11].In addition, semiconducting materials support integrated device realization by virtue of their robust, compact, and compatible features which go hand-in-hand with the existing technology[2].

4.2 Oxide Semiconductor: ZnO

From the perspective of nonlinear optical materials, oxide semiconductor i.e. ZnO has been widely investigated because they exhibit tunable optical properties [10, 11]. We can tune their optical and NLO properties as they provide a means to control their nucleation sites [12,13]. In addition Zinc oxide (ZnO) materials have been an interesting topic of research because they possess a wide (3.4 eV) and direct band gap as well as large exciton binding energy [12,13]. They generally form in the hexagonal crystal structure [12]. An important property of ZnO lattice is the possibility of doping with transition metal ions and 4f-elements which tailor the physical properties significantly. The doping in ZnO is being mainly aimed at the realization of n and p-type conductivity and room temperature magnetic behavior [14]. However in the recent times, linear and NLO characteristics of ZnO-based nanostructured species are topics of significant theoretical and experimental interest [15-20]. This is because of the fact that in comparison to bulk, ZnO nanostructures exhibit enhanced nonlinear effects and fast response time due to material and structural resonance effects [10,11]. ZnO nano and microstructures varying in size can be grown using various methods [12]. The methods employed to prepare such ZnO nanostructures primarily determine their optical, physical as well as chemical characteristics [12]. This is due to the surface morphology and arrangements of ZnO nanoclusters [12,13]. Due to the special features of ZnO nanostructures, various applications like electronic, biomedical and nanophotonics-based on ZnO nanostructures have been demonstrated [21-23]. In addition, ZnO sub-wavelength nanostructures exhibit a number of promising applications like field emission, sensors, UV photonic devices, and piezoelectric nanogenerators [24-28]. For example, optical confinement in ZnO-nanorods leads to improved optical emission properties. Due to this enhanced emission, ZnO rods are

useful in UV lasing [29, 30]. Unequal atomic dimensions of Zn and O results in enhanced NLO response in ZnO. Also due to high inherent polar potentials, ZnO and ZnO based structures show large NLO response [31]. Over the last decade, NLO properties like effective nonlinear absorption coefficients (β_{eff}) and intensity dependent refractive index (n_2) have been investigated in different forms of ZnO. NLR phenomena like self-focusing and self-defocusing have been previously reported for ZnO thin films [32, 33]. However, it was observed that the change from self-focusing to self-defocusing happen only between on- and off-resonant conditions [34, 35].

As mentioned previously, methods employed to prepare the ZnO sample has a direct bearing on it's structural, linear as well as the nonlinear optical properties [10-12]. For example, the bandgap and hence its optical as well as electronic properties can be tuned by defects [36,37]. The intrinsic or extrinsic defects in ZnO directly impact its linear and nonlinear optical properties [10-12]. It is important to note that the effect of intrinsic defects in ZnO cannot be prevented. However, the intrinsic defects in ZnO sample could be minimized depending on the preparation technique [11,12]. Intrinsic defects such as O vacancies and Zn interstitials make ZnO an n-type semiconductor [12]. Unintentionally doped or undoped ZnO exhibit n-type conductivity having large electron densities [12,38]. Irimpan *et al.* clearly demonstrated the role of intrinsic defects or the impact of preparation technique on the NLO properties in ZnO thin films [39]. The authors showed that the ZnO films prepared by pulsed laser ablation and dip-coating exhibit reverse saturable absorption (RSA) while the self-assembled ZnO film exhibit saturable absorption (SA) [39]. In another work, Irimpan *et al.* also investigated the dependence of NLO properties on ZnO nanocolloids [40]. They

showed that nonlinear characteristics are strongly affected by the particle size [40]. The role of extrinsic defects on linear as well as NLO properties have also been investigated in the recent time [41]. Ren *et al.* demonstrated that Nickel (Ni) doping in ZnO nanowires leads to structural and morphology modifications. This leads to enhancement in light emission efficiency [41]. Torres *et al.*, using Z- scan, showed the difference in NLO properties of Ni-doped ZnO films at femtosecond and picosecond time-scale laser pulses. Observed differences in the NLO properties are attributed to the resulting structural and morphology changes linked to the Ni doped-ZnO nanostructures [42].

In the recent years, ZnO nanorods have attracted significant interest for a number of novel device applications [43, 44]. Interest in ZnO nanorods is due to its large lateral surfaces and also it can be prepared by various techniques on a variety of substrates with low defect density [41, 45]. Moreover when doped with transition metals such as Mn, Ni, Cr, ZnO shows enhanced electronic, magnetic and optical properties [41, 46,47]. However, among all transition metal doped ZnO nanostructure, Mn-doping in ZnO is important due to various reasons. [48]. The equilibrium solubility limit of transition metals such as Mn is more than 10 mol % in ZnO [12]. Also, Mn is an isovalent impurity for Zinc and the ionic radius of Mn^{2+} and Zn^{2+} are comparable [49]. Also when doped with transition metals such as Mn, Ni, Cr, it has been demonstrated that ZnO exhibit room-temperature ferromagnetism [48, 49-53]. Therefore Mn-doped ZnO is a suitable material for optoelectronic devices [12, 54]. The ferromagnetic behavior is due to the stable secondary phase of oxygen deficient Mn_xO_y [55]. Ferromagnetic ordering in Mn-doped ZnO nanostructures results in a magnetization-induced change in NLO susceptibilities ($\chi_{ijk}^{(2)}$, $\chi_{ijkl}^{(3)}$ etc.). This change in NLO

susceptibilities is supposed to impact the efficiencies for NLO phenomena like SHG, self-focusing, and self-defocusing [56]. Therefore in view of this, it is necessary to study the dependence of the NLO properties in Mn-doped ZnO nanostructure. We believe that the NLO behavior exhibited by extrinsic defects induced ZnO will differ from bulk ZnO or thin-films [12,56]. However investigations of NLO properties due to Mn doping in ZnO based nanostructures has not yet been done. Therefore in order to ascertain the role of Mn-induced defects as well as geometry, a detailed study of the NLO properties in Mn-doped ZnO nanorods is essential. In this study, we carried out a detailed investigation of the NLO properties for various concentrations of Mn-doping in ZnO nanorods using nanosecond laser. Nonlinear absorption coefficients and intensity dependent refractive-index have been investigated in Mn-doped ZnO nanorods prepared by hydrothermal method [57]. The third-order NLO characteristics of Mn-doped ZnO nanorods were carried out using the Z-scan method with 532 nm wavelength laser in sub-nanosecond regime [58].

4.3 Description of Mn-Doped ZnO Nanorods

In this study, we have carried out NLO characterization for five different kinds of samples prepared by hydrothermal method [59]. All the samples have been prepared by Dr. P. K. Sahoo and A. Singh at School of Physical Sciences, NISER on commercially available 500 nm thick glass substrate which is sputter-coated with indium tin oxide (ITO) layer. In order to prepare Mn-doped ZnO nanorods, the substrates were immersed in an aqueous solution in a Borosil bottle. The solution is made up of 0.5M hexamethylenetetramine (HMTA) , 0.5M Zinc Nitrate hexahydrate, and 0.5%, 1.5%, 2.0%, 2.5% (molar percentage) Manganese chloride tetrahydrate

respectively. All set of the sample was refluxed at 90^0 C on the oven for 6 hours. Then after the Borosil bottles were allowed to cool down up to room temperature. After this samples were thoroughly rinsed in DI water to remove the residual salt and surfactant.

4.4 Experimental Section: Z-scan Method

In order to determine the NLO characteristics, like n_2 and β_{eff} in undoped and Mn-doped ZnO Nanorods, Z-scan method was employed [58]. Our Z-scan set up comprises a Q-switched diode-pumped solid-state (DPSS) laser having 0.7 ns pulse width and can operate at a variable repetition rate (single shot to 100 kHz). DPSS laser deliver 532 nm. The experiment was carried out at 40 Hz repetition rate. This helps us to minimize the thermal contribution to n_2. In order to change the intensity (or power), we used a half wave plate and a polarizing-beam-splitter. A converging lens (f=150mm) was used to focus the beam to a spot size of $w_0 \approx$ 45μm. This results in a Rayleigh length ($z_0 = \pi w_0^2/\lambda$) of $\approx$ 12 mm. The Mn-doped ZnO nanorods samples were translated 100 mm along the z-axis of the beam. The transmitted power through the samples was measured using fast photodetector (Model S120C; Thorlabs Inc.) in both the Z-scan configuration.

4.5 NLO Measurements in Mn-Doped ZnO Nanorods

In most general and simple case, the NLO properties like NLA and NLR in an optical system is the interaction of two different light beams [1-3]. During the interaction, if two light beams can change their phase, then it is referred to as NLR, whereas if there is an amplitude change due to the interaction, then it is called NLA [58]. It is important to mention that NLA phenomena take place only if there is certain energy resonance condition [2]. Since the discovery of nonlinear optics, the NLO properties of semiconductors are investigated and continue to be studied and investigated

because of its importance in optical technologies [60]. Due to the fact that semiconductors are efficient for light emission and detection, they can be applied in optical technologies for manipulating signals and short pulse production [1-3]. Here, we concentrate on the NLO behavior of Mn-doped ZnO nanorods in the transparency region. In other words, we have investigated the NLA and NLR of Mn-doped ZnO nanorods with laser pulses having energy below the bandgap energy of the optical system. In the transparency region, the nonlinear response is due to the bound electronic nonlinearities or the free carrier created by two-photon absorption [2,61,62]. In this case, the response time of the optical nonlinearity is very fast which is dictated by the virtual lifetime of the relevant transitions and can be treated as instantaneous [1].

4.5.1 OA Z-scan Measurements

OA Z-scan is used to determine the NLA coefficient of the nonlinear medium [1,58]. NLA correspond to the imaginary part of third-order susceptibility [58]. As the name suggests, NLA leads to depletion of the laser beam due to absorption by means of two-photon absorption (TPA) or multiphoton absorption (MPA). It has been demonstrated that NLA phenomena like TPA or MPA, results in suppression of the peak and enhancement of valley in the CA Z-scan measurement [58]. However, NLA phenomena like saturable absorption (SA), suppress the valley and enhance the peak in the CA Z-scan measurement. In order to determine the effective NLA coefficient (β_{eff}) of undoped and Mn-doped ZnO nanorods, we have performed OA measurements at incident on-axis laser intensity of $\approx$ 1-3 GW/cm^2. Figs 4.1 (a-d) shows the representative experimental traces showing NLA (SA and TPA) for the OA Z-scan measurements for Mn-doped ZnO rods with 532 nm nanosecond laser pulses.
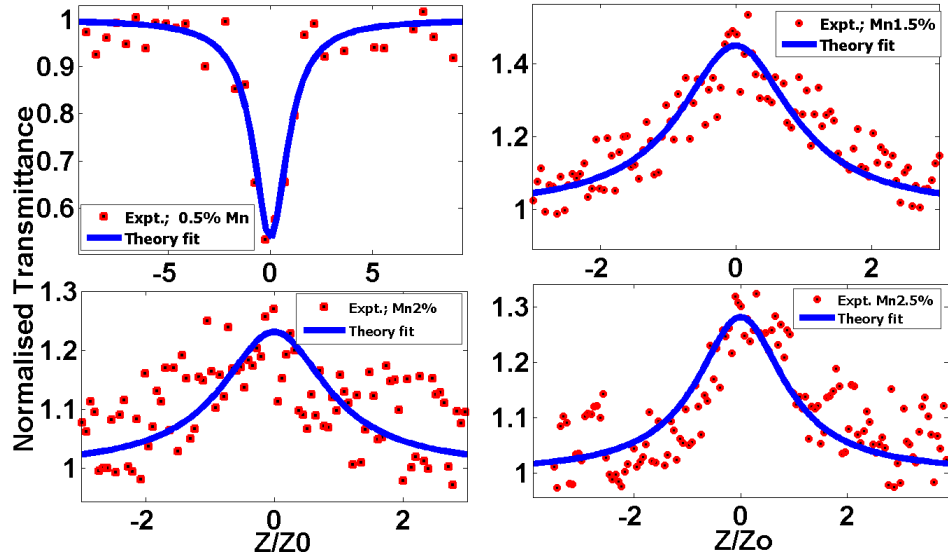
Fig.4.2 Open Aperture Z-scan traces for varying Mn-doping concentration in ZnO rods with 532 nm wavelength and 0.7 ns pulses.

We can observe from the height of the peak and dip in the OA Z-scan experimental data (Fig. 4.2 (a-d)) that all the four ZnO samples exhibit a clear dependence on the Mn doping concentrations. As evident from Fig. 4.2 (a), OA Z-scan traces for 0.5 % Mn-doped ZnO rods exhibit a transmission drop (dip) at the focal plane (z=0). The dip at the focal plane in OA Z-scan data indicate that 0.5 % Mn-doped ZnO rods have a positive value of effective nonlinear absorption (β_{eff}). However, it is interesting to note from Fig. 4.2 (b), (c) and (d), that OA Z-scan features observed in the higher concentration of Mn-doping in ZnO rods exhibit a peak at the focal plane (z = 0). Therefore, higher Mn-doping concentrations in ZnO nanorods results in saturable absorption (SA). This behavior of SA at 532 nm is yet to be observed prior to this work, in case of ZnO or any other metal doped ZnO nanostructures. For comparison, we also performed the OA Z-scan experimental data for pure ZnO samples. The OA measurements for pure ZnO nanorods also reveal the positive value of effective nonlinear absorption coefficients (β_{eff}). Also to determine the impact of the substrate,

we have performed OA Z-scan transmission of the substrate at similar laser fluence. We observe that Z-scan normalized transmittance exhibited negligibly weak variation; therefore, we can say that there is a negligible contribution from the substrate. In order to determine the effective nonlinear absorption coefficient, the OA Z-scan experimental data were fitted using the relation 2.10 [58].

Table 4.1 Effective NLA coefficients (β_{eff}) of doped and undoped ZnO samples.

Sample	β_{eff} (cm/W)	Laser Parameters: Wavelength (λ), Pulse width (FWHM)	References
ZnO Thin films	4.20×10^{-9}	532nm; 25 ps	[63]ref.
ZnO Thin films	-1.53×10^{-7}	830nm; 175fs	[64]ref.
ZnO Nanorods	5.61×10^{-6}	815nm; 85fs	[65]ref.
ZnO Thin films	-0.61×10^{-6}	815nm; 85fs	[66]ref.
ZnO Nanorods	5.90×10^{-7}	800nm; 130fs	[67]ref
ZnO Nanorods	3.5×10^{-5}	532 nm; 0.7 ns	Thesis work
0.5% Mn Conc. in ZnO nanorods	1.32×10^{-5}	532nm; 0.7ns	Thesis work
1.5% Mn Conc. in ZnO Nanorods	-1.03×10^{-5}	532nm; 0.7ns	Thesis work
2% Mn Conc. in ZnO Nanorods	-4.17×10^{-6}	532 nm; 0.7ns	Thesis work
2.5% Mn Conc. inZnO Nanorods	-5.45×10^{-6}	532nm; 0.7ns	Thesis work

Our NLO investigation revealed that the nonlinear absorption coefficient values as well their sign differ widely in comparison with the most of previously reported values as shown in table 4.1. As observed in table 4.1, there is an inconsistency with respect to the sign of β_{eff} in ZnO thin films. However, it is clear that the β_{eff} values for the ZnO rods doped with Mn exhibits an enhancement in values compared to previously reported values for ZnO thin-films and rods. In order to understand this weak nonlinear absorption coefficient, we note down the observation made by Schmidt-Grund *et al.*[67]. The authors report that doping process leads to change in the energy states of the ZnO samples and sometimes even there is a red shift of the bandgap [63,68]. On comparing our linear absorption data, we do observe that there is a shift in the optical resonance as well as the generation of defect states in Mn-doped ZnO nanorods [69]. This condition of a shift in optical resonance is the potential cause for the observed weak nonlinear absorption leading to SA behavior in higher Mn-doped ZnO rods.

This variation in NLO properties of Mn-doped ZnO or any other doped semiconductors could also be caused by the modifications in the band structure, morphology as well as structural arrangement [67,68]. Therefore, the observed peaks in OA Z-scan normalized transmittance (Figs. 4.1(b-d)) which indicate a weak nonlinear absorption or SA behavior could be attributed to modification in the energy eigenstates as well as a shift in the band-edges (or bandgap) in ZnO nanorods. In other words, the non-availability of unoccupied states at high irradiance in higher concentration doped ZnO results in weakening of nonlinear optical absorption. As a consequence, the expected TPA behavior for pure ZnO nanorods and that for 0.5%

Mn-doped ZnO rod are completely suppressed and taken over by a peak in the OA transmission which characterizes SA behavior.

We would also like to mention that the difference in the nonlinear coefficients (Table 4.1) could also be due to the difference in the pulse width or due to thermal effects in previous results. Generally, the nonlinear coefficients in the materials depend upon a number of factors like wavelength, pulse duration, repetition rate and peak power of the laser pulse. Generally the study of NLO coefficients with different laser pulses and wavelength help us to determine the physical nature of the nonlinearities as optical nonlinearities due to excited states and two photon absorption etc. will behave differently for different pulse widths.

4.5.2 CA Z-scan Measurements

As discussed in chapter 2 and 3, CA Z- scan is used to study the NLR properties of the nonlinear medium. The n_2 corresponds to the real part of $\chi^{(3)}$ [1,58,70]. In order to determine the nonlinear refractive index (n_2) of the ZnO rods having different Mn concentration, we have carried out the CA Z-scan measurements with nanosecond laser pulses. Measurements were carried out at a peak laser intensity of $\approx$ 1-3 GW/cm^2. Fig 4.3 (a-d) shows the representative experimentally measured traces showing NLR as observed in the CA Z-scan when done with 532 nm nanosecond laser pulses. It is evident that the CA Z-scan experimental data Mn-doped ZnO nanorods (Fig 4.3(a-d)) are characterized by pre-focal maxima and post-focal minima which is a signature of negative value for the nonlinear refractive index (n_2). For understanding the mechanism behind such an NLR behavior and making a comparison, we also
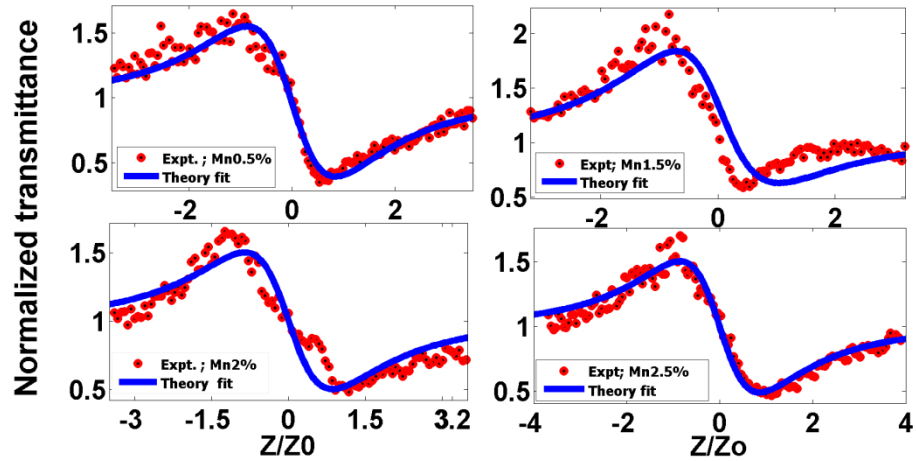
Fig. 4.3 CA Z-scan curve for varying Mn-doping concentration in ZnO nanorods with 532 nm and 0.7 ns pulses.

performed the CA Z-scan transmission of undoped ZnO rods at 532 nm which have a similar pattern as that for Mn-doped ZnO nanorods [69].

In order to determine the n_2, the CA Z-scan data was fitted using the standard relation 2.16 [58]. The NLR results are presented in table-4.2 for various ZnO samples. It is evident from our investigations that all the samples of ZnO nanorods, exhibit the self-defocusing effect. Also, our investigation reveals that the nonlinear refractive index values are an order of magnitude higher as compared to ZnO thin-films. This enhancement in n_2 values could be attributed to the modifications in the morphology and geometrical arrangements. In addition, the alteration in the electronic bandgap has an important bearing on n_2 value measurement [67,68,71].

It is worthwhile to mention that, there exists a Fabry-Perot-like localized resonance in the samples. This is because the end faces of the ZnO nanorods are optically flat and therefore the nanorods or nanowires act as a cylindrical optical cavity. As the optically flat and parallel end faces of the nanorods provides requisite optical feedback for a resonant cavity and hence the ZnO nanorods are analogous to macroscale Fabry-

81

Perot resonators [72-76]. Also ZnO has high refractive index (2.45) which causes more efficient total internal reflection in the ZnO nano/micro configurations resulting in the local field enhancement [73, 77]. Therefore, the factors such as Fabry perot resonances which facilitates field localization as well as quantum confinement could possibly lead to increase in the measured values for n_2.

Table 4.2 Summary of n_2 values of Mn-doped and undoped ZnO samples.

Sample	n_2 (cm^2/W)	Laser Parameters: Wavelength (λ), Pulse width (FWHM)	References
ZnO thin films	-0.90×10^{-14}	532nm; 25 ps	[63]ref.
ZnO thin films	2.57×10^{-11}	830nm; 175fs	[64]ref.
ZnO Nanorods	3.11×10^{-10}	815nm; 85fs	[65]ref.
ZnO thin films	5.57×10^{-11}	815nm; 85fs	[66]ref.
ZnO Nanorods	2.1×10^{-10}	532 nm; 0.7 ns	This work
0.5% Mn in ZnO Nanorods	-1.88×10^{-10}	532nm; 0.7ns	Thesis work
1.5% Mn in ZnO Nanorods	-1.59×10^{-10}	532nm; 0.7ns	Thesis work
2% Mn in ZnO Nanorods	-1.25×10^{-10}	532 nm; 0.7ns	Thesis work
2.5% Mn in ZnO Nanorods	-1.34×10^{-10}	532nm; 0.7ns	Thesis work

4.6 Summary

In this chapter, I have presented the impact of Mn-doping on NLO properties in ZnO nanorods. The motivation behind this study is to show that NLO properties are

strongly influenced by the geometrical arrangements as well as modification in the energy eigenstates of a doped species. Such an assertion is based on the fact that the electronic bandgap in semiconductors, which is determined by energy eigenspectrum of ZnO nanorod variant, primarily determines the NLO response. A clear impact on the NLO properties with Mn-doping concentration was observed in ZnO nanorods. The change from TPA to SA absorption with Mn-doping in ZnO could be attributed to modifications in structure, morphology, and shift of optical resonance. In pure and 0.5 % Mn-doped ZnO rods, strong TPA behavior was observed. In CA Z-scan measurements, all the samples with different Mn-doping concentration exhibited self-defocusing. In addition, the n_2 values have been significantly high as compared to ZnO thin films. The nanostructured morphology of ZnO and the associated alterations the same due to Mn-doping ought to be the cause of variation in linear and NLO properties. The enhancement in NLR by the sample has the potential application for all-optical switching. Additionally, the SA behavior exhibited by strongly-doped ZnO nanorods could find widespread applicability for mode-locking in ultrashort pulse generation.

Bibliography

[1] M. Sheik-Bahae and M. P. Hasselbeck, Third-order optical nonlinearities, in OSA Handbook of Optics, (McGraw-Hill2001), Vol. IV, Chap. 17.

[2] R. W. Boyd. *Nonlinear Optics*. Academic Press, second edition, 2003.

[3] M. Sheik-Bahae and E. W. Van Stryland, Optical nonlinearities in the transparency region of bulk semiconductors, in Nonlinear Optics in Semiconductors I, vol. 58,

Semiconductors and Semimetals, E. Garmire and A. Kost, Eds.: Academic Press, 1999, pp. 257-318.

[4] H. M. Gibbs, *Optical bistability: controlling light with light*. Orlando: Academic Press,1985.

[5] M. N. Islam, *Ultrafast fiber switching devices and systems*. Cambridge England; New York, NY, USA: Cambridge University Press, 1992.

[6] E. W. Van Stryland, Y. Y. Wu, D. J. Hagan, M. J. Soileau, and K. Mansour, Optical limiting with semiconductors, J. Opt. Soc. Am. B **5**, 1980-1988 (1988).

[7] M. Haiml, R. Grange, and U. Keller, Optical characterization of semiconductor saturable absorbers, Appl. Phys. B **79**, 331–339 (2004).

[8] B. S. Wherrett, A. C. Walker, and F. A. P. Tooley, Nonlinear refraction for CW optical bistability, in *Optical nonlinearities and instabilities in semiconductors*, H. Haug, Ed. Boston: Academic Press, 1988.

 [9] A. Miller, D. A. B. Miller, and S. D. Smith, Dynamic Non-Linear Optical Processes in Semiconductors, Advances in Physics **30**, 697-800 (1981).

[10] H. Morkoc and U. Ozgur, Zinc oxide: fundamentals, materials and device technology, WILEY-VCH Verlag GmbH & Co. KGaA, Weinheim, 2009.

[11] A. B. Djurisic and Y. H. Leung, Optical properties of ZnO nanostructures, Small 2, 944–961 (2006).

[12] U. Ozgur, Y. I. Alivov, C. Liu, A. Teke, M. A. Reshchikov, S. Doğan, V. Avrutin, S.-J. Cho, and H. Morkoç, A comprehensive review of ZnO materials and devices, J. Appl. Phys. **98**(4), 041301 (2005).

[13] E. Fortunato, A. Gonçalves, A. Pimentel, P. Barquinha, G. Gonçalves, L. Pereira, I. Ferreira, and R. Martins, Zinc oxide, a multifunctional material: from material to device applications, Appl. Phys., A Mater. Sci. Process. **96**(1), 197–205 (2009).

[14] M. S. R. Rao and T. Okada, *ZnO Nanocrystals and Allied Materials* (Springer, 2014).

[15] V. M. Axt and S. Mukamel, Nonlinear optics of semiconductor and molecular nanostructures; a common perspective, Rev. Mod. Phys. **70**, 145 (1998).

[16] Y. Kayanuma, Quantum-size effects of interacting electrons and holes in semiconductor microcrystals with a spherical shape, Phys. Rev. B **38**, 9797 (1988).

[17] S. T. Tan, B. J. Chen, X. W. Sun, W. J. Fan, H. S. Kwok, X. H. Zhang, and S. J. Chua, Blueshift of the optical band gap in ZnO thin films grown by metal-organic chemical vapor deposition, J. Appl. Phys. **98**, 013505 (2005).

[18] K. K. Nagaraja, S. Pramodini, A. Santhosh Kumar, H. S. Nagaraja, P. Poornesh, and D. Kekuda, Third-order nonlinear optical properties of Mn-doped ZnO thin films under CW laser illumination, Opt. Mater. **35**, 431 (2013).

[19] J. H. Lin, Y. J. Chen, H. Y. Lin, and W. F. Hsieh, Two-photon resonance assisted huge nonlinear refraction and absorption in ZnO thin films, J. Appl. Phys. **97**, 033526 (2005).

[20] Y. P. Chan, J. H. Lin, C. C. Hsu, W. F. Hsieh, Near-resonant high order nonlinear absorption of ZnO thin films, Optics Express **16** (24), 19900-19908(2008).

[21] B. Claflin, D. C. Look, and D. R. Norton, Changes in electrical characteristics of ZnO thin films due to environmental factors, J. Electron. Mater. **36**(4), 442–445 (2007).

[22] J. W. Rasmussen, E. Martinez, P. Louka, and D. G. Wingett, Zinc oxide

nanoparticles for selective destruction of tumor cells and potential for drug delivery applications, Expert Opin. Drug Deliv. **7**(9), 1063–1077 (2010).

[23] S. John, S. Marpu, J. Li, M. Omary, Z. Hu, Y. Fujita, and A. Neogi, Hybrid zinc oxide nanoparticles for biophotonics, J. Nanosci. Nanotechnol. **10**(3), 1707–1712 (2010).

[24] M. H. Koch, P. Y. Timbrell and R. N. Lamb, The influence of film crystallinity on the coupling efficiency of ZnO optical modulator waveguides, Semicond. Sci. Technol. **10,** 1523–1527(1995).

[25] Y. W. Zhu, H. Z. Zhang, X. C. Sun, S. Q. Feng, J. Xu, Q. Zhao, B. Xiang, R. M. Wang and D. P. Yua, Enhanced field emission from ZnO nanorods via thermal annealing in oxygen, Appl. Phys. Lett. **83**, 144–146 (2003).

[26] C. J. Lee, T. J. Lee, S. C. Lyu, Y. Zhang, H. Ruh and H. J. Lee, Field emission from well-aligned zinc oxide nanowires grown at low temperature, Appl. Phys. Lett. **81**, 3648–3650 (2002).

[27] T. Gao and T. H. Wang, Synthesis and properties of multipod-shaped ZnO nanorods for gas-sensor applications, Appl. Phys. An **80**, 1451–1454 (2005).

[28] Z. L. Wang and J. Song, Piezoelectric nanogenerators based on zinc oxide nanowire arrays, Science **312**, 242–246 (2006).

[29] Z. Fan, D. Dutta, C. J. Chien, H. Y. Chen, E. C. Brown, P. C. Chang and J. G. Lu, Electrical and photoconductive properties of vertical ZnO nanowires in high-density arrays, Appl. Phys. Lett. **89**, 213110 (2006).

[30] Y. C. Kong, D. P. Yu, B. Zhang, W. Fang and S. Q. Feng, Ultraviolet-emitting ZnO nanowires synthesized by a physical vapor deposition approach, Appl. Phys. Lett. **78**, 407–409 (2001).

[31] B. F. Levine, A New Contribution to the Nonlinear Optical Susceptibility Arising from Unequal Atomic Radii, Phys. Rev. Lett. **25**, 440–443(1970).

[32] B. E. Urban, J. Lin, O. Kumar, K. Senthilkumar, Y. Fujita, and A. Neogi, Optimization of nonlinear optical properties of ZnO micro and nanocrystals for biophotonics, Opt. Mater. Express **1**(4), 658–669 (2011).

[33] A. I. Ryasnyanskiy, B. Palpant, S. Debrus, U. Pal, and A. L. Stepanov, Optical nonlinearities of Au nanoparticles embedded in a zinc oxide matrix, Opt. Commun. **273**(2), 538–543 (2007).

[34] P. Bermel, A. Rodriguez, J. D. Joannopoulos, and M. Soljacić, Tailoring optical nonlinearities via the Purcell effect, Phys. Rev. Lett. **99**(5), 053601 (2007).

[35] V. Yannopapas, Enhancement of nonlinear susceptibilities near plasmonic metamaterials, Opt. Commun. **283**(8), 1647–1649 (2010).

[36] B. E. Sernelius, K. F. Berggren, Z.-C. Jin, I. Hamberg and C. G. Granqvist, Band-gap tailoring of ZnO by means of heavy Al doping, Phys. Rev. B: Condens. Matter Mater. Phys. **37**, 10244 (1988).

[37] A. G. Ali, F. B. Dejene and H. C. Swart, Effect of Mn doping on the structural and optical properties of sol-gel derived ZnO nanoparticles, Cent. Eur. J. Phys. **10**(2), 478–484 (2012).

[38] T. Minami, H. Sato, H. Nanto, and S. Takata, Optical Properties of Aluminum Doped Zinc Oxide Thin Films Prepared by RF Magnetron Sputtering, Jpn. J. Appl. Phys., Part 2 **24**, L781 (1985).

[39] L. Irimpan, A. Deepthy, Bindu Krishnan, L. M. Kukreja, V. P. N. Nampoori, and P. Radhakrishnan, Effect of self-assembly on the nonlinear optical characteristics of ZnO thin films, Opt. Commun. **281(10)**, 2938-2943(2008).

[40] L. Irimpan, V. P. N. Nampoori, and P. Radhakrishnan, Size-dependent enhancement of nonlinear optical properties in nanocolloids of ZnO, J. Appl. Phys. **103**, 033105 (2008).

[41] Q. J. Ren, S. Filippov, S. L. Chen, M. Devika, N. Koteeswara Reddy, C. W. Tu, W. M. Chen, and I. A.Buyanova, Evidence for coupling between exciton emissions and surface plasmon in Ni-coated ZnOnanowires, Nanotechnology **23**(42), 425201 (2012).

[42] C. Torres-Torres, B. A. Can-Uc, R. Rangel-Rojo, L. Castañeda, R. Torres-Martinez, C. I. García-Gil, and A. V. Khomenko, Optical Kerr phase shift in a nanostructured nickel-doped zinc oxide thin solid film, Opt. Express **21**, 21357 (2013).

[43] C. C. Yi, C. Wang, and W. I. Park, ZnO nanorods: synthesis, characterization and applications, Semicond. Sci. Technol. **20**, S22 (2005).

[44] Y. Y. Zhang, M. K. Ram, E. K. Stefanakos, and D. Y. Goswami, Synthesis, Characterization, and Applications of ZnO Nanowires, J. Nanomater **624520**, 2012(2012).

[45] I. C. Robin, B. Gauron, P. Ferret, C. Tavares, and G. Feuillet, Evidence for low density of nonradiative defects in ZnO nanowires grown by metal organic vapor-phase epitaxy, Appl. Phys. Lett. **91**, 143120 (2007).

[46] T. Dietl, H. Ohno, F. Matsukura, J. Cibert, and D. Ferrand, Zener Model Description of Ferromagnetism in Zinc-Blende Magnetic Semiconductors, Science **287**, 1019 (2000).

[47] Y. J B *et al.*, Ferromagnetism in Dilute Magnetic Semiconductors through Defect Engineering: Li-Doped ZnO, Phys. Rev. Lett. **104**, 137201(2010).

[48] Y. S. Wang, P. J. Thomas and P. O'Brien, Optical Properties of ZnO Nanocrystals Doped with Cd, Mg, Mn, and Fe Ions, J. Phys. Chem. B **110**, 21412–21415 (2006).

[49] R. K. Sharma, S. Patel, and K. C. Pargaien, Synthesis, characterization and properties of Mn-doped ZnO nanocrystals, Adv. Nat. Sci.: Nanosci. Nanotechnol. **3**, 035005 (2012).

[50] J. R. Neal, A. J. Behan, R. M. Ibrahim, H. J. Blythe, M. Ziese, A. M. Fox, and G. A. Gehring, RoomTemperature Magneto-Optics of Ferromagnetic Transition-Metal-Doped ZnO Thin Films, Phys. Rev. Lett. **96**(19), 197208 (2006).

[51] A. C. Mofor, A. El-Shaer, A. Bakin, A. Waag, H. Ahlers, U. Siegner, S. Sievers, M. Albrecht, W. Schoch, N. Izyumskaya, V. Avrutin, S. Sorokin, S. Ivanov, and J. Stoimenos, Magnetic property investigations on Mn-doped ZnO Layers on sapphire, Appl. Phys. Lett. **87**(6), 062501 (2005).

[52] W. Yan, Z. Sun, Q. Liu, Z. Li, Z. Pan, J. Wang, S. Wei, D. Wang, Y. Zhou, and X. Zhang, Zn vacancy induced room-temperature ferromagnetism in Mn-doped ZnO, Appl. Phys. Lett. **91(6)**, 062113 (2007).

[53] B. B. Straumal, S. G. Protasova, A. A. Mazilkin, A. A. Myatiev, P. B. Straumal, G. Schütz, E. Goering, and B. Baretzky, Ferromagnetic properties of the Mn-doped nanograined ZnO films, J. Appl. Phys. **108**(7), 073923 (2010).

[54] H. Y. Peng, G. P. Li, J. Y. Ye, Z. P. Wei, Z. Zhang, D. D. Wang, G. Z. Xing, and T. Wu, Electrode dependence of resistive switching in Mn-doped ZnO: Filamentary versus interfacial mechanisms, Appl. Phys. Lett. **96**(19), 192113 (2010).

[55] D. C. Kundaliya *et al.*, On the origin of high-temperature ferromagnetism in the low-temperature-processed Mn-Zn-O system, Nat. Mater. **3**, 709–714 (2004).

[56] J. S. Miller and M. Drillon, Magnetism: Molecules to materials V, WILEY-VCH Verlag GmbH & Co. KGaA, Weinheim, 43–44 (2005).

[57] J. B. Cui, C. P. Daghlian, U. J. Gibson, R. Pusche, P. Geithner and L. Ley, Low-temperature growth and field emission of ZnO nanowire arrays, J. Appl. Phys. **97**, 044315 (2005).

[58] M. Sheik-Bahae, A. A. Said, T.-H. Wei, D. J. Hagan and E. W. Van Stryland, Sensitive measurement of optical nonlinearities using a single beam, IEEE J. Quantum Electron. **26**, 760–769 (1990).

[59] A Singh, K Senapati, B Satpati, M Kumar, PK Sahoo, Nanoscale interface engineering in ZnO twin nanorods for proposed phonon tunnel devices, Physical Chemistry Chemical Physics **17** (6), 4277-4282(2015).

[60] Elsa Garmire, Nonlinear optics in daily life, Opt. Express 21, 30532-30544 (2013)

[61] M. Sheik-Bahae and E. W. Van Stryland, Optical nonlinearities in the transparency region of bulk semiconductors, in Nonlinear Optics in Semiconductors I, E. Garmire and A. Kost, Eds., Semiconductors and Semimetals, vol. 58 (Academic, Boston, 1999).

[62] A. A. Said, M. Sheik-Bahae, D. J. Hagan, T. Wei, J. Wang, J. Young, and E. W. Van Stryland, Determination of bound-electronic and free-carrier nonlinearities in ZnSe, GaAs, CdTe, and ZnTe, J. Opt. Soc. Am. B 9, 405 (1992).

[63] X. Zhang, H. Fang, S. Tang and W. Ji, Determination of two-photon-generated free-carrier lifetime in semiconductors by a single-beam Z-scan technique, Appl. Phys. B: Lasers Opt. **65**, 549–554(1997).

[64] J. H. Lin, Y. J. Chen, H. Y. Lin and W. Hsieh, Two-photon resonance assisted huge nonlinear refraction and absorption in ZnO thin films, J. Appl. Phys. **97**, 033526 (2005).

[65] H. W. Lee, K. M. Lee, S. Lee, K. H. Koh, J. Y. Park, K. Kim and F. Rotermund, Ultrafast third-order optical nonlinearities of vertically-aligned ZnO nanorods, Chem. Phys. Lett. **447**, 86–90 (2007).

[66] S. K. Min, C.-H. Oh, G. J. Lee, Y. P. Lee, S. K. Min and S. H. Han, Nonlinear Optical Properties of ZnO Nanorods Prepared by Using the Electro-deposition Method, J. Korean Phys. Soc. **55**, 1005–1008 (2009).

[67] R. Schmidt-Grund, N. Ashkenov, M. M. Schubert, W. Czakai, D. Faltermeier, G. Benndorf, H. Hochmuth, M. Lorenz, and M. Grundmann, Temperature-dependence of the refractive index and the optical transitions at the fundamental band-gap of ZnO, Phys. of Semicond. 28th Int. Conf. 271–272 (2007).

[68]P. Pushparajah, A. K. Arof and S. Radhakrishna, Physical properties of spray pyrolyzed pure and doped ZnO thin films, J. Phys. D Appl. Phys. **27**(7), 1518–1521 (1994).

[69] A. Singh, S. Kumar, R. Das, and P. K. Sahoo, Defect-assisted saturable absorption characteristics in Mn-doped ZnO nano-rods RSC Adv. **5**, 88767 (2015).

[70] D. N. Christodoulides, I. C. Khoo, G. J. Salamo, G. I. Stegeman, and E. W. Van Stryland, Nonlinear refraction and absorption: mechanisms and magnitudes, Adv. Opt. Photon. **2(1),** 60-200 (2010).

[71] C. Torres-Torres, M. Trejo-Valdez, H. Sobral, P. Santiago- Jacinto and J. A. Reyes-Esqueda, Stimulated Emission and Optical Third-Order Nonlinearity in Li-Doped ZnO Nanorods**,** J. Phys. Chem. C **113**, 13515–13521 (2009).

[72] R. Hauschild *et al.*, Stimulated emission from ZnO nanorods, phys. stat. sol. **243**, 853–857 (2006).

[73] Y. Chen and Y. Chen, Enhanced random lasing in ZnO nanocombs assisted by Fabry–Perot resonance, Opt. Express **19**, 8728-8734 (2011)

[74] H. Dong, B. Zhou, J. Li, J. Zhan, L. Zhang, Ultraviolet lasing behavior in ZnO optical microcavities, Journal of Materiomics **3**, 255-266(2017).

[75] J. C Johnson, H. Yan, P. Yang, and R. J. Saykally, Optical cavity effects in ZnO nanowire lasers and waveguides. J. Phys. Chem. B **107**, 8816–8828 (2003).

[76] X. H. Wu, A. Yamilov, H. Noh, H. Cao, E. W. Seelig, and R. P. H. Chang, Random lasing in closely packed resonant scatterers, J. Opt. Soc. Am. B **21**(1), 159–167 (2004).

[77] S. Arab, P. D. Anderson, M. Yao, C. Zhou, P. D. Dapkus, M. L. Povinelli and S. B. Cronin, Enhanced Fabry-Perot resonance in GaAs nanowires through local field enhancement and surface passivation**,** Nano Res. **7(8)**, 1146–1153 (2014).

Chapter 5
Controlling Light-Matter Interactions in Periodically

Stratified Media

In this chapter, I theoretically and experimentally discuss a novel scheme for controlling light-matter interactions in a periodically stratified media. The idea is executed through excitation of optical Tamm plasmon (OTP), a kind of surface waves that exits at the boundary of a distributed-Bragg-reflector (DBR) and a thin plasmon-active metal layer. The polaritonic behavior of an OTP mode allows an alternative nomenclature as Tamm plasmon polariton (TPP) mode. A brief introduction of OTP mode properties in the metal-DBR planar structure is discussed which is followed by a review of the present status of OTP modes. In the subsequent section, I focus on optimizing the structural parameters so as to tune the quality factor of the OTP modes. The third section describes the utility of hybrid-OTP for refractive index sensor. In the final section, I explore the possibility of OTP modes in the planar structure being employed for temperature sensing. In this chapter, all the theoretical analysis has been carried out by employing standard transfer matrix method for a planar configuration.

5.1 Optical Tamm Plasmon Modes and Its State of Art

Igor Tamm in 1932 proposed an electronic state confined at the surface of crystalline solids called Tamm states [1]. An optical analog of Tamm states was proposed in 2007 by Kaliteevski *et al.* where electron potential was replaced by the Distributed Bragg reflector or periodically stratified medium [2]. Subsequently, in 2008, Sasin *et al.* experimentally showed the presence of optical Tamm plasmon (OTP) states [3]. These OTP modes are an electromagnetic surface mode that exists at the boundary of distributed Bragg reflector (DBR) and a plasmon-active metal layer or at the interface

between two DBR having overlapping stop bands [2,4]. The confinement of this surface electromagnetic field is due to the negative dielectric constant of metal and the stop band of the DBR [2]. However, the confinement in the Bragg mirror is not because of total internal reflection (TIR) but a consequence of photonic stop band arising from the periodicity of multilayer dielectric structure. These OTP modes are also called Tamm plasmons polaritons (TPPs). They possess interesting features which make them useful for various applications. These TPP modes are interface states which display maximum field at the metal-dielectric interface and therefore exhibits confined field enhancement [3]. TPPs modes exhibit following characteristics

- ❖ TPPs are excited inside the band gaps of photonic crystals and dispersion curve is parabolic in nature.

- ❖ In comparison to conventional surface plasmon (SP) modes, TPP modes exist for both the polarization i.e. transverse electric (TE) and transverse magnetic (TM) [5-7].

- ❖ The separation between the TE and TM polarizations varies quadratically with the in-plane k vector.

- ❖ Complex architectures like prisms or gratings are not needed for exciting TPP modes [2]. This is due to the fact that TPPs in-plane k vector is close to zero and therefore can be excited directly.

- ❖ TPP mode excitation is possible using normal as well as oblique illumination. [8].

- ❖ TPPs modes resonance wavelength depends on a number of factors like the metal thickness, the thickness of dielectric adjacent to metal, metal types [9, 10].

Recently, activity in study associated with TPP modes has increased because of a number of applications. Present state of art of TPP modes includes a number of applications like coupling of surface waves to TPP modes [11], TTP based lasers [12,13], Optical nonlinear study using TPP modes [14], light trapping [15], all-optical switching [16] and sensing [17, 18] which have been suggested and observed experimentally. There are quite a few studies which focus on enhancing the fluorescence using TPP coupled emissions [9]. R Badagua *et al.* have carried out extensive studies in this area of fluorescence modification in materials using TPP modes [19, 20].

TPP mode has been of significant interest in the field of nonlinear optics. Afinogenov *et al.* demonstrated enhancement of SHG intensity due to excitation of TPPs modes [21]. Lee *et al.* in their recent study proposed enhanced NLO effects due to TPPs in 1-dimensional photonic crystal (DBR) structures [14]. Their results implied that very surface-enhanced Raman scattering signals can be enhanced and NLO effects could be observed with much lower threshold light intensities. In the field of NLO, Xue *et al.* theoretically investigated enhanced third-harmonic generation (THG) in the heterostructure with a DBR and a thick metal film [22]. Nonlinear Tamm states are proposed in layered metal-dielectric metamaterials by Iorsh *et al.* in 2011 [23]. Gubaydullin *et al.* in their recent work demonstrated the enhancement in the probability of spontaneous emission due to excitation of TPPs modes [24]. Recently Shukla *et al.* proposed the excitation of TPP modes in one-dimensional quasi-periodic photonic crystal [25]. Very recently, quite a few investigations have been aimed at the possibility of inter-modal coupling between surface plasmons and TPP modes [26-27]. The strong coupling between the TPP and surface plasmon modes have been

demonstrated as an anti-crossing behavior in their dispersion relations. The utility of conventional TPP modes and hybrid TPP modes in a sensing application has also been reported theoretically as well as demonstrated experimentally [17, 18, 28]. Single photon emission is also possible using TPP structures [29]. Recently, Li *et al.* demonstrated the concept of planar hot-electron photodetector utilizing the concept of TPPs with a DBR, a Schottky junction, and metal layer. The structure shows enhanced cavity coupling and TPPs resonance and therefore light-trapping efficiency could be enhanced manifolds [30]. Fang *et. al.* studied the characteristics of the coupled states of SPPs, magnetic-defect and TPPs modes for a system of semi-infinite DBR having metal and magneto-optical films [31]. The authors showed that the dispersion properties of SPPs mode are strongly influenced by the magnetic-defect states and TPPs modes. Also, the influence on SPPs due to the presence of magnetic-defect states get enhanced by the hybrid coupled states resonances. Fang *et. al* also employed TMM to understand the surface modes properties in semi-infinite DBR having a layer of the metal film [32]. The authors observed that the metal film changes the characteristics of surface waves in the semi-infinite DBR considerably. Recently the introduction of ultrafast lasers started the investigations of temporal properties of TPPs modes [33, 34]. Earlier, SPP mode width and lifetime have also been investigated and found to be of the order of several nanometers and hundreds of fs respectively which improves significantly in case of TPP modes [35]. The recent investigation in this direction showed the changes in fs pulse envelope when reflected from a TPP structure [33]. Features of TPP modes for carrying out basic scientific research have been studied by Grossmann *et al.* and Kaliteevski *et al*. [36,37]. For example, Grossmann *et al.* have shown that TPP exhibit strong coupling with

quantum-well excitons [36] and Kaliteevski *et al.* have also demonstrated that TPP modes show strong coupling of exciton-polaritons [37].

5.2 Structural Optimization and Tuning the Quality Factor of Optical Tamm Modes

Since the first experimental demonstration of TPP modes in 2008 by Sasin *et al.,* TPP has been intensively studied in the last few years [10-12, 17-21, 24-30]. The DBR-metal structure that supports TPP modes could be designed to operate at a chosen frequency with a possibility of monolithic integration. However, one disadvantage of TPP modes is that its field are strongly confined at the interface of DBR-metal film. Therefore, a crucial challenge of precisely controlling and manipulating TPP mode-field still persists. Also, due to advancement in laser technology, it is essential to investigate the photon relaxation mechanism and lifetime of TPP modes, which is defined by the characteristics of metal-DBR geometry [33].

Recent studies on TPPs modes are focused on the criticality coupling of light to TPPs modes [10, 38, 39]. By using the concept of admittance loci, Chang *et al.* investigated the dependence of TPPs wavelength on DBR structures [10]. However, an extensive theoretical and experimental study for understanding the factors governing the coupling efficiency is still required.

DBR properties and plasmonic metal films are the two important factors that determine the coupling efficiency of TPPs modes. Properties like DBR bilayers, refractive index difference between the two dielectric medium greatly influence the TPPs resonance. The properties of plasmonic metal film that affects TPP lifetime and resonance are its thickness and absorption

coefficients [33]. Investigations of the quality factor (Q-factor) and a lifetime of TPPs resonance is essential to create novel photonic devices [33]. Therefore for efficient coupling of light to TPP modes, metal and DBR parameters are needed to be optimized. In this section, we basically study the propagation characteristics of TPPs modes for ascertaining the influence of metal films and DBR on the Q-factor of TPPs in DBR-metal structure. Experimentally, we estimate the coupling efficiency and lifetime of TPPs mode from its transmission or reflection spectrum. As we know that the excitation of TPPs mode leads to a narrow peak (in transmission spectrum) or a narrow dip (in reflection spectrum) within the photonic stop band (PBG).

5.2.1 Theoretical Framework

Fig 5.1 shows the schematic of the TPP structure. The structure consists of a DBR and a metal film. Here the DBR consists of Ta_2O_5 and SiO_2. The DBR terminates with the Ta_2O_5 layer. Ta_2O_5 layer is followed by a metal layer of gold (Au) and Silver (Ag) in this work. The DBR dielectrics thicknesses chosen to form a quarter-wavelength stack condition at the operational wavelength.
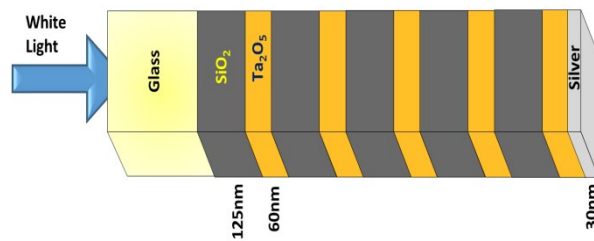
Fig 5.1 Schematic of the TPPs structure

The properties of TPPs modes using standard TMM for the DBR-metal structure have been analyzed. The DBR reflectivity is given by the relation [40],

$$|\mathbf{r}_N|^2 = \frac{|C|^2}{|C|^2 + \left[\sin(K\Lambda)/\sin(NK\Lambda)\right]^2}$$

(5.1)

where $|C|^2 = \dfrac{|r_i|^2}{1-|r_i|^2}$ and 'r_I' is the reflection coefficient of one unit of DBR. 'K' is the Bloch wavevector for the DBR which is complex inside the photonic bandgap and 'N' is the number of DBR unit cells [40]. Metal reflection coefficients r_M is given by the Fresnel relation [2],

$$r_M = (n_A - n_M)/(n_A + n_M)$$

(5.2)

where $n_M = \sqrt{\varepsilon(\omega)}$ is the complex refractive index of the metal and n_A is the dielectric refractive index adjacent to the metal. The relative permittivity $\varepsilon(\omega)$ of metals in the Drude model is expressed as:

$$\varepsilon(\omega) = 1 - \frac{\omega_p^2}{(\omega^2 + i\gamma\omega)}$$

(5.3)

where ω_p the plasma frequency, and γ is the collision frequency [26]. Assuming γ is small and $\omega \ll \omega_p$, equation 5.2 is modified as [26]

(5.4)

$$r_M \approx \exp(i[(1-s)\pi + 2(n_A/n_A')^{2s} n_A'(\omega/\omega_p)])$$

Here, $s = 1$ or 0 for TM or TE polarization and $n_A' = \sqrt{n_A^2 + n_i^2}$. Here, n_i is the imaginary part of the effective refractive index for TPP modes [41]. Therefore, the reflectivity from metal-DBR geometry is expressed by the relation $R = |\mathbf{r}_N|^2 |\mathbf{r}_M|^2$. Therefore, metal, as well as DBR properties, influence the TPPs Q-factor and lifetime. To study the dependence on DBR

bilayers, we plot the reflectivity for Ag-DBR geometry. Plasma wavelength and collision frequency values are taken from Johnson *et al.* [42]. Reflection spectra for N = 4, 6, 8, 10 and 12 when d_1 = 60 nm (Ta$_2$O$_5$), d_2 = 125 nm (SiO$_2$) and d_m = 30 nm (Ag) are illustrated in Fig. 5.2 (a). Here, N is the number of bilayers of the DBR. The simulations were performed using the material refractive indices as given by Bright *et al.* [43, 44]. As observed in Fig. 5.2, the reflectivity decreases to a minimal value for N = 6 and the reflectivity minimum shifts upward as we increase the number of unit cells. Also, it is evident that for higher values of N, the reflectivity variation is narrower for the TPPs resonance. In Fig. 5.2 (b), the reflectivity spectra for Ag-DBR configuration having varied Ag thicknesses (d_m) are shown with N = 6, which clearly shows the influence of d_m on TPP resonance. It is evident that the TPP excitation reaches a minimum value in the reflection spectrum when d_m = 30 nm. With the increase in d_m, TPP resonance turns sharper and the reflectivity minimum shifts upward.
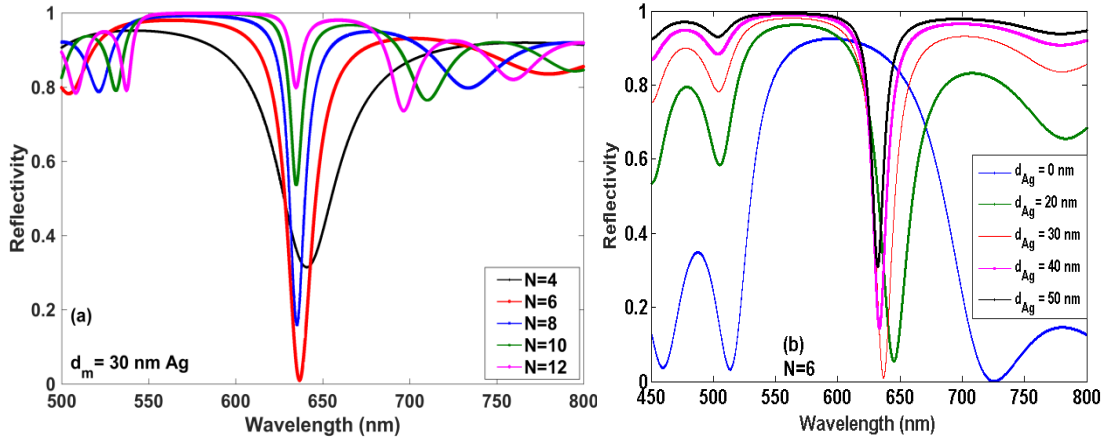
Fig 5.2. (a) Reflection spectra for varying DBR bilayers and d_m = 30 nm for Ag (b) Reflection spectra for varying Ag thickness and N = 6 of DBR.

Therefore it is clear from the Fig. 5.2 (a) and (b) that the excitation efficiency of TPP mode is affected by the number of bilayers in DBR and d_m. This is connected to the phase change in

reflection coefficients from the metal and DBR. Since, the excitation of TPP mode is governed by the phase matching conditions that require $\phi_{left} + \phi_{right} = 0$ where ϕ_{left} and ϕ_{right} are the phase of backscattered radiation of light traveling from right to left and left to right respectively at the metal-DBR interface [2, 45]. Naturally, the condition of perfect coupling or zero reflectance requires the aforementioned condition to be satisfied exactly at the Ag-DBR interface [38]. In Figs. 5.2 (a) and (b), the above phase matching condition is satisfied for N = 6 and d_m = 30 nm. As evident from Fig 5.2(a) and (b), the linewidth of TPP resonance decreases with increase in N and d_m. The increase in linewidth is due to increase in reflectivity of the Ag-DBR geometry [46, 47]. Therefore, the decrease in linewidth with an increase in DBR pairs or metal thickness provides a means to improve the Q-factor of the TPPs mode. It is important to observe and inferred from Fig. 5.2 (a) and (b) that for a given metal thickness, the choice of N becomes important in achieving maximum coupling efficiency.

Based on above observations, we need to observe the influence of 'N' and 'dm' variation together on the narrowness and reflectivity minima of TPPs modes. In order to understand the influence of coupling efficiency on metal-DBR parameters, reflectivity minima (R_{min}) is simulated as a function of N and d_m for the metals gold (Au) and silver (Ag). In the simulation, light is assumed to be incident from the substrate side. Fig. 5.3 (a) illustrates a color map showing the shift in R_{min} as a function of N and d_m. As observed in Fig. 5.3(a), there is strong coupling to TPP modes for all N≤9. However, for DBR with N≥ 10, the coupling efficiency reduces. It is also important to observe from Fig. 5.3(a) that the coupling efficiency maximizes only under certain conditions. The optimum metal thickness d_m(opt) is ≈ 46 nm and N= 6 for highest coupling efficiency. On the other hand, the optimum value of d_m increases to 60 nm when N= 7. In a qualitative sense, coupling efficiency could also

be observed in Fig. 5.3 (b) where the metal thickness is plotted as a function of N. In comparison to Fig. 5.3(a), Fig. 5.3(b) also exhibits optimum metal thickness for a
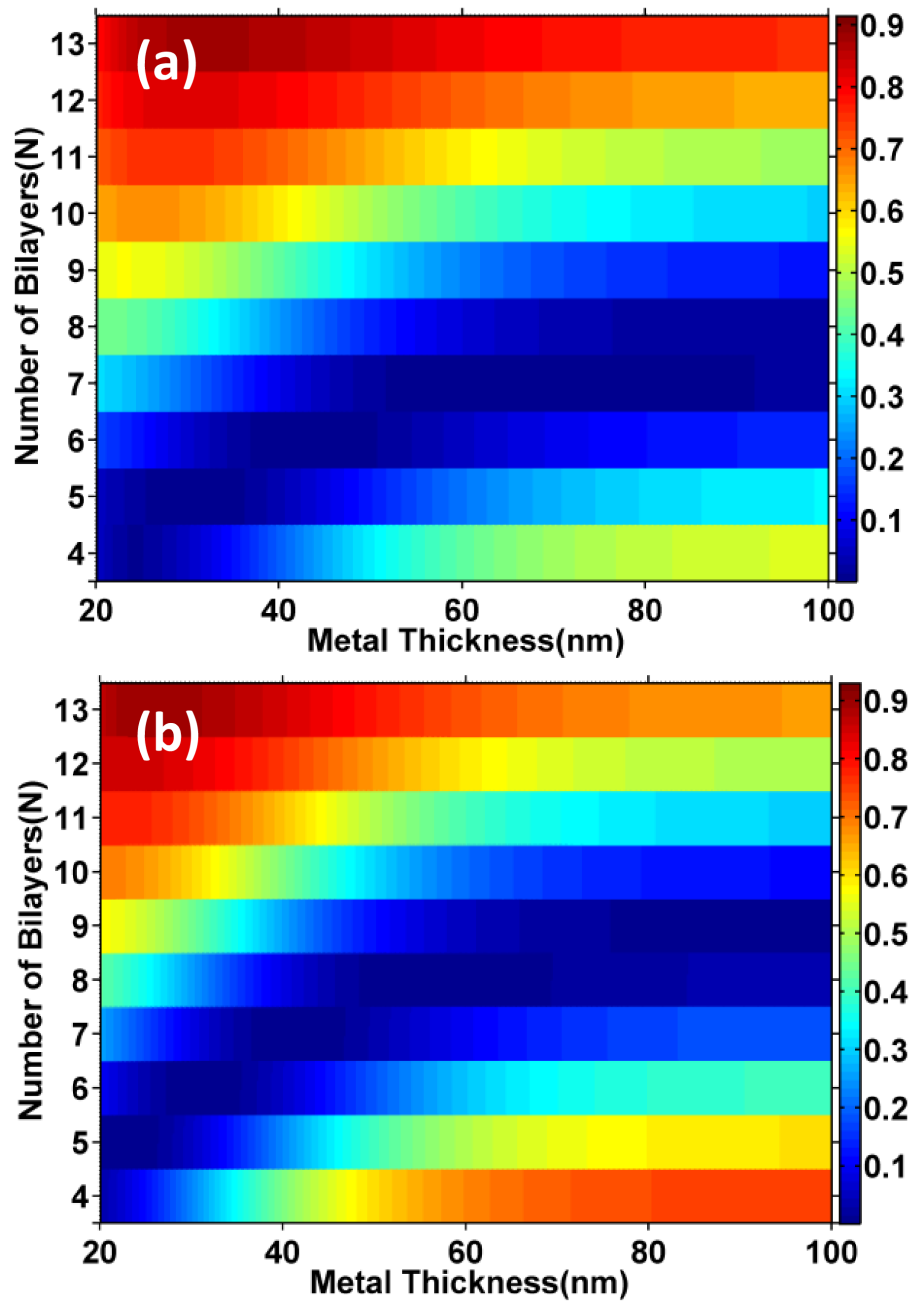
Fig 5.3 Variation of reflectivity minimum (R_{min}) of the metal-DBR geometry as a function d_m and N at normal incidence for (a) Au-(TiO_2/SiO_2)-based DBR and (b) Ag-(TiO_2/SiO_2)-based DBR. Color bar represents R_{min}.

given N where R_{min} is smallest. For the silver case dm(opt) ≈ 36 nm, d_m(opt) ≈ 46 nm and d_m(opt) ≈ 60 nm for N= 6, N= 7 and N= 8 respectively in order to maximize the coupling efficiency. As observed the coupling efficiency reduces for N ≥ 11 as per Fig. 5.3(b). From Figs. 5.3(a) and 5.3(b), it is easy to conclude that dm, as well as N, influence the coupling efficiency of TPP modes. The study also reveals that the plasmon metal also influences the Q-factor of the TPPs modes.
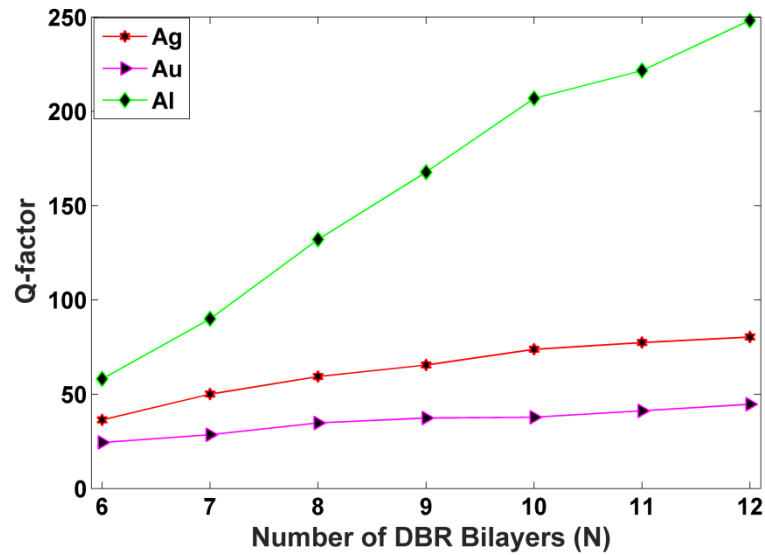
Fig 5.4 Variation of Q-factor for TPPs modes with DBR Bilayers

In order to bring out an alternate viewpoint, we have calculated the Q-factor as a function of N with d_m = 30 nm for Au, Ag and Al. The variation of Q-factor with N is shown in Fig. 5.4. We can clearly observe from Fig. 5.4 that with the increase in DBR bilayers, the Q-factor increases for all the plasmon-active metals. However, an important point to observe is that Q-factor is maximum for Al and minimum for Au. The difference in coupling efficiency is due to the difference in imaginary part of the dielectric constant of plasmon active metals. The imaginary part of dielectric constant is largest for Al and hence highest coupling efficiency,

103

However, due to rapid oxidation of Al, Au becomes the most suitable candidates for applications based on TPP modes.

To get a better picture, we have illustrated the dependence of Q-factor and lifetime of TPPs modes on metal thicknesses for Ag and Au as shown in Figs 5.5 (a) and (b). In case of Ag, Q-factor of the TPPs mode is $\approx$ 40-50 for d_m = 30 nm and scales almost linearly with the increase in metal thickness up to 50 nm for all values of N. The Q-factor decreases for d_m> 50 nm. The decrease in Q-factor for d_m> 50 nm is related to the saturation of reflectivity from Ag layer. Also with the increase in metal thickness, the absorption losses in metal also increase which in turns influences the Q-factor.
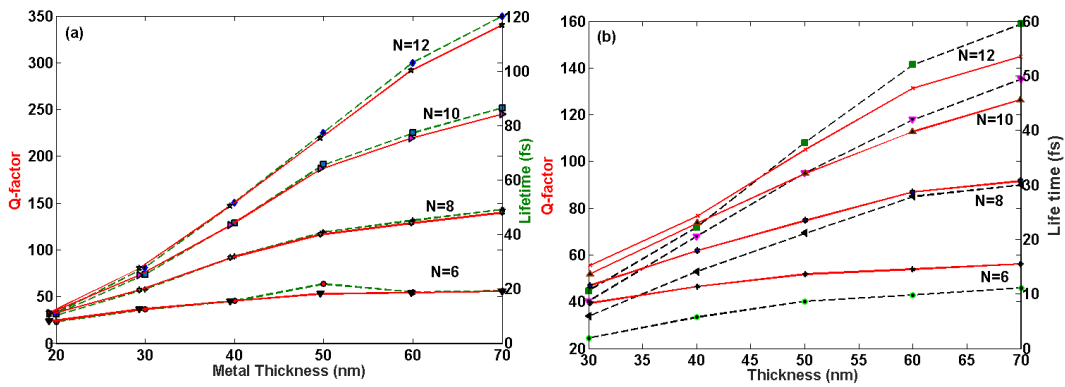
Fig 5.5 Q-factor and lifetime of TPPs modes as a function thickness for (a) Silver (Ag) and (b) Gold (Au)

As photons lifetime of TPPs mode is directly proportional to the Q-factor, therefore the similar trend is observed for the lifetime as well. The Q-factor and lifetime of TPPs mode in case of Ag (Fig. 5.5(a)) are almost 2 times larger as compared to Au Ag (Fig. 5.5(b)). Larger values in case of Ag are due to the greater magnitude of the imaginary component of dielectric constant for Ag in comparison to that for Au [48]. Hence, proper choice of metal, its thickness, DBR bilayers is important for applications based on high Q-factor TPPs modes.

5.2.2 Experimental Configuration and Reflectivity Measurements

Dependence of TPPs coupling efficiency on metal thickness is illustrated experimentally in this section. In order to perform the experiments, I have used dielectric plane mirrors in place of DBR. An experimental set-up for exciting TPPs modes is shown in Fig. 5.6 (a). The experimental set-up consists of a fiber-coupled white light source (WLS) having $\approx$ 260 nm broad spectrum (see Fig. 5.6(b)). WLS is non-uniform in the visible region as shown in Fig. 5.6(b).
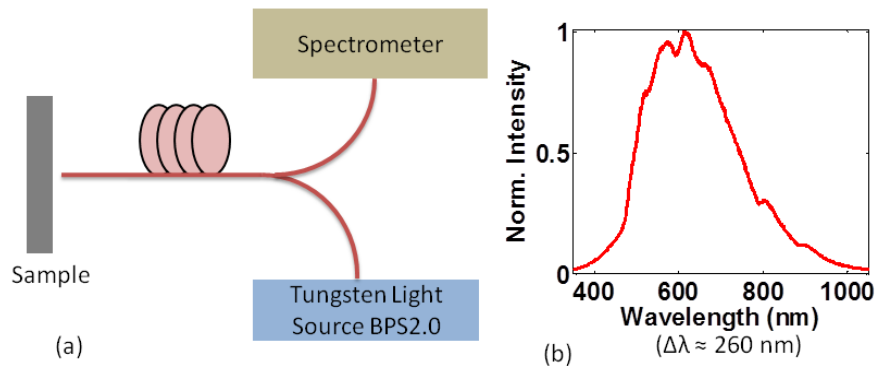
Fig 5.6 (a) Schematic of the experimental set up for TPPs mode excitation. (b) Nonuniform white light source.

The light is launched with an optical fiber on metal-deposited Braggs mirrors and the reflection from the surface is collected by the same optical fiber before feeding it to the spectrometer (Model: BRC112P-V, BWTek Inc.; Resolution – 0.5 nm). For exciting TPP modes, 30 nm and 60 nm of Gold (Au) and 30 nm of silver (Ag) thin-films were deposited on dielectric Braggs mirrors (Castech Inc.), namely 'mirror +30nm Au' and 'mirror +60 nm Au' and 'mirror + 30 nm Ag' respectively. Without metal depositions, the reflectivity of the plane mirrors is >99% over a wavelength range of 520−670 nm. For experimental observation of

TPPs modes, WLS is launched normally on the metal-mirror configuration and reflected beam is measured as shown in Fig 5.6(a). The reflection spectra for the bare mirror and metal deposited mirrors are illustrated in Fig. 5.7. The reflections spectra are shown in Fig. 5.7 are characterized by a sharp reflectivity minima appearing within the DBR stopband [2, 9].
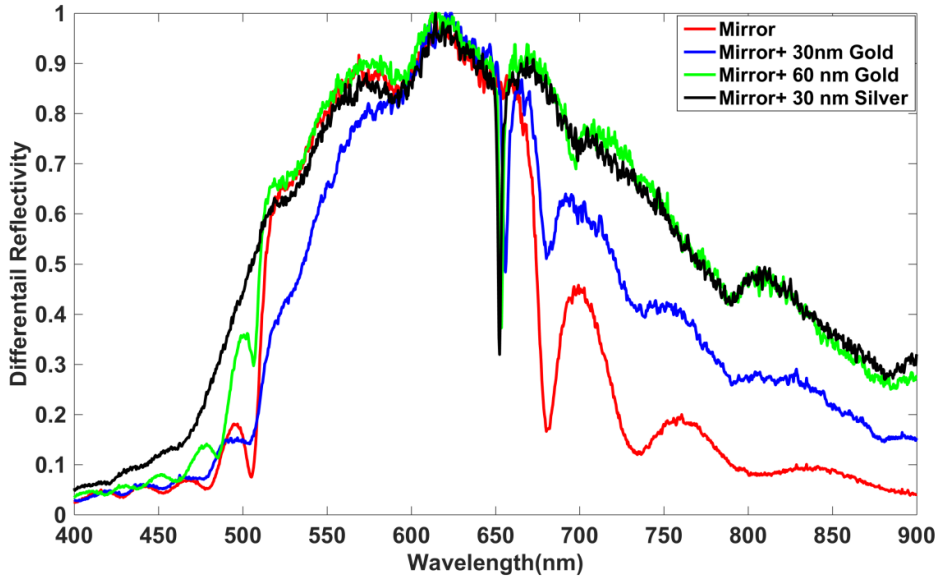
Fig 5.7 Experimentally Measured Reflection Spectra.

5.2.3. Q- Factor and Life-Time of Optical Tamm Modes

It is straightforward to observe from Fig. 5.7 that metal (Ag and Au) deposited plane mirrors shows a narrow dip in its reflectance spectra inside the high reflection band (stop band) of the plane mirror. This narrow dip in the high reflection region of the mirror is a signature of TPP mode excitation. Metal deposited mirrors namely "mirror + 30 nm Au", "mirror + 60 nm Au" and "mirror + 30 nm Ag" shows TPP excitation at 656 nm, 653.5 nm 652.5 nm wavelength respectively. The reflection spectra of TPP modes were fitted using Lorentzian function and calculated the linewidth of the TPPs resonance whose values are given in table-5.1. As clearly

observed from Fig. 5.7 and table 5.1, R_{min} is associated with the TPP modes are strongly affected by the plasmon active metal as well as its thickness. As we can observe from Fig. 5.7, the dip corresponding to TPP mode is sharper for "mirror +60 nm Au" as compared to "mirror + 30 nm Au" i.e. TPP resonance sharpened with the increase in metal thickness. Also, dip corresponding to TPP mode was blue shifted for a 60 nm thick Au-film deposited mirror. From Fig. 5.7, it is also clearly observed that the dip in the case of "mirror + 30 nm Ag" sample is sharper and blue-shifted as compared to "mirror+60nmAu" and "mirror +30 nm Au" samples. Sharpness and smaller linewidth in case of Ag deposited mirror is due to the large value of its imaginary dielectric constant as compared to Au [10]. Sharp resonances in the reflection or transmission spectra provide a better platform for sensing application due to higher detection-accuracy or improved signal-to-noise ratio (SNR) [48]. Based on the observations, we determined the Q-factor of the TPP resonance. Q-factor is defined by the ratio of energy stored within the cavity to the energy loss per optical time period multiplied by a factor of 2π. Alternatively, in terms of resonance wavelength (λ_{tp}) and linewidth ($\Delta\lambda$), Q-factor is expressed by the relation ($Q = \lambda_{tp}/\Delta\lambda$) [10]. Basically, Q-factor is a measure of the energy losses from within the cavity. Here, the value of TPP resonance width ($\Delta\lambda$) is influenced by energy loss via the metal film, DBR, as well as due to scattering by rough metal and DBR surfaces [49].

Table 5.1 Q-factor for the TPPs modes for metal deposited broadband mirror

Samples	Resonance Wavelength (λ_{tp})	FWHM ($\Delta\lambda$)	Error	Q-factor
'DBR+30 nm Au'	656.00	3.92	±0.067	167.40
'DBR+60 nm Au'	653.50	2.60	±0.155	251.0
'DBR+30 nm Ag'	652.50	2.36	±0.085	277.0

The *Q*-factor determined for the three metal deposited mirrors are tabulated in table-5.1. We found that the *Q*-factor of the TPP mode, in the case of silver λ_{tp} = 652.5 nm), is ≈ 1.65 times as that for gold (λ_{tp} = 656 nm). Experimental observations also suggest that the *Q*-factor of TPPs mode can be modified by varying d_m or by using plasmonic metals. The excitation of TPP modes at the metal-DBR boundary is comparable to modes in a Fabry-Perot cavity [34]. The TPP structure could be treated like a Fabry-Perot cavity having "zero" gap between the metal and DBR. Therefore, the photons trapped inside the structure due to excitation of TPPs mode could be characterized by the cavity lifetime (τ_{tp}). The cavity lifetime is governed by many factors like DBR and metal reflectivity as well as thickness [33]. TPP lifetime could be evaluated similarly to cavity lifetime by the expression ($\tau_{tp} = Q\lambda_c/2\pi c$). The τ_{tp} for three different cases are found to be 58.00 fs, 87.00 fs, and 96.00 fs respectively.

5.3 Hybrid-Tamm Modes for Refractive Index Sensing

5.3.1 Motivation

The TPPs modes excited at the boundary of a metal film and a DBR shows a number of possibilities in terms of sensing scheme and its simple structural implementations. This is because the TPPs mode based sensors can be operated at a particular wavelength (or a number of wavelengths), and can work with all plasmonic metals (Ag, Au, and Al). Also, TPPs mode, which is excited as a narrow dip in the high reflection band of the DBR exists for both TE and TM polarizations and at an oblique angle as well [9, 50]. Enhancement in light and light localization at metal-DBR boundary due to excitation of TPPs modes have been utilized for various purposes like light trapping [15] and lasing [11,12], nonlinear optics [14], optical switches [16], fluorescence enhancement [19, 20]. Reflection dip or transmission peak corresponding

to TPP mode excitation have been utilized for refractive index sensing (RIS) [17, 18]. However, these sensors require the use of mesoporous multilayers as Typical TPPs mode field are restricted at the metal-DBR boundary. Due to mode confinement, the TPPs resonance wavelength is not affected by the ambient medium. Due to the absence of TPPs field interaction with the ambient medium, the TPPs-modes resonance wavelengths are not affected [18, 19]. Therefore in order to change the TPPs-modes resonance wavelengths properties as the characteristics of the ambient medium change, we configure a system in which a coupled mode could be excited.

In order to excite coupled TPP modes, I have proposed a geometry in which an analyte layer is sandwiched between two 'metal-DBR' structures. The geometrical configuration is illustrated in Fig. 5.8(a). The DBR or one-dimensional photonic crystal in the configuration comprises Ta_2O_5/SiO_2 multilayers [50, 51]. Here, by altering the cavity configuration, we can control the coupled Tamm modes or the hybrid TPP modes as per the targeted application. Also, for this geometry, field-localization is significant in the analyte region due to the strong coupling between TPPs modes [51]. The proposed sensing configuration has following advantages over the typical SPP based sensors.

1. Unlike surface plasmon polariton modes that are TM-polarized, Tamm plasmon modes can be excited by incident waves of both orthogonal TE- and TM- polarizations, and are characterized by parabolic dispersion with different 'effective masses' for TE- and TM-polarized Tamm plasmons.

2. As surface plasmons are TM-polarized non radiating modes, therefore comples architectures involving high index prism and grating are involved for their excitation. However such configyrations are not required for the excitation of

the TPP modes. This is due to the fact that TPPs in-plane k vector is close to zero and therefore can be excited directly.

3. Unlike surface plasmons, TPP modes excitation is possible using normal as well as oblique illumination.

4. Tunability of the TPP mode. An important requirement for optical sensors is the ability to tune the spectral range of operation, so that the device may be tuned to the optimum region for a specific target. TPP mode tuning is easily obtained, simply by changing the thickness, refractive index of the DBR or porosity of the constituting DBR bilayers.

5. FWHM of TPP mode varies from 2 to 5 nm, however the optical sensors based on SPR configuration typically exhibit FWHM≈ 40–50 nm. Therefore TPP based sensor has better detection accuracy (DA) as compared to SPR based sensor.
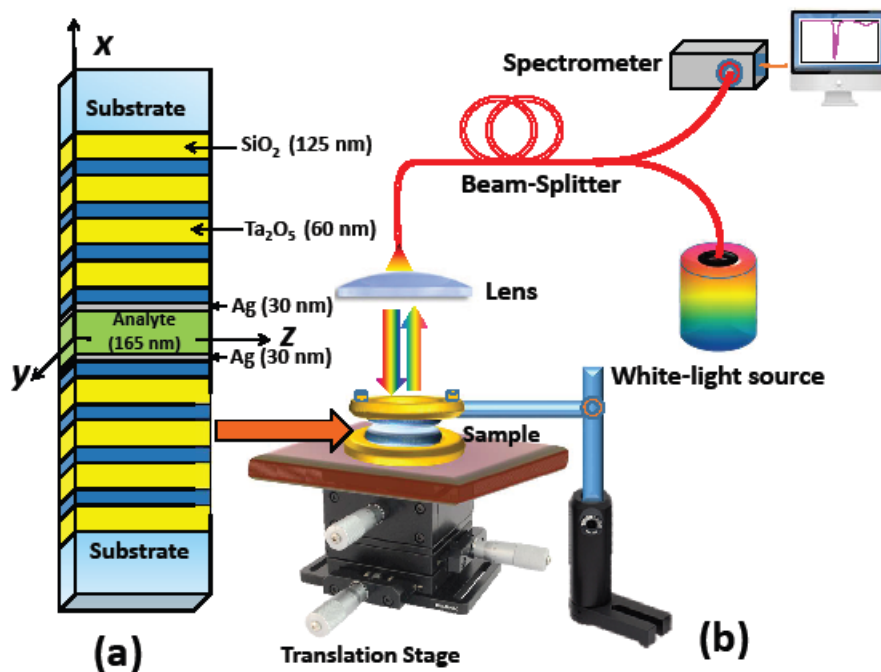
Fig. 5.8 (a) Configuration for exciting coupled TPPs modes. (b) The experimental set-up for RIS measurements.

5.3.2 Structure for Exciting Hybrid Optical Tamm Modes

The DBR-metal-cavity-metal-DBR configuration for exciting coupled TPPs modes is schematically presented in Fig. 5.8 (a) and the experimental configuration for the RIS measurements is illustrated in Fig. 5.8(b). WLS is launched on dual 'metal-DBR' structures as illustrated in Fig. 5.8(b). At normal incidence, the reflected light is collected by the same optical fiber before being sent to the spectrometer. The experimental design provides a means to change the analyte refractive index [52]. For simulating the reflection spectra from the metal-DBR structure, we choose Ag as metal and each DBR having 8 bilayers of Ta_2O_5/SiO_2. Ag thickness is taken to be 30 nm and the refractive index value is used from Johnson *et al.* [42]. The material dispersion relations for Ta_2O_5 and SiO_2 are taken from Kobayashi *et al.* work [53]. We have used d_1 = 60 nm and d_2 = 125 nm so as to form a quarter-wavelength stack and have a high reflection band in the visible region (530 -730 nm) as illustrated in Fig. 5.9 (a).

5.3.3 Numerical Results on Hybrid Tamm Modes

To calculate the reflection spectrum of a multi-layered structure, we used the TMM and the cavity thickness d_a is taken to be 140 nm [32]. Also, the analyte index is taken to be n_a = 1:33. The simulated reflection spectra for dual 'Ag-DBR' configuration is presented in Fig. 5.9 (a) (solid curve) which depicts two nearly placed dips inside the high reflection band of Ta_2O_5-SiO_2 DBR. The dips in the reflection spectra occurs at λ_{r1} = 659 nm and λ_{r2} = 670 nm. Such dips in reflectivity are associated with the coupling of two individual TPPs modes formed at Ag-DBR boundary. It is important to mention here that d_a = 140 nm is in order avoid cavity-modes [53]. There is a reduction of absorption in the metal film due to excitation of the hybrid TPPs mode
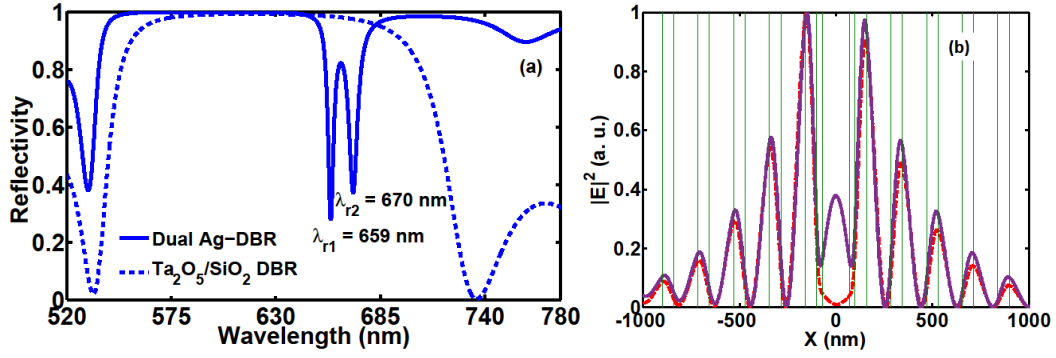
Fig 5.9 (a) Numerically simulated spectrum for dual "Ag-DBR" configuration with $n_a = 1{:}33$ and $d_a = 140$ nm. (b) Normalized field intensity for Mode-1 (dotted curve) and Mode -2 (solid curve).

[54]. Hybrid mode dips at λ_{r1} and λ_{r2} is assigned as anti-symmetric (Mode-1) and symmetric mode (Mode -2) based on symmetry in dual Ag-DBR structure (about $x = 0$). The normalized hybrid mode field intensity for both modes are illustrated in Fig. 5.9 (b). Field intensity represented in Fig. 5.9 (b), clearly illustrates the symmetric and anti-symmetric field variation about $x = 0$. Mode-2 shows the significant existence of a field in the analyte region (see Fig. 5.9 (b)) and therefore the resonance wavelength of Mode - 2 is expected to change with the change in the analyte index. In order to understand the variation in dispersion properties of Mode – 2, the reflectivity map $R(n_a, \lambda)$ on the plane of analyte index (n_a) and wavelength (λ) at normal incidence are presented in Figs. 5.10 (a), (b), and (c) respectively. We can observe from Figs 5.10 that the λ_{r1} corresponding to Mode-1 experience an imperceptible shift. However, λ_{r2} corresponding to Mode-2 shows a marginal shift as n_a varies (see Fig. 5.10(a)). It is important to observe that the shift in λ_{r2} is large as illustrated in Figs. 5.10 (b) (for $d_a = 80$ nm) when n_a change from 1.33 to 1.53. The mode-2 (λ_{r2}) shows a maximum shift for $d_a = 165$ nm (see Fig. 5.10 (c) as n_a changes from 1.33 to 1.53. Qualitatively, the shift in coupled TPPs mode wavelength could be analyzed by observing the change in

112
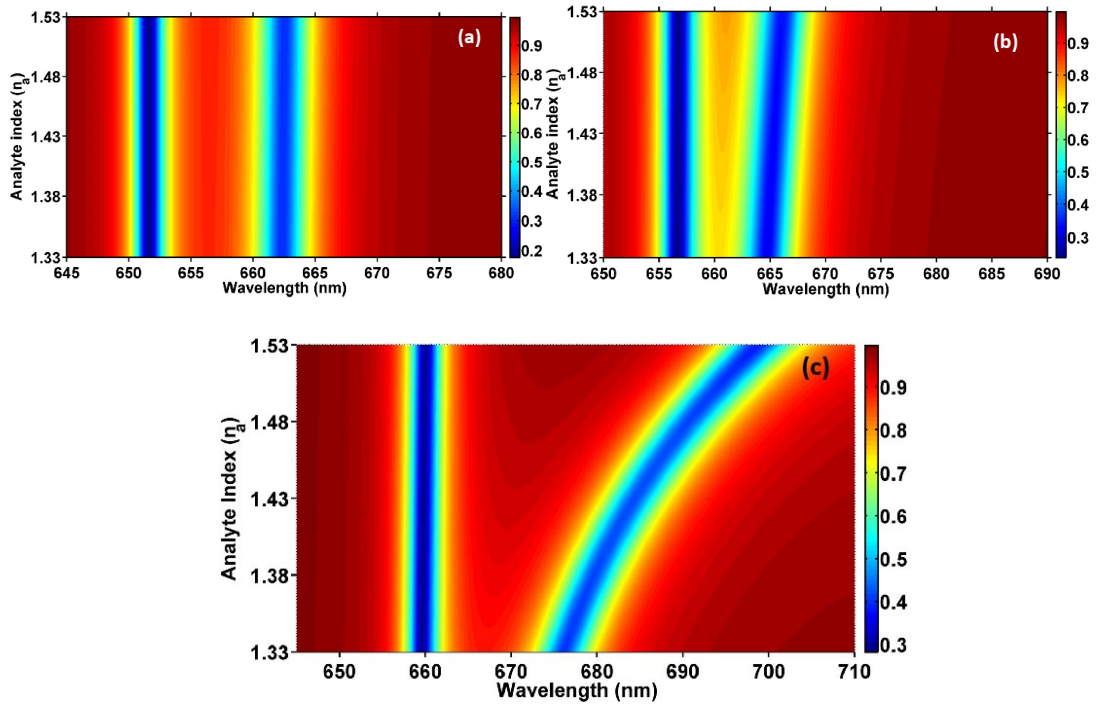
Fig. 5.10 Reflectivity map $R(n_a,\lambda)$ of the coupled TPPs mode when (a) $d_a = 20.0$ nm, (b) $d_a = 80.0$ nm and (c) $d_a = 165.0$ nm. Color-bar represents reflectivity.

Mode -2 field distribution. The mode-2 field intensity is illustrated in Figs. 5.11(a), (b) and (c). The field intensity for mode-2 with $d_a = 20$ nm is presented in Fig. 5.11(a), when $n_a = 1.33$ and $n_a = 1.53$. Around the region $x = 0$ (see Fig 5.11(a)), the variation in Mode-2 field intensity is imperceptible when n_a is varied. Again around the region $x=0$ (see Fig 5.11(b)), when $d_a = 80$ nm, the variation in mode-2 field intensity is small but observable. However, variation in mode-2 field intensity is appreciably large for $d_a = 165$ nm ((see Fig 5.11(c))). This variation in field intensity is the cause behind the large shift in Mode-2 resonance wavelength with the change in n_a. This variation in mode-2 resonance wavelength could be utilized for the sensing scheme. it is important to mention that the proposed sensing scheme could be used for biochemical sensing as well [55-57].
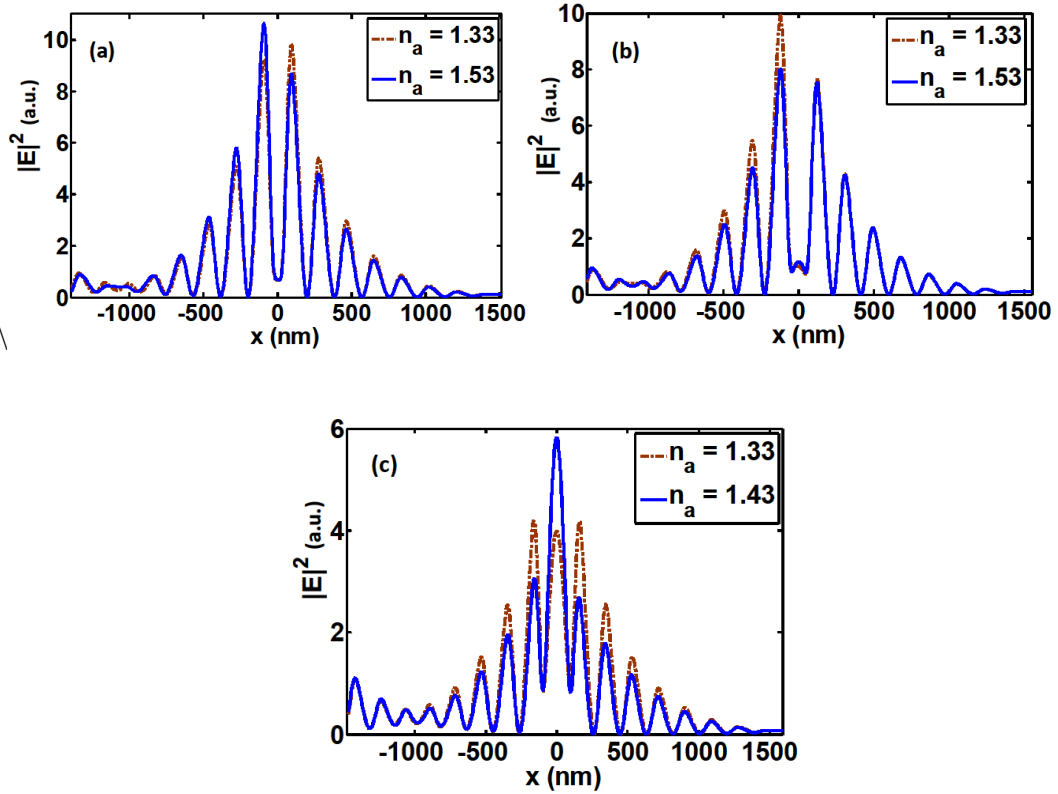
Fig 5.11 Field intensity for Mode-2 when (a) d_a = 20.0 nm, (b) d_a = 80.0 nm and (c) d_a = 165.0 nm.

From the aforementioned description, it is clear that λ_{r1} of Mode-1 does not show any shift as n_a change, however, λ_{r2} of Mode-2 exhibits a significant shift for variation in n_a for $d_a \geq$ 50nm. This variation in λ_{r2} with analyte index is the basis of my proposed "self-referenced sensor". Sensing is called self-referenced because λ_{r1} for Mode -1 does not change and λ_{r2} for Mode – 2 exhibits large change with variation in n_a [58-61].

5.3.4 Hybrid Optical Tamm Modes Sensor Characteristics

In view of the observations made in the previous section, we have investigated the coupled TPPs mode sensor characteristics by calculating the shift in λ_{r2} with respect to λ_{r1}. To determined the sensitivity of the proposed sensor, we assumed d_a = 165.0 nm as a maximum

shift in λ_{tp} was observed for this case (see Fig. 5.10 (a), (b) and (c)). The sensitivity is defined as $S_n = |\delta\lambda_r|/\delta n_a$, where $\delta\lambda_r = \lambda_{r2} - \lambda_{r1}$ as per Fig. 5.9(a). For the same geometry, detection accuracy (DA) is defined as the inverse of FWHM of Mode-2. We also calculated FOM of the proposed sensor and is defined as FOM = S_n/ FWHM. FOM is an essential quantity to analyze sensor performance.
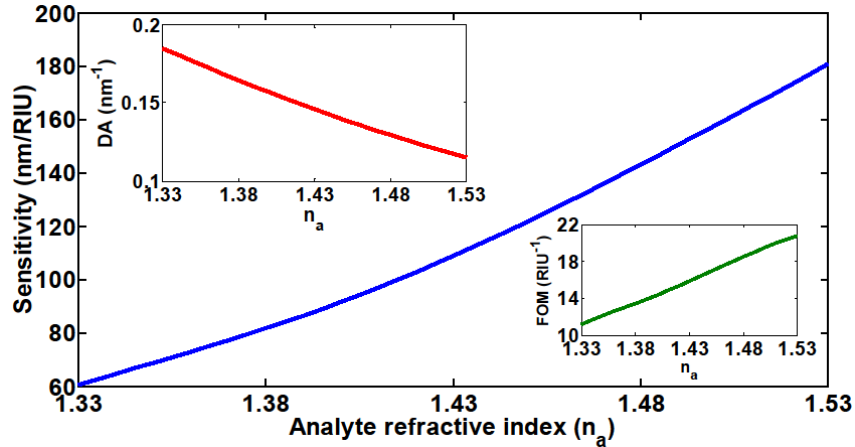
Fig 5.12 Variation of sensitivity, DA, and FOM for the hybrid-TPP mode sensor as a function of the analyte index (n_a).

The variation of S_n, DA (inset) and FOM (inset) for the proposed TPP hybrid-mode sensor as analyte index (n_a) varies are illustrated in Fig 5.12. From the Fig 5.12, it is clear that the sensitivity varies nonlinearly from 65.0 nm/RIU to 180.0 nm/RIU. The proposed coupled TPPs mode RIS shows FOM of 11-21 /RIU (see Fig. 5.12).

5.4 Refractive Index Sensing with Distributed Bragg Reflectors

5.4.1 Motivation

In the last few years, refractive index sensor (RIS) based on photonic crystals and TPP based structures have been intensively studied [17, 18, 28, 56, 67]. Amongst them,

one important configuration for refractive index sensing is a microcavity or analyte region filled with a biochemical component. These structures are famous for their easy control of the optical design and easy fabrication. Also, the proposed RIS could be used in the wavelength of our interest by optimizing the DBR. For controlling the characteristics of the microcavity modes and to apply it for any practical applications, the field distribution in the cavity plays an important role. In this study, we propose a RIS comprising a DBR and investigate its sensing properties. With the proposed architecture, we can excite the cavity modes. The excitation of the cavity modes leads to a narrow dip in the stop band of the DBR. Mode excitation leads to field enhancement in the region between metal and DBR.

In this section, we investigate the impact of cavity thickness; angle of incidence (AOI), metal (Ag, Al, Au) and light polarization on the sensor performance. The RIS design is very simple to implement as the sample is only made up of a metal film on top of DBR. The present RIS is advantageous over other with respect to its excitation-detection mechanism.

5.4.2 Structure Design for Cavity-Mode Excitation

The cavity based RIS configuration is presented in Fig. 5.13 (a). Configuration presented in Fig. 5.13 (a) is comprised of a cavity sandwiched between a thin metal and a DBR. The gap of the proposed configuration placed between the metal film and DBR is the basis of cavity mode excitation and hence could be utilized for RIS. The cavity refractive index (n_a) influences the mode resonance (λ_c). Therefore on varying n_a in the cavity, the λ_c of the mode changes. In this study, I have taken 8 DBR unit cells of Ta_2O_5/SiO_2 with thicknesses 60 nm and 130 nm respectively to form a quarter-wavelength stack. The chosen quarter-wavelength stack results in band gap
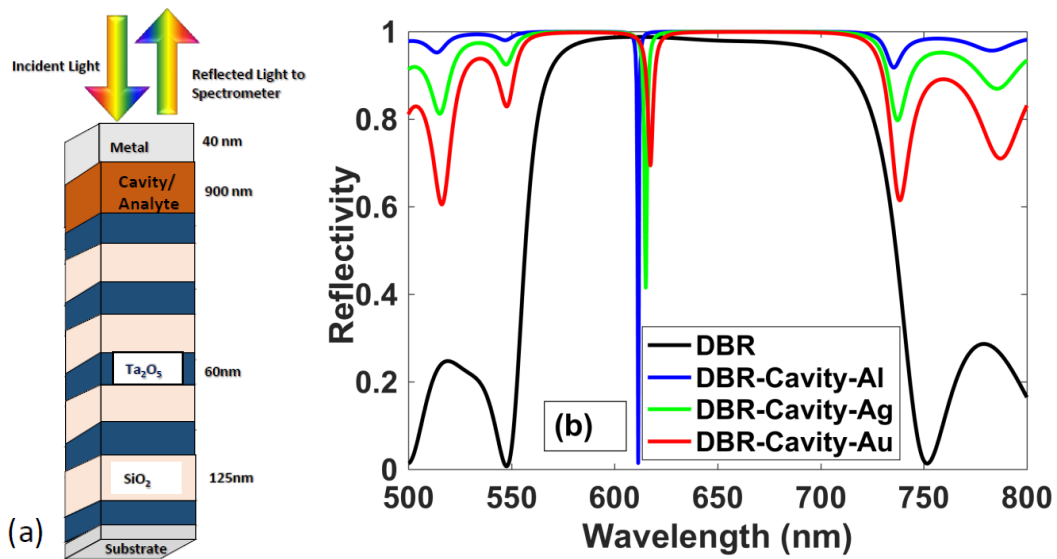
Fig 5.13 (a) Design of the cavity structure (b) Reflectivity of the structure with $n_a = 1.33$ and $d_a = 900$ nm.

from 550 nm to 750 nm as illustrated in Fig. 5.13 (b). Ta_2O_5 and SiO_2 refractive index values are used from Kobayashi *et al.* work [53]. To begin with, the cavity thickness (d_c) and d_m are taken to be 900 nm and 40 nm for simulation work. This study investigates the role of metals (such as gold, silver, and aluminum) on the sharpness and resonance wavelength. Theoretical analysis is carried out with various metals to Fig out their impacts on sensitivity and DA of the RIS. Theoretically, we analyzed the propagation characteristics of the proposed design (see Fig. 5.13 (a)) using TMM [40, 63]. In the analysis, the cavity region refractive index is varied. Lightwave oscillates inside the cavity and a new kind of surface wave called cavity-mode is formed in the cavity region. The cavity modes λ_c are susceptible to the variation in n_a. To investigate the RIS properties, a shift in λ_c is monitored from transmittance, reflectance or absorption spectra.

5.4.3. Impact of Cavity Thickness and Metals on Cavity Modes

In order to calculate the reflectivity of the proposed RIS configuration, we employed the TMM [40, 63]. In Fig. 5.13(b), we present the reflectivity at 90^0 for different plasmon active metal layers of identical thickness. Sharp minima inside the stop band correspond to the formation of the cavity-modes [8]. I have also investigated the effect of metals on the λ_c of cavity mode and is illustrated in Fig. 5.13(b). Different metals result in variation in λ_c for the cavity modes. Also sharper reflection spectra for Al with respect to that of Au and Ag is due to the larger value of ε^{img} of Al. In addition, the difference in reflectivity drop could be explained on the basis of metal imaginary dielectric constant value as well as on the perfect phase matching condition $r_M r_{DBR}=1$ where r_M and r_{DBR} are reflection coefficients of the metal and DBR [2]. In order to study the impact of plasmon-active metals on the cavity resonance wavelength and its sensing characteristics, reflectivity with varied n_a is shown in Figs. 5.14(a), (b) and (c) respectively. The n_a refractive indices used in the simulation are chosen in such a way that it corresponds to methanol, water, isopropanol, 2-methoxyethanol and chloroform
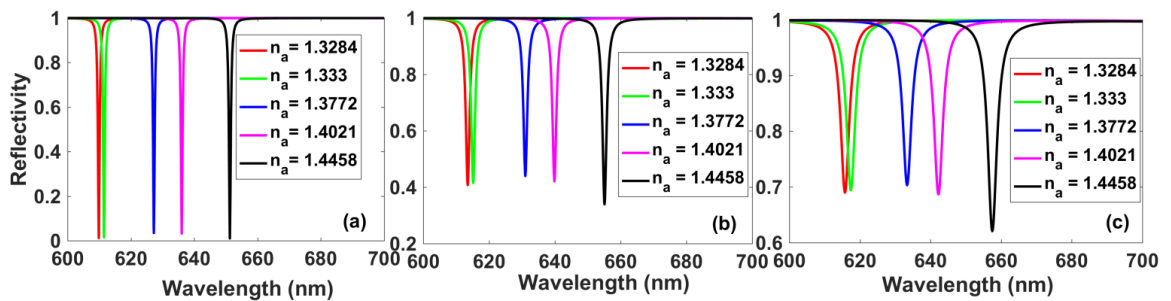
Fig 5.14 Reflection spectra of the cavity-mode calculated by TMM for different plasmon active metals ((a) Aluminum; (b) Silver; (c) Gold).

having a refractive index (RI) of 1.3284, 1.333, 1.3772, 1.4021 and 1.4458 respectively [56]. As illustrated in Fig. 5.14, R_{min} and λ_c of the cavity-mode changes when n_a varies from 1.3284 to 1.4458. Qualitatively, the shift in λ_c is the result of cavity mode excitation and its field interaction with the analyte refractive index [25]. Also it is evident (see Figs 5.14) the narrowness or the sharpness of the cavity-mode strongly depends on the metals. Also, it is important to note that due to narrow and sharp resonance, the width is minimum for Al. This provides a practical platform for sensing application with an improved signal-to-noise ratio (SNR) and DA.

5.4.4 Cavity Mode Sensing Characteristics

In view of the observations made in the previous section, we have investigated the sensing characteristics of the metal-cavity-DBR geometry. Fig. 5.15 (a) shows the cavity-mode λ_c variation with respect to n_a of the cavity for RIS. The graph is plotted for metals (Al, Ag, Au) with $d_a = 900$ nm. From Fig. 5.15 (a), we can clearly observe that the λ_c increases linearly with the increase in n_a. Sensitivity is defined as $S_n = \Delta\lambda/\Delta n_a$ and was calculated to be $\simeq 355$ nm/RIU for $d_a = 900$ nm. As observed in Fig. 5.15 (b), sensitivity has been calculated for $d_a = 900$ nm as this thickness maximizes the (S_n) value and helps to avoid additional modes in the
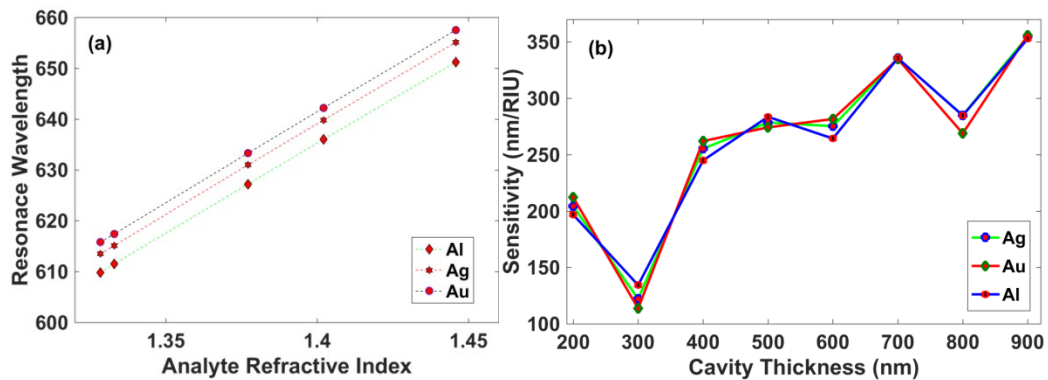
Fig 5.15 (a) Variation of the cavity-mode resonance wavelength with analyte index. (b) Cavity thickness dependent Sensitivity (S_n).

cavity [54]. Additional modes in the cavity lead unavoidably enhance the detection complexity. The proposed design is important from the perspective that it results in field confinement in the cavity and hence could be utilized for sensing purposes [28,51,68]. Since the proposed refractive index sensing scheme is based on 1DPC, therefore it could be employed in the desired band [18].

5.4.5 Impact of Incident Angle on Sensitivity

In general, the cavity and TPPs mode are dispersive and hence they are susceptible to variation in the AOI [3]. In order to find out its implications, the sensitivity versus AOI variation is illustrated for both the polarizations (TE and TM) in Fig. 5.16. It is apparent from the Fig. 5.16 that the S_n tends to increase with the increase in AOI for both TE and TM modes. It is important to note that the S_n for TM-mode increases up to 30° AOI and then after, tends to decrease (See Fig 5.16(Green line)). Also, the S_n for TM-mode is smaller with respect to the TE-mode. This is due to the fact that the variation in λ_c is larger for TE-mode with respect to TM-mode. In order to understand this, we note that the stop band in DBR is formed due to multiple reflections from the
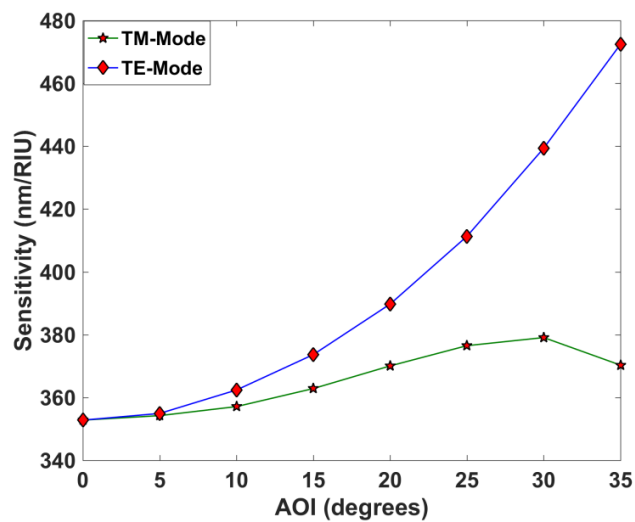
Fig 5.16 Variation of S_n as a function of AOI for the TE and TM polarized light.

DBR multilayers [69, 70]. Afinogenov *et al.* demonstrate that the TM-mode reflectivity reduces as AOI increases and finally, reflectivity becomes zero at Brewster's angle [70]. Due to this, stopband edges smoothen and therefore the dip corresponding to the λ_c becomes broad. In other words, the decrease in TM mode reflectivity results in poor confinement of the mode field and hence decreases in S_n. However, larger S_n of the TE-mode is because of to its large group velocity dispersion with respect to TM-mode. Also the reflectivity of TE-mode increases with increase in AOI. Increase in reflectivity leads to strong field confinement and hence increase in S_n.

5.5 Tamm-Plasmon Resonance Based Temperature Sensor

In this section, we discuss experimental results and theoretical modeling of a temperature sensing scheme using the phenomenon of Tamm-plasmon resonance. We deployed a scheme where controlled heating Ag deposited DBR is carried out and alterations in the coupling efficiency to TPP modes is noted. The DBR is comprised of periodically stacked multilayers of Ta_2O_5 and SiO_2. Such an experiment allows the study of the TPP mode confinement as well as the accurate determination of temperature. We systematically investigate the reflectivity minima (depicting coupling efficiency) of the excited TPP mode when the Ag-DBR sample is heated. We found that the reflectivity minima corresponding to TPPs mode shift upwards with an increase in temperature. The metal-DBR configuration supporting TPPs mode is theoretically analyzed as well.

5.5.1 Optical Tamm Modes Excitation Setup

The configuration which supports TPPs modes is consists of a DBR and a metal

film (Ag) as shown in Fig. 5.17 (a). The presented structure in Fig. 5.16 (a) supports a TPPs mode at Ag-DBR interface according to the resonance condition for micro-cavity modes. A representative of the experimental configuration for exciting TPPs mode is presented in Fig. 5.17(b).
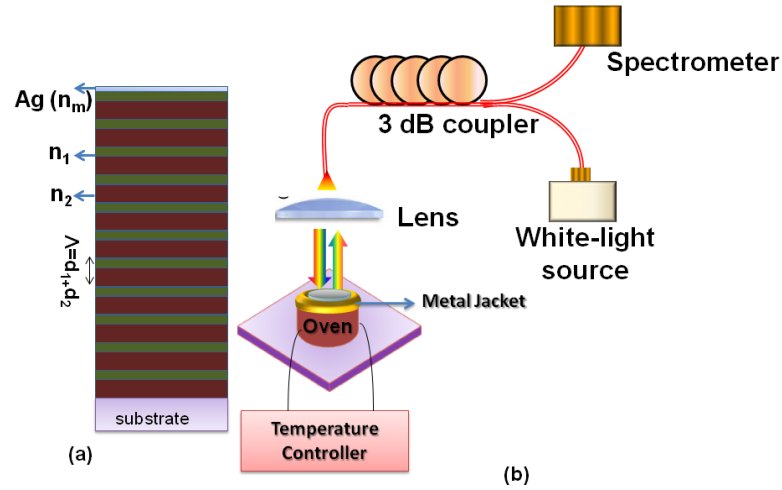
Fig 5.17(a) Schematic of the metal-DBR structure. (b) TPPs excitation and detection configuration for studying the temperature dependent TPP mode characteristics at normal incidence.

The structure in Fig. 5.17 (a) shows a DBR with periodically stacked multilayers of refractive indices n_1 and n_2 having thicknesses d_1 and d_2 respectively. Here the DBR or one-dimensional photonic crystal is a conventional plane mirror comprised of periodic dielectric stacks satisfying the Bragg's condition (Laser Optik, Germany). At normal incidence, the plane mirror shows a stop band from $\approx$ 520-680 nm. For exciting TPPs modes, we deposited 30 nm thick (d_m) Ag film on the plane mirror (Laser Optik, Germany).

5.5.2 Optical Tamm Mode Reflectivity Measurements

   The experimental set-up for studying the temperature dependence of TPPs characteristics at normal incidence is shown in Fig 5.16 (b). For exciting TPPs mode, WLS is incident normally on the "DBR-metal" geometry and the reflected light is collected by the same optical fiber before being sent to the spectrometer. Reflection spectrum of the investigated structure is illustrated in Fig. 5.17. As observed (see Fig. 5.17) the reflection spectra show a dip at $\lambda_r \approx 652.5$ nm inside the high reflection region (stop band) of the bare mirror. The sharp dip in the reflection spectrum inside the high reflection band of the mirror is due to excitation of a TPPs mode. The TPPs mode is excited and confined at the Ag-DBR boundary according to the phase-matching or resonance condition [2]. FWHM of the excited TPP mode was calculated and determined to be $\Delta\lambda \approx 2.2$ nm. This corresponds to a Q-factor of ≈ 296. From the Fig 5.17, it could also be observed that the excitation of the TPPs mode is near the
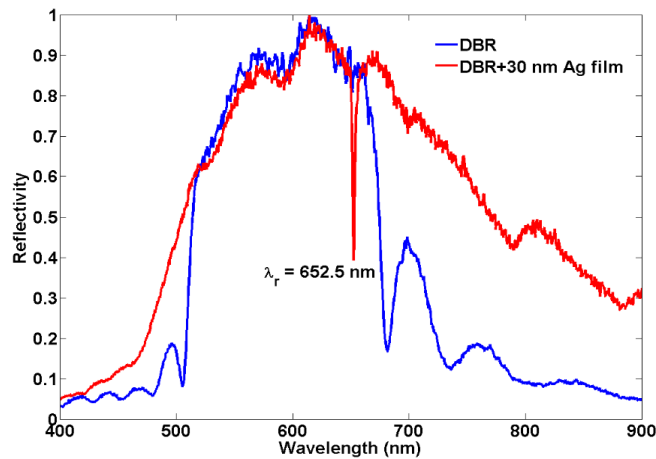
Fig 5.18 Measured reflectivity from DBR (Blue) and "DBR-metal" (Ag) thin film (Red) versus wavelength of unpolarized light at normal incidence.

low-frequency edge of the high reflection region of the mirror. TPPs excitation is near the low-frequency band due to asymmetric configuration of the bare mirror. When

unpolarized light is incident on the metal-DBR geometry at an oblique angle, the TPPs degeneracy is separated. Reflection spectrum of the Ag-DBR configuration at 45^0 AOI is shown in Fig. 5.19, which shows two distinct nearby sharp resonances associated with TM and TE polarized TPPs mode. As evident from Fig. 5.19 TM and TE polarized TPPs mode shift to the longer frequency with the increase in AOI from 0° to 90°. The shift to longer frequency is due to modified Bragg's law [71]. This is essentially due to the fact that unlike SPP modes that are TM polarized, TPP modes excitation is possible for both orthogonal TM and TE polarizations [72]. In addition, the orthogonal TE, as well as TM polarized mode are characterized by parabolic dispersion curves depicting different effective masses for TE and PM polarized TPP modes. As observed in Fig 5.19, the TM-TPP resonance is excited at $\lambda_{r(TM)} = 593$ nm and TE-TPP is excited at $\lambda_{r(TE)} = 605$ nm for AOI = 45^0.
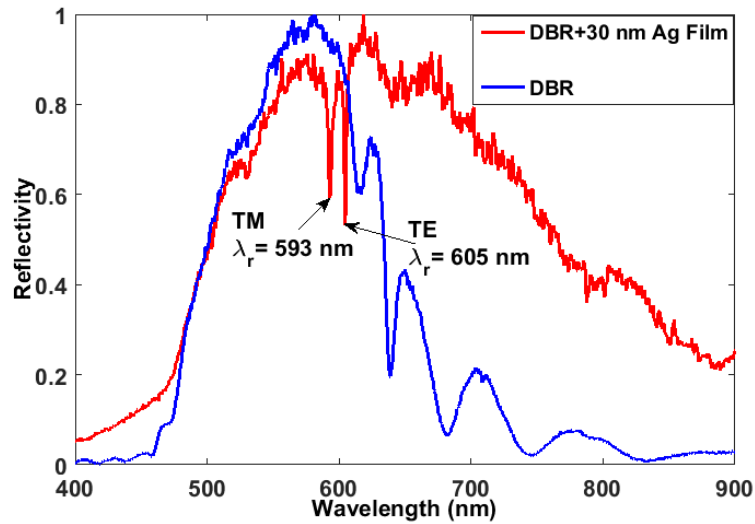
Fig 5.19 Experimentally measured reflection spectra of the bare mirror (Blue) and mirror with Ag film (Red) for 45° AOI with an unpolarized light.

To determine the impact of temperature on TPPs mode, the metal deposited mirror is housed in an oven which provides uniform heating to the sample (see Fig. 5.17(b)).

The temperature dependent reflection spectra of Ag-DBR configuration is illustrated in 5.20. As observed in Fig. 5.20, the R_{min} corresponding to TPPs mode decreases as we increase the temperature. This is due to the fact that the TPP resonance turns weaker according to the phase matching condition [2]. This temperature dependence of reflection spectra of the metal-DBR system provides an alternative way to determine the temperature change. Fig. 5.20 clearly illustrates that the variation in reflectivity minima (ΔR_{min}) of the TPPs-mode is prominent at a lower temperature. However, the variation in ΔR_{min} turns smaller at higher temperatures. Such observations essentially indicate that the conditions of perfect coupling or phase matching conditions for exciting TPPs modes changes with a change in temperatures (see Fig. 5.20) [38]. The upward shifts of TPPs mode indicate that the conditions of
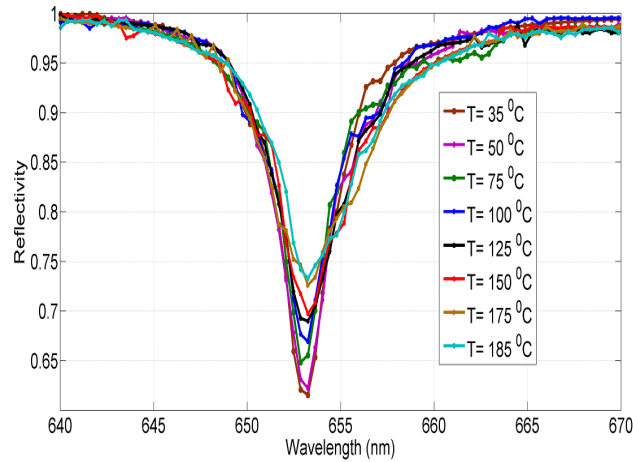
Fig 5.20 Reflection spectra of "DBR + 30 nm Ag" thin-film at varied temperature for normal incidence.

perfect coupling turns weaker with an increase in higher temperature. However, the change in refractive index with temperature for Ta_2O_5 and SiO_2 is considerably small and hence negligible. Chu *et al.* [73] demonstrated $dn/dT \approx 2.36 \times 10^{-6}$/K for Ta_2O_5, however $dn/dT \approx 8 \times 10^{-6}$/K for SiO_2 according to Matsuoka *et al.* [74]. But, the

(dn/dT) of Ag is $\approx 2.5 \times 10^{-4}$/K. Therefore the dn/dT value for Ag is an order of magnitude larger as compared to dn/dT of Ta_2O_5 and SiO_2 unit cells [75]. Hence the variation in the R_{min} of Ag-DBR configuration mainly results from the temperature dependence of 'ε' for Ag film. The inherent change in a layer thickness of Ta_2O_5 and SiO_2 due to thermal expansion could possibly shift the TPP resonance wavelength (λ_r) which was not observed [3]. However, the presented temperature measurement configuration involves a change in R_{min} which is negligibly affected by the thermal expansion of dielectric materials constituting the DBR.

5.5.3 Temperature Sensitivity of Ag-DBR Structures
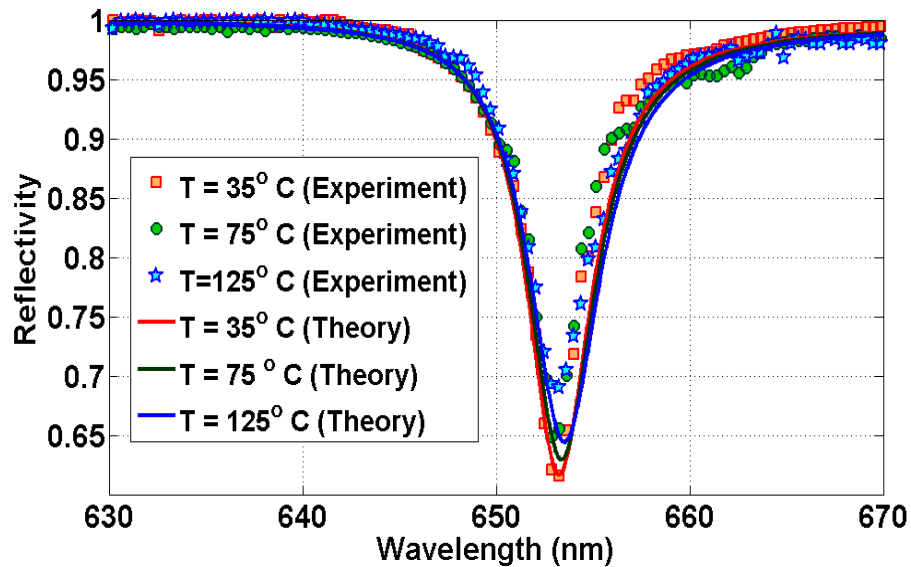
Fig. 5.21 Dependence of R_{min} of TPPs as a function of temperature.

Experimentally measured values of reflection spectra, as well as theoretically modeled reflection spectra by transfer-matrix method (TMM) for "DBR+30 nm Ag" structure at temperature T = 35^0 C, 75^0 C and 125^0 C, are shown in Fig. 5.21 for normal incidence. It is clear from the Fig 5.20 that the TMM-based model nearly

matches with the experimentally measured reflection spectra (dotted curve). It is also evident (See Fig. 5.21) that the $\Delta\lambda$ of the TPPs resonance does not change much with temperature. In order to measure the performance, we define the sensitivity (S_R) of the proposed temperature sensor as the ratio of the variation in reflectivity minimum (ΔR_{min}) from the "DBR-metal" structure to the change in temperature (ΔT) at a given AOI i.e. $S_R = \Delta R_{min}/\Delta T_{AOI}$ [76]. For measuring S_R, reflectivity minimum (R_{min}) of the reflection spectra are plotted with respect to temperature (T) in Fig. 5.22. The plot shows the variation is linear at low temperature; however at a higher temperature, the deviation is not linear. The slope of the plot gives us sensitivity and is calculated to be $S_R = 7.8\times10^{-4}/°C$. It is important to mention here that SPR-based temperature sensors exhibit a sensitivity of $\approx 3.5\times10^{-4}/°C$ [77, 78].
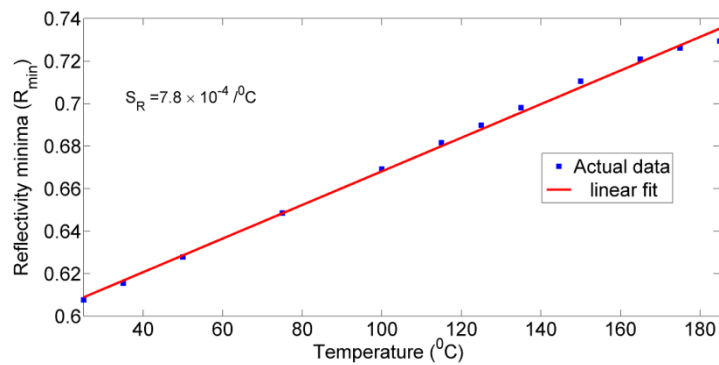
Fig 5.22 Change in R_{min} as a function of temperature for "metal-DBR" at normal incidence.

5.6 Summary

The strongly localized electromagnetic modes lead to field enhancement in case of TPP modes which have been used for various applications. This chapter begins with a discussion and review of the present status of TPPs modes. We have theoretically and

experimentally investigated the factors influencing the lifetime and Q-factor of TPPs modes. In this chapter, I have also proposed a refractive-index sensor scheme utilizing coupled modes in dual 'Ag-DBR' configuration. Coupled or hybrid TPPs modes are excited due to coupling between two TPP modes at the metal-DBR boundary. We have also shown that a micro-cavity in between metal and DBR geometry is a powerful tool for light trapping and hence can be utilized for refractive index sensing. The proposed hybrid and cavity modes sensing configuration could be employed in the desired wavelength range. We have also been able to demonstrate a TPPs based temperature sensor in a simple metal-DBR structure. The reflection dip or R_{min} corresponding to excitation of TPPs-modes exhibit a change with temperature. The change in R_{min} with temperature is being utilized for temperature measurement.

Bibliography

[1] I. Tamm, Uber eine mögliche Art der Elektronenbindung an Kristalloberflächen, *Zeitschrift für Physik* **76**, 849 (1932).

[2] M. Kaliteevski, I. Iorsh, S. Brand, R. Abram, J. Chamberlain, A. Kavokin, and I. Shelykh. Tamm plasmon-polaritons: Possible electromagnetic states at the interface of a metal and a dielectric Bragg mirror, Physical Review B **76**, 165415 (2007).

[3] M. E. Sasin, R. P. Seisyan, M. A. Kaliteevski, S. Brand, R. A. Abram, J. M. Chamberlin, A. Yu. Egorov, A. P. Vasil'ev, V. S. Mikhrin, and A. V. Kaovkin, Tamm plasmon polaritons: Slow and spatially compact light, Applied Physics Letters **92**, 251112(2008).

[4] A. V. Kavokin, I. A. Shelykh, and G. Malpuech, Lossless interface modes at the boundary between two periodic dielectric structures, Physical Review B **72**, 233102 (2005).

[5] E. Kretschmann and H. Raether, Radiative decay of nonradiative surface plasmons excited by light, Z. Naturforsch A **23**, 2135–2136 (1968)

[6] H. Zhou, G. Yang, K. Wang, H. Long, and P Lu, Multiple optical Tamm states at a metal-dielectric mirror interface, Opt. Lett. **35**, 4112-4114(2010)

[7] C. Symonds, A. Lemaître, E. Homeyer, J. C. Plenet J C, and J. Bellessa, Emission of Tamm plasmon/exciton polaritons, Appl. Phys. Lett. **95**, 151114 (2009)

[8] K. Leosson, S. Shayestehaminzadeh, T. K. Tryggvason, A. Kossoy, B. Agnarsson, F. Magnus, S. Olafsson, J. T. Gudmundsson, E. B. Magnusson, and I. A. Shelykh, Comparing resonant photon tunneling via cavity modes and Tamm plasmon polariton modes in metal-coated Bragg mirrors, Opt. Lett. **37**, 4026-4028 (2012).

[9] Y. Chen, D. Zhang, L. Zhu, Q. Fu, R. Wang, P. Wang, H. Ming, R. Badugu, J. R. Lakowicz, Effect of Metal Film Thickness on Tamm Plasmon-Coupled Emission, Phys. Chem. Chem. Phys. **16**, 25523–25530 (2014).

[10] C. Y. Chang, Y. H. Chen, Y. L. Tsai, H. C. Kuo, K. P. Chen, Tunability, and Optimization of Coupling Efficiency in Tamm Plasmon Modes, IEEE J. Sel. Top. Quantum Electron. **21** 460020 (2015)

[11] M. Lopez-Garcia M, Y. L. D. Ho, M. P. C. Taverne, L. F. Chen, M. M. Murshidy, A. P. Edwards, M. Y. Serry, A. M. Adawi, J. G. Rarity, and R. Oulton, Efficient out-coupling and beaming of Tamm optical states via surface plasmon polariton excitation, Appl. Phys. Lett. **104**, 231116 (2014)

[12] G. Lheureux, S. Azzini, C. Symond, P. Senellart, A. Lemaître, C. Sauvan, J. P.Hugonin, J. J.Greffet, J. Bellessa, Polarization-Controlled Confined Tamm Plasmon Lasers, ACS Photonics **2**, 842-848 (2015).

[13] C. Symonds, G. Lheureux, J. P. Hugonin, J. J. Greffet, J. Laverdant, G. Brucoli, A. Lemaitre, P. Senellart, and J. Bellessa, Confined Tamm plasmon lasers, Nano Lett. **13,** 3179–3184 (2013)

[14] K. J. Lee, J. W. Wu, and K. Kim, Enhanced nonlinear optical effects due to the excitation of optical Tamm plasmon polaritons in one-dimensional photonic crystal structures, Opt. Express **21**,28817–28823 (2013)

[15] X. L. Zhang, J. F. Song, X. Bi Li, J. Feng, and H. B. Sun, Light trapping schemes in organic solar cells: A comparison between optical Tamm states and Fabry-Perot cavity modes, Org. Electron. **14,** 1577–1585 (2013).

[16] C. Tamm and C. Weiss, Bistability and optical switching of spatial patterns in a laser, J. Opt. Soc. Am. B **7,** 1034–1038(1990)

[17] W. L. Zhang, F. Wang, Y. J. Rao, and Y. Jiang, Novel sensing concept based on optical Tamm plasmon, Opt. Express **22**, 14524-14529 (2014).

[18] B. Auguie, M. C. Fuertes, P. C. Angelome, N. L. Abdala, G. J. A. A. Soler Illia, and A. Fainstein, Tamm Plasmon Resonance in Mesoporous Multilayers: Toward a Sensing Application, ACS Photonics **1**, 775-780(2014).

[19] R. Badugua, E. Descrovib, and J. R. Lakowicza, Radiative decay engineering 7: Tamm state-coupled emission using a hybrid plasmonic-photonic structure, Analytical Biochemistry **445(3)**, 1-13 (2014).

[20] R. Badugu and J. R. Lakowicz. Tamm state-coupled emission: Effect of probe location and emission wavelength, J. Phys. Chem. C **118(37)**, 21558-21571 (2014).

[21] B. I. Afinogenov, V. O. Bessonov, and A. A. Fedyanin, Second-harmonic generation enhancement in the presence of Tamm plasmon-polaritons, Opt. Lett. **39**, 6895-6898 (2014)

[22] Chun-hua Xue, Hai-tao Jiang, Hai Lu, Gui-Qiang Du, and Hong Chen, Efficient third-harmonic generation based on Tamm plasmon polaritons, Opt. Lett.**38**, 959-961 (2013).

[23] I. Iorsh, I. V. Shadrivov, P. A. Belov, and Y. S. Kivshar, Nonlinear Tamm states in layered metal-dielectric metamaterials, Phys. Status Solidi **6(**1), 43–45 (2012).

[24] A. R. Gubaydullin, C. Symonds, J. Bellessa, K. A. Ivanov, E. D. Kolykhalova, M. E. Sasin, A. Lemaitre, P. Senellart, G. Pozina and M. A. Kaliteevski, Enhancement of spontaneous emission in Tamm plasmon structures, Sci Reports **7**, 9014(2017).

[25] Mukesh Kumar Shukla and Ritwick Das, Tamm-plasmon polaritons in one-dimensional photonic quasi-crystals, Opt. Lett. **43**, 362-365 (2018).

[26] R. Das, T. Srivastava, R. Jha, Tamm-plasmon and surface-plasmon hybrid-mode based refractometry in photonic bandgap structures, Opt. Lett. **39**, 896–899 (2014).

[27] B. I. Afinogenov, V. O. Bessonov, A. A. Nikulin, A. A. Fedyanin, Observation of hybrid state of Tamm and surface plasmon-polaritons in one-dimensional photonic crystals, Appl. Phys. Lett. **103**, 061112 (2013).

[28] S. Kumar, M. K. Shukla, P. S. Maji and R. Das, Self-referenced refractive index sensing with hybrid-Tamm-plasmon-polariton modes in sub-wavelength analyte layers, J. Phys. D. Appl. Phys. **50,** 375106(2017).

[29] S. V. Poltavtsev, Yu. V. Kapitonov, J. Vondran, D. R. Yakovlev, C. Schneider, M. Kamp, S. Höfling, R. Oulton, I. A. Akimov, A. V. Kavokin, and M. Bayer, Photon echoes from (In, Ga)As quantum dots embedded in a Tamm-plasmon microcavity, Phys. Rev. B **95**, 035312(2017).

[30] R. Li, C. Zhang, and X. Li, Schottky hot-electron photodetector by cavity-enhanced optical Tamm resonance, Appl. Phys. Lett. **110**, 013902(2017).

[31] Y. T. Fang, Y. X. Ni, H. Q. He and J. X. Hu, Effect of hybrid state of surface plasmon–polaritons, magnetic defect mode and optical Tamm state on nonreciprocal propagation, Opt. Commun **320**, 99-104(2014).

[32] Y. T. Fang, X. H. Song, L. Z. Lu, J. J. Wang, Y. X. Jiang, and M. Zhu, Surface waves with near-zero or negative group velocity on one-dimensional photonic crystal coated with one metal film, Opt. Commun. **228**, 129-134 (2013).

[33] B. I. Afinogenov, A. A. Popkova, V. O. Bessonov, and A. A. Fedyanina, Measurements of the femtosecond relaxation dynamics of Tamm plasmon-polaritons, Appl. Phys. Lett. **109,** 171107 (2016)

[34] P. Melentiev, A. Afanasiev, and V. Balykin, Optical Tamm state on a femtosecond time scale, Phys. Rev. A **88,** 053841(2013).

[35] A. Politano and G. Chiarello, Tuning the lifetime of the surface plasmon upon sputtering Phys, Status Solidi RRL **3,** 136–138(2009).

[36] C. Grossmann, C. Coulson, G. Christmann, I. Farrer, H. Beere, D. Ritchie, and J. Baumberg. Tuneable polaritonics at room temperature with strongly coupled Tamm plasmon polaritons in metal/air-gap microcavities, Appl. Phys. Lett. **98**, 231105(2011).

[37] M. Kaliteevski, S. Brand, R. A. Abram, I. Iorsh, A. V. Kavokin, and I. A. Shelykh. Hybrid states of Tamm plasmons and exciton polaritons. Applied Physics Letters, 95:251108 (2009).

[38] B. Auguie, A. Bruchhausen, and A.Fainstein, Critical coupling to Tamm plasmons, J. Opt. 17, 035003(2015)

[39] S Kumar and R Das, On the tunability of quality-factor for optical Tamm plasmon modes, J. Opt.19 (9), 095001 (2017).

[40] P. Yeh, A. Yariv, and C. S. Hong, Electromagnetic propagation in periodic stratified media. I. General theory, J. Opt. Soc. Am. **67** 423-438(1977)

[41] X L Zhang, J F Song, X B Li, J Feng and H B Sun, Strongly Localized Evanescent Optical Tamm States at Metal-DBR Interface, J. Lightwave Technol. **3** 11654-1659 (2013).

[42] P B Johnson and R W Christy, Optical Constants of the Noble Metals, Phys. Rev. B **6**, 4370 (1972).

[43] T. J. Bright, J. I. Watjen, Z. M. Zhang, C. Muratore, A. A. Voevodin, D I Koukis, D. B. Tanner, and D. J. Arenas, Infrared optical properties of amorphous and nanocrystalline Ta_2O_5 thin films, J. Appl. Phys. **114** 083515 (2013).

[44] G. Ghosh, M. Endo, T. and Iwasaki, Temperature dependent Sellmeier coefficients and chromatic dispersions for some optical fiber glasses, J. Lightwave Technol. 12 1338(1994).

[45] S. Brand, R. A. Abram, and M. A. Kaliteevski, Bragg reflector enhanced attenuated total reflectance, J. Appl. Phys. **106**,113109 (2009).

[46] Y. Xiang, P. Wang, W. Cai, C.F. Ying, X. Zhang and J. Xu, Plasmonic Tamm statesdual enhancement of light inside the plasmonic waveguides, J. Opt. Soc. Am. B

31, 2769-2722 (2014).

 [47] S. K. S. Rahman, T. Klein, S. Klembt, J. Gutowski, D. Hommel and K. Seband, Observation of a hybrid state of Tamm plasmons and microcavity exciton polaritons Sci. Rep. **6,** 34392(2016).

[48] B. D. Gupta and R. K. Verma, Surface plasmon resonance-based fiber optic sensors: principle, probe designs, and some applications, J. Sensors **2009,** 979761(2009)

[49] M. E. Sasin, R. Seisyan, M. A. Kaliteevski, S. Brand, R. Abram, J. Chamberlain, A. Y. Egorov, A. Vasilev, V. Mikhrin, and A. Kavokin, Tamm plasmon polaritons: Slow and spatially compact light Appl. Phys. Lett., **92,** 251112 (2008).

[50] B. I. Afinogenov, V. O. Bessonov, A. A. Nikulin, and A. A. Fedyanin, Observation of hybrid state of Tamm and surface plasmon-polaritons in one-dimensional photonic crystals Appl. Phys. Lett. **103,** 061112 (2013).

[51] Y. Fang, L. Yang, Wa Kong and Na Zhu, Tunable coupled states of a pair of Tamm plasmon polaritons and a microcavity mode J. Opt. **15**, 125703(2013).

[52] K. V. Sreekanth, Y. Alapan, M. ElKabbash, Efe Ilker, M. Hinczewski, Umut A. Gurkan, A. De Luca and Giuseppe Strangi, Extreme sensitivity biosensing platform based on hyperbolic metamaterials Nature Mater **15**, 621-627 (2016).

[53] M. Kobayashi, H. Terui, Refractive index and attenuation characteristics of SiO_2 - Ta_2O_5 optical waveguide film, Appl. Opt. **22**, 3121-3127 (1989).

[54] M. A. Kaliteevski, A. A. Lazarenko, D. Ilinskaya, Yu. M. Zadiranov, M. E. Sasin D. Zaitsev, V. A. Mazlin, P. N. Brunkov S. I. Pavlov, A. Yu. Egorov, Experimental demonstration of reduced absorption of light by intracavity metallic layers, Plasmonics **10,** 281-284 (2015).

[55] Y. L. Jin, J. Y. Chen, L. Xu, and P. N. Wang, Refractive index measurement for biomaterial samples by total internal reflection, Phys. Med. Biol. **51**, 371–379 (2006).

 [56] M. Shaban, A. M. Ahmed, E. Abdel-Rahman and H. Handy, Tunability and Sensing Properties of Plasmonic/1D Photonic Crystal, Sci. Rep. **7,** 41983 (2017)

[57] C. López-Quesada, A.-S. Fontaine, A. Farre, M. Joseph, J. Selva, G. Egea, M. D. Ludevid, E. Martín-Badosa, and M. Montes-Usategui, Artificially-induced organelles are optimal targets for optical trapping experiments in living cells, Biomed. Opt. Express **5**, 1993-2008 (2014).

[58] S. K. Srivastava and I. Abdulhalim, a Self-referenced sensor utilizing extra-ordinary optical transmission from metal nanoslits array, Opt. Lett. **40**, 2425-2428 (2015)

[59] M. Abutoama, I. Abdulhalim, Angular, and Intensity Modes Self-Referenced Refractive Index Sensor Based on Thin Dielectric Grating Combined With Thin Metal Film, IEEE J. Sel. Top. Quantum Electron. **23**, 1-9 (2017).

[60] C. Yang C and S. O. Oyadiji, Theoretical and experimental study of self-reference intensity- modulated plastic fiber optic linear array displacement sensor, Sens. Actuators A: Phys. **222**, 67-79 (2015).

[61] Xu-Lin Zhang, Jing Feng, Xiao-Chi Han, Yue-Feng Liu, Qi-Dai Chen, Jun-Feng Song, and Hong-Bo Sun, Hybrid Tamm plasmon-polariton/microcavity modes for white top-emitting organic light-emitting devices, Optica **2**, 579-584 (2015).

[62] R. Jha, J. Villatoro, G. Badenes and V. Pruneri, Refractometry based on a photonic crystal fiber interferometer, Opt. Lett. **34**, 617-619 (2009).

[63] R. Das, T. Srivastava, R. Jha, Guided mode Analysis of Tamm-Plasmon Polariton at Metal Heterostructure Dielectric Interface J. Lightwave Technol. **32**, 1221-1225 (2014).

[64] N. Luan, C. Ding, J. Yao, A Refractive Index and Temperature Sensor Based on Surface Plasmon Resonance in an Exposed-Core Microstructured Optical Fiber, IEEE Photonics Journal **8**, 1-8 (2016).

[65] P. Bhatia, B. D. Gupta, Surface-plasmon-resonance-based fiber-optic refractive index sensor: sensitivity enhancement, Appl. Opt. **50**, 2032-2036 (2011).

[66] R. Jha, A. K. Sharma A K, High-performance sensor based on surface plasmon resonance with chalcogenide prism and aluminum for detection in infrared, Opt. Lett. **34**, 749-751 (2009).

[67] W. Xu, M. Lin, C. Chen, C. Chang, and K. Chen, in *JSAP-OSA Joint Symposia 2016 Abstracts, OSA* (2016).

[68] Pavel S. Pankin, Stepan Ya. Vetrov, and Ivan V. Timofeev, Tunable hybrid Tamm-microcavity states, J. Opt. Soc. Am. B **34**, 2633-2639 (2017).

[69] C. J Wu, Y. H. Chung, B. J. Syu, and T. J. Yang, Progress in electromagnetic research, **102**, 81, (2010).

[70] B.I. Afinogenov, A. A. Popkova, V. O. Bessonov, and A. A. Fedyanina, Measurements of the femtosecond relaxation dynamics of Tamm plasmon-polaritons, Appl. Phys. Lett. **109**, 171107(2016).

[71] X. Wang, X. Hu, Y. Li, W. Jia, C. Xu, X. Liu, J. Zi, Enlargement of omnidirectional total reflection frequency range in one-dimensional photonic crystals by using photonic heterostructure, Appl. Phys. Lett. **80** (2002).

[72] R.V. Nair, R. Vijaya, Three-dimensionally ordered photonic crystal heterostructure with a double photonic stop band, J. Appl. Phys. **102**, 056102 (2007).

[73] A. Chu, H. Lin, and W. Cheng, Temperature dependence of refractive index of Ta_2O_5 Dielectric Films, J. Electron. Mater. **26**, 889–892 (1997).

[74] J. Matsuoka, N. Kitamura, S. Fujinaga, T. Kitaoka, and H. Yamashita, the Temperature dependence of refractive index of SiO_2 glass, J. Non-Cryst. Solids **135**, 86–89 (1991).

[75] H. P. Chiang, P.T. Leung, and W. S. Tse, The surface plasmon enhancement effect on absorbed molecules at elevated temperatures, J. Chem. Phys. **108**, 2659 (1998).

[76] N. Liu, M. Mesch, T. Weiss, M. Hentschel, and H. Giessen, Infrared perfect absorber and its application as plasmonic sensor, Nano Lett. **10**, 2342-2348 (2010).

[77] H. P. Chiang, Y. C. Wang, P. T. Leung, and W. S. Tse, A theoretical model for the temperature-dependent sensitivity of the optical sensor based on surface-plasmon resonance, Opt. Commun. **188**, 283-289 (2001).

[78] K. Q. Lin, L. M. Wei, D. G. Zhang, R. S. Zheng, P. Wang, Y.-H. Lu, and H. Ming, "Temperature effects on prism-based surface plasmon resonance sensor," Chin. Phys. Lett. **24**, 3081–3084 (2007).

Chapter 6
Conclusions and Future Outlook

In this thesis entitled "Linear and Nonlinear Optical Effects in Sub-Wavelength structures", I have basically focused on three major projects. The first two projects focus on the nonlinear optical measurements (such as NLR and NLA) in (a) organic thin-films and (b) inorganic (semiconducting) sub-wavelength species. The third project involves detailed description and experimental investigations on optical properties of optical surface modes in a periodically-stratified medium and its possible applications.

Below, the contributions and achievements of the three major projects are summarized. Based on the investigations and results, the possibilities for future work are suggested.

1. Nonlinear Optical Properties of Organic Semiconductors.

In this work, I have experimentally investigated the influence of phase change on NLO properties of organic semiconductors (metal-free and metal-phthalocyanine; abbreviated as Pc and MPc respectively) thin films. Annealing the as-prepared (α-phase) Pc and MPc films produces stable β-phase due to structural re-orientation. We have observed that both the phases exhibit remarkably different linear and nonlinear properties. Therefore, the investigations on determining nonlinear optical coefficients in thin-films with different phases have practical significance towards optimizing the nonlinear Figure of merit.

I have determined the NLR and NLA coefficients of both the phases of Tetra-tert-butyl-phthalocyanine (Pc), Copper(II)2,9,16,23-Tetra-tert-butyl-29H,31H-

phthalocyanine (CuPc) and Zinc(II) 2,9,16,23-Tetra-tert-butyl-29H,31H-phthalocyanine (ZnPC) films using Z-scan method. Our results reveal that as-prepared Pc, CuPc, and ZnPc exhibit large NLR and comparatively smaller NLA whereas the annealed variant has greater NLA. To the best of our knowledge, we report the first observation of fifth-order NLO response in as-prepared (α-phase) of metal-free Pc thin-film which was depicted in an unusual dual peak-valley feature in Z-scan transmittance. Metallo-phthalocyanine thin films also exhibit a discernible difference in NLR at 1064 nm wavelength. The measurements revealed that the CA Z-scan measurements on CuPc films exhibit "peak-valley" characteristics from which we conclude that it possesses negative n_2. However, the CA Z-scan experiments for ZnPc exhibits "valley-peak" signature from which we conclude that it possesses positive n_2. The difference in NLA mechanisms for CuPC and ZnPc was clearly evident from the OA Z-scan measurements. Both phases of ZnPc exhibit saturable absorption (SA) whereas CuPc exhibits reverse-SA (or RSA) behavior. In order to compare the functionality in nonlinear optics based devices, we estimated the Figure of merit (FOM_1 and FOM_2) for metal-free Pc thin-films as well as Metallo-phthalocyanine thin-films.

This work was carried out in collaboration with Dr. S. M. Dharmaprakash and K. V. Anil Kumar of Mangalore University. The work gave material for two publications:

"Phase-dependent ultrafast third-order optical nonlinearities in metallophthalocyanine thin films", S. Kumar, K.V.A. Kumar, S.M. Dharmaprakash, R. Das, *J. Appl. Phys,* **2016**, 120 (12), 123104.

"Impact of α→ β transition in the ultrafast high-order nonlinear optical properties of metal-free phthalocyanine thin films", K.V.A. Kumar, S. Kumar, S.M. Dharmaprakash, R. Das, *J. Phys. Chem. C,* **2016,** 120 (12), 6733-6740.

2. Nonlinear Optical Properties of Inorganic Semiconductors.

In this project, I used Z-scan method to determine NLO properties of inorganic semiconductors (Mn-doped ZnO) nanorods prepared by hydrothermal method. I have carried out detailed investigations of NLA and NLR properties of ZnO nanorods having different Mn doping concentrations. I have experimentally illustrated that Mn-doping concentration changes the NLA and NLR properties of the ZnO nanorods as compared to undoped variants. The difference in NLO properties is attributed to the modifications in energy eigenstates of doped variants through the appearance of defect states within the bandgap as well as deep in the bands. CA Z-scan method reveals self-defocusing effects for Mn-doped ZnO nanorods and undoped ZnO rods. Saturable absorption and two-photon absorption (TPA) was observed and associated NLA coefficients were determined at 532 nm using an ns laser. In pure and 0.5 % Mn-doped ZnO rods, strong TPA behavior was observed while SA was prominent at higher Mn doping concentration. The change from TPA to SA absorption with Mn-doping in ZnO is attributed to the modifications in structure, morphology, and shift of optical resonance.

This work was carried out in collaboration with Dr. P K Sahoo and Avanendra Singh, School of Physical Sciences, NISER. The work gave material for one publication:

"Defect-assisted saturable absorption characteristics in Mn-doped ZnO nano-rods", A. Singh, S. Kumar, R Das, PK Sahoo, *RSC Advances*, **2015,** (108), 88767-88772.

3. Controlling Light-Matter Interactions in Periodically Stratified Medium.

In this section, detailed investigations of the optical properties of optical surface states in a planar configuration have been explored. I have theoretically and experimentally investigated the factors influencing the lifetime and Q-factor of TPP modes. Basically, the TPP modes are optical surface modes which are formed at the boundary of metal and a distributed-Bragg-reflector (DBR). In a metal-DBR configuration, I have performed reflection and transmission measurements to explore the conditions required for TPP excitations. From the reflection spectrum, TPP mode propagation characteristics are determined. Reflection spectrum of TPP modes reveals that metal thickness, metal types, and DBR unit cells play an important role in getting a zero reflectivity and sharper resonance. In the next part of this project, I have proposed a refractive-index sensor based on coupled TPP modes in dual 'silver (Ag)-DBR' configuration. Coupling of TPP modes at the metal-DBR boundary is achieved through an analyte medium. Based on the shift in the resonance wavelength for one of the hybrid-mode as a function of analyte refractive index, a plausible working mechanism for refractive index sensor is proposed. I have also shown that a micro-cavity in between metal and DBR geometry is a powerful tool for light trapping and excitation of cavity mode which could employ for developing sensitive and accurate refractive index sensors. The proposed sensing schemes could be potentially applied to the field of bimolecular and biochemical detection. A different aspect of this project, investigates theoretically as well as experimentally, the applicability of TPP

for temperature measurement. The observation suggests that the reflection minima or R_{min} corresponding to excitation (or coupling) efficiency of TPP-modes exhibit a variation as a function of temperature. The change in R_{min} with temperature could be deployed for developing robust temperature measurement schemes. The detail of this project is described in chapter 5. This research work has resulted in five publications:

"Refractive index sensing using a light trapping cavity: A theoretical study", S. Kumar and R. Das, *J. Appl. Phys*, **2018**, *123*, 233103.

"Coupling to Tamm-plasmon-polaritons: dependence on structural parameters", A. Kumari, S. Kumar, M.K. Shukla, G. Kumar, P.S. Maji, R. Vijaya, R. Das, *Journal of Physics D: Applied Physics*, **2018,**51 (25), 255103.

"Self-referenced refractive index sensing with hybrid-Tamm-plasmon-polariton modes in sub-wavelength analyte layers", S. Kumar, M.K. Shukla, P.S. Maji, R. Das *Journal of Physics D: Applied Physics*, **2017**, 50 (37), 375106.

"On the tunability of quality-factor for optical Tamm plasmon modes", S. Kumar, R. Das, *Journal of Optics*, **2017**, 19 (9), 095001.

"Tamm-plasmon resonance based temperature sensor in a Ta_2O_5/SiO_2 based distributed Bragg reflector", S. Kumar, P.S. Maji, R. Das, *Sensors and Actuators A: Physical*, **2017**, 260, 10-15.

Future Outlook

The investigations carried out in this thesis may lead to the following possibilities for future work:

Our findings pave a way for further experimental investigations on morphological phase and spectrum-dependent nonlinear optical effects in various derivatives of

phthalocyanine and other organic compounds. Based on linear optical properties of quite a few organic thin films, there is a strong anticipation that phase and pulse width dependent NLO properties of such variants in the visible region could exhibit novel features. This could be of prime significance in optoelectronic industry.

Based on our investigation it becomes necessary to carry out phase dependent study in phthalocyanine thin films in order to assess the NLO properties accurately and for optimizing the nonlinear FOM.

The saturable absorption (SA) observed in Mn-doped ZnO nanorods opens up the possibility of obtaining optical limiting and transmission enhancement simultaneously.

Detail NLO investigations of Mn-doped ZnO nanorods and similar nanostructures will provide important information's regarding ZnO based materials as saturable absorbers for laser mode-locking

In addition, investigations of the spectral dependence of changes in refractive index in Mn-doped ZnO nanorods are essential to understanding its dispersion properties and various applications.

Further, the studies on TPP modes as well as micro-cavity modes necessarily entail the development of appropriate experimental schemes for refractive index sensing through hybrid-mode and cavity-modes in metal-DBR configuration.

Field enhancement due to excitation of TPPs modes may lead to various nonlinear optical (NLO) effects. Further studies may lead to observations of change in refractive index in metal-DBR structure with a few mW on resonance laser excitation source.